Characterization of Thermal-Mechanical Properties and Optimal Selection of Coke Drum Materials

by

Hafijur Rahman

A thesis submitted in partial fulfillment of the requirements for the degree of

Master of Science

Department of Mechanical Engineering
University of Alberta

Abstract

Coke drums, critical equipment in petroleum industry, experience severe thermal-mechanical loading during operations and, the safety and integrity of the coke drum are important to the industries. The tendency of material selections of the coke drum is increasing towards with higher content of Chrome and Molly as the base and 410S stainless steel as the cladding material. Coke drums made of these materials are still experiencing the same type of failure or damage due to high stress developed in the coke drum shell during the operation. The thermo-elastic behavior of the coke drum with currently used materials under thermal and mechanical cyclic loadings is analyzed by using finite element method. It is found that the mismatching of coefficient of thermal expansions of the clad and base materials of coke drum is the main reason to induce very high stress in clad layer that can exceed its yield strength. An alternative combination of SA302B as the base and nickel alloy N06625 as the cladding material is suggested; with this new combination the stress developed in the drum shell is very low according to the coupled thermo-elastic analysis due to their matching coefficient of thermal expansions. The thermal-mechanical properties of those materials are experimentally obtained in the laboratory. To find more accurate and practical results, thermal elastic-plastic analysis is also performed for both pairs of clad and base materials. It is found that permanent deformation is caused in the first cycle of operation and plastic shakedown occurs in the clad layer of the coke drum with the currently used material combination. But there is no permanent deformation happened in the coke drum shell with the new selected material combination, which can be recommended as an optimal material combination for the coke drum.

Acknowledgements

The author would like to acknowledge with gratefulness to his supervisors Dr. Zihui Xia and Dr. Xiaodong Wang for their guidance, constant support, intuitive suggestions and relentless encouragement.

Gratitude is extended to Dr. Jie Chen and Mr. Bernie Faulkner, who helped me to use the experimental facility, equipment and the associate testing procedure.

The author would like to take the opportunity to thank the other members of the Collaborative Research and Development (CRD) Project group, past and present, for offering support and excellent technical discussions during the weekly group meetings. The author gratefully acknowledges the computing support provided by the Department of Mechanical Engineering, University of Alberta.

INDEX

List of Figures

List of Tables

Chapter 1 Introduction

1.1 Introduction

Coke drums are insulated vertically oriented cylindrical pressure vessels used in the delayed coking process. Delayed coking process is used to convert heavy oil residue to produce gas product and petroleum coke. The tops and bottoms of the coke drums are elliptical and conical respectively. The dimensions of the coke drums are commonly 4 m to 9 m in diameter, and around 25 m in height. The pressure inside the coke drum varies from 100 to 500 kPa, and the maximum operating temperature ranges from 427 to 482°C. Around 10 cm of fiberglass insulator with stainless steel or aluminum sheet covering is installed on the outside of the coke drum for heat conservation [1].

Coke drum is subjected to severe thermal-mechanical loadings in the temperature range from arbitrary to 480^{o} C in each operating cycle, including the processing stages of steam testing, vapor heating, oil filling , steam and water quenching and un-heading. A typical coke drum operation is shown in Fig. 1.1. This figure shows the measured temperature history at a specified location of an 18-hour operation cycle [2]. The process is commencing with preheating the drum by flowing the steam from the bottom of the drum to the top. The temperature of the steam testing is increasing rapidly at the beginning and then becomes stable after 1.2 hours. The reason of the steam preheating is to ensure if there are any leaks to be repaired before starting the operation of the coke drum. A similar phenomenon is observed at the vapor heating stage. The flow of hydrocarbon

vapor reduces the thermal shock experienced when hot, heavy oil is injected into the drum. The oil filling stage is beginning by injecting the heavy oil from the bottom of the coke drum. The temperature of the whole coke drum increases simultaneously to a very high temperature even though the oil level is still at low, because the coke drum is filled up with hot oil vapor rapidly. The oil filling stage generally takes from 10 to 24 hours [1]. After that, coke drums are cooled down by injecting high rate of quench water from the bottom of the coke drum. At this stage, since there is a big difference of temperatures between the surfaces below the water and above the water, high stress developed in the coke drum as a result of severe bending. During un-heading stage, extraction of coke is completed by cutting the solid coke using rotating high-pressure water stream. Finally, the coke drum is checked again and reheated to continue for the next operation.

Since the coke drum is filled with hot oil and subsequently quenched with water, coke drum undergoes severe thermal-mechanical loadings. The intense thermal cycling during quenching stage is the root cause of the shell bulging [3], which leads the cracking and failure of the shell of the coke drums. Therefore, the severe thermal-mechanical loadings cause lives of the coke drum to be shortened. The average operational life of the coke drum is above ten years [1]. During their operational lives, coke drums have also to go through a series of repairs due to the damage that result in high cost associated with the production loss.

Therefore, it is important to improve the reliability and to extend the lives of the coke drums, which will save the maintenance cost, increase the production and especially ensure the safety of the operation.

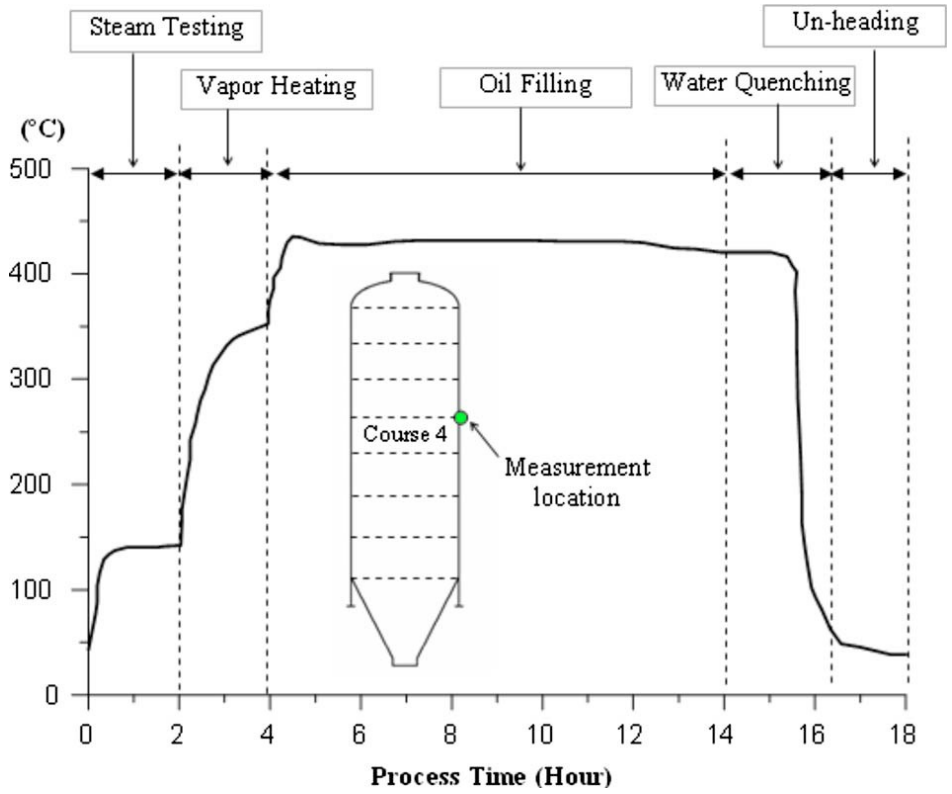

Figure 1.1: A typical thermal cycle of the coke drums [2].

1.2 Review of the Currently Used Coke Drum Materials

Coke drums are generally constructed with two layers of materials: base and clad. The thickness of the base varies from 0.014 to 0.042 meters. Internally, the coke drums are clad with liner materials whose thickness ranges from 0.002 to 0.0032 meters [1].

In the early days, coke drums were constructed using plates of carbon steel (mild steel). To increase the useful life and reduce the down time, in recent years coke drums have been constructed from low alloy steel such as Carbon-1/2 Moly, 1 Chrome-1/2 Moly and 2 ¼ Cr – Mo or even higher alloying elements. Most modern coke drums are fabricated with 405 or 410S stainless steel as a clad material for corrosion resistance [4]. Typical materials used in the coke drum are listed in Table 1.1.

Table 1.1: Typical materials used in coke drums. [3]

Base Metal	Type	Clad Metal	Type
SA516 Gr70	Carbon Steel	AISI 405	13 Cr
SA204 Gr C	Carbon - ½Moly	SA240 TP410S	12 Cr
SA387 Gr 11 CL 2	1 ¼ Cr – ½ Moly		
SA387 Gr 12 CL 2	1Cr – ½ Moly		
SA387 Gr 22 CL 2	2 ¼ Cr – ½ Moly		

1996 API Coke Drum Survey Report showed that the tendency of material selections of the coke drum is towards higher content of Chrome and Molly [4]. The selection of cladding material began an increase in the use of TP410S stainless steel. These materials are considered because of their higher yield strength and better creep resistance. However, coke drums made of these materials are still experiencing the same type of failure or damage [3]. For example, Bagdasarian et al. [5] found that increase of the Chrome and Molly in alloy does not increase the service life of the coke drums.

1996 API Coke Drum Survey also indicated that service induced bulging occurred in 57% of the surveyed coke drum. Among them, 70% of the cracks occurred at bulged

areas [4]. Therefore, it is important to set proper guidelines for selecting suitable materials for the coke drums that will increase the reliability of the coke drum sand be economically beneficial for upgrading heavy oil process in the petroleum refineries.

1.3 Importance of Alternative Selection of Coke Drum Materials

Most of the studies assign the discontinuity of the weld zones and abrupt change of the temperature during quenching to the failure mechanism of the coke drum, which are truly important issues to consider for the design and fabrication of the coke drums [1, 5-9]. Xia et al [2] indicated that even with the presence of discontinuity and abrupt temperature change during quenching, coke drum would operate safely if the stress developed in the coke drum could be controlled within the elastic range. Therefore, lowering the stress and strain in coke drums is important issue to be considered in the design of the coke drums.

Xia et al. [2] also performed a finite element analysis (FEM) of the coke drum with TP410S as the clad material and SA387-22-2 as their base material. And they concluded that the major source of stress developed in the coke is due to the mismatch of the CTE's of the base and clad layers of the coke drum. Therefore, better selection of the coke drum materials based on the CTE's can achieve some contributions to the reliability of the coke drums.

Nikic et al. [10] extended the work of the Xia et al. [2] to find better material candidates for the coke drums. The authors developed two FEA models considering different combinations of clad and base materials; (a) The first one was the elastic-plastic analysis

of one-course of the coke drum to examine the stress in clad and base layer caused by the thermal cycle with in-phase internal pressure, and (b) The second one was the thermo-elastic transient analysis to investigate the stress in the clad and base layer during the quenching operation stage. He also checked the influence of CTEs, thermal conductivities and Young's modulus of the coke drum materials on the stress level in the quenching stage.

The research results obtained by Nikic et al. [10] indicated that a significant improvement can be achieved by using nickel based alloys N06600 and N06625 due to their matching CTEs with the base materials and higher yield strength compared to TP410S stainless steel. The author also found that SA302C showed a significant advantage over the other base materials because of its combination with N06625 resulting low von Mises equivalent stress to yield strength ratio in the clad layer. Due to unavailability of material SA302C in the market, SA302B is chosen as a base material in the present studies due to the similarities of their thermal and mechanical properties. Therefore, N06625 as clad material paired with SA302B as base material, an alternative selection of coke drum materials, can be an opportunity in improvement of reliability of coke drums.

1.4 Importance of Characterization of the Thermal-Mechanical Properties of Coke Drum Materials

Accurate thermal elastic-plastic analyses of the coke drums depend on how precisely the characterization of the thermal-mechanical properties of the coke drum materials was done. Xia et al and Nikic et al. [2, 10] in their research obtained mechanical and thermal

properties from ASME database. But ASME provides only minimum specified yield and tensile strengths of the materials obtained from the monotonic tensile stress-strain curves, which are generally conservative to use in practical application and not suitable to include in cyclic loading conditions. Hence, it is essential to determine more accurate thermal & mechanical properties of the desired materials.

Xia et al [2] indicated that coke drums are designed with respect to the ultimate strength of the material according to the ASME Sec. VIII, Division 1. The other factors considered for the selection of the materials and thickness of the coke drums are: internal operating pressure, and hydrostatic pressure due to oil filling and water quenching [2]. Most of the researchers confirmed that low cycle fatigue is the principle failure mechanism of the coke drums, due to high stress developed during the quenching of the process cycle [11]. Therefore, though the coke drums are subjected to cyclic thermal and mechanical loadings, they are not well designed based on fatigue criterion.

Therefore, using monotonic material properties to design coke drum may cause error in prediction of the fatigue life of the coke drum materials. For the cyclic loading applications, it is important to use materials' cyclic mechanical properties.

1.5 Introduction of the Present Work

The present study focuses on optimal selection of coke drum materials. There are three main objectives of the current research works:

1) To characterize basic thermal-mechanical and isothermal low cycle fatigue properties of the coke drum materials.
2) To develop a coupled thermo-elastic finite element (FE) model of the coke drum to analyze the stress/strain field in the drum shell for two pairs of base and clad material combinations; one is currently used material combination (TP410S/SA387-22-2) and another is the optional material combination (N06625/SA302B) .
3) To develop a thermal elastic-plastic FE model of the coke drum to analyze more accurately the stress/strain field for the same two pairs of base and clad materials.

Optimal selection of materials for coke drums can increase the reliability and performance of the coke drums as discussed earlier. Therefore, in the present study, at first the mechanical and thermal properties of the alternative coke drum materials of N06625 and SA302B are experimentally obtained from a series of relevant tests performed in our laboratory. Experimental investigations of the coke drum materials are important to obtain more accurate and deeper understanding of the mechanical properties. These properties are then summarized and compared with the properties of currently used coke drum materials. To more accurately study material response under cyclic (fatigue) loading, cyclic stress-strain curves of those materials are obtained. Strain amplitude - isothermal low cycle fatigue life curves of the coke drum materials are also obtained for estimation of the fatigue lives of those materials under given cyclic loading conditions.

A finite element (FE) based coupled thermo-elastic model of the coke drum is developed using FEM code ANSYS. Special care is taken to model the thermal and mechanical boundary conditions and assumptions associated with the FE model in a reasonable and justifiable manner. This relative simple FE analysis provides guidelines for the selections of materials and, operating parameter (such as water rising speeds during quenching stage) etc. The stress/strain distributions in the drum shell for those two pairs of base and clad materials are also obtained and compared. It is found that the maximum stress in the clad of the studied coke drum with the materials combination of SA387-22-2/TP410S exceeds the yield strength.

To obtain more accurate and practical results, finite element based thermal elastic-plastic model of the coke drum is developed using the temperature distribution history data from the coupled thermal-elastic analysis. The bilinear kinematic hardening model is adopted for this analysis in which the required materials' bilinear properties are obtained from the tested cyclic stress-strain curves. Finally, the mechanical behavior of the coke drum with two different pairs of materials is investigated by comparing the stress/strain fields obtained from the simulation results. The present study provides some guidelines for the future design and manufacturing of more robust coke drums.

Chapter 2 Characterization of Mechanical and Low Cycle Fatigue Properties of SA302B and N06625

2.1 Introduction

To select suitable materials for a design and numerical modeling of a structure, obtaining accurate material properties are important. Though material properties can be obtained from ASME-material database [12], but ASME provides a minimum specified yield and tensile strength of the materials which are generally conservative to use in practical application. Hence it is important to determine more accurate thermal & mechanical properties of the desired materials. Our studied coke drum is made of SA240 TP410S as a clad layer and SA387-22-2 as a base layer. Nikic and Xia et al [10] suggested an optional material combination consisted of Inconel 625 or UNS N06625 (60Ni-22Cr-9Mo-.5Cb) as a clad layer and SA302B (Mn-1/2Mo) as a base layer due to their matching CTEs. This new material combinations reduces the stress level in the clad layer. The specified compositions of the material N06625 and SA302B at ambient temperature, which are provided by material supplier, are given in Table 2.1. These material compositions are consistent with the ASME standard [13, 14].

Table 2.1: Limiting Chemical Composition, % of N06625 and SA302 Gr. B [13, 14].

Test materials	Nominal Composition (%)										
Elements	C	Cr	Mn	Mo	P	S	Ni	Si	Co	Al	Cu
SA 302 Gr B	0.11	0.27	1.16	0.48	0.015	0.016	0.24	0.24	-	0.027	0.035
N06625	0.1	22	0.5	9	0.015	0.015	60	0.5	3.5	-	-

The objective of this chapter is to characterize the mechanical and thermal properties of optional material combination of N06625 /SA302B and comparison of their properties with the currently used material combination TP410S/SA-387-22-2. Jie et al [3, 17] performed all the relevant tests and obtained the mechanical and thermal properties of the materials of latter combination. For this reason, only the tests of the two materials N06625 and SA302B were performed and their properties will be presented and discussed in this chapter. Jie and Xia et al [3] have developed a thermal-mechanical material testing system in our lab as shown in Fig. 2.1, which is capable to perform tests under monotonic or cyclic loadings at room or elevated temperatures. The testing system primarily made up of a servo-controlled hydraulic MTS machine, an electric resistance heating furnace, a set of water-cooled grips, an extensometer and, a data acquisition and control system [3]. The more details of this testing system can be found in Ref. [3].

Since the operating temperature of the coke drum is in between arbitrary temperature to 480^{o}C, all the tests were carried out at four different temperatures, that is, at room temperature, 100^{o} C, 250^{o} C and 480^{o} C, respectively. Four types of tests (monotonic, cyclic, CTE measurement and Isothermal low cycle fatigue) were performed on both materials. Monotonic test is used to determine the modulus of elasticity, yield strength, ultimate strength and the percentage of elongation of the materials. Cyclic stress-strain curves from cyclic tests are required to more accurately study material response under cyclic (fatigue) loading. Isothermal low cycle fatigue tests were performed to obtain materials strain amplitude-fatigue life curves of those materials based on the two materials at specific temperature.

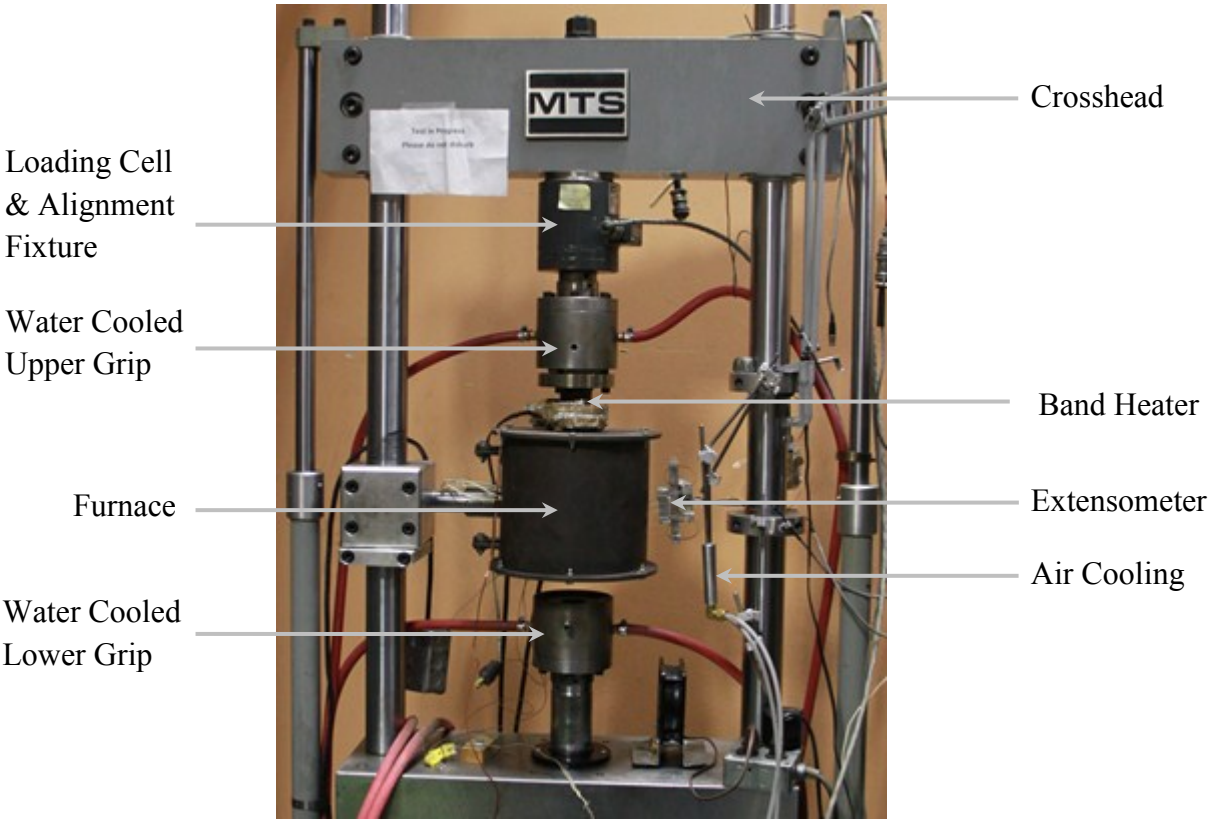

Figure 2.1: Thermal-mechanical material testing system during CTE measurement test.

2.2 Specimen Geometry

Cylindrical threaded specimens were designed and manufactured according to ASTM E8 standard [15] to carry out all the tests. There were in total 84 specimens prepared and tested. The dimensions of the cyclic and monotonic test specimens are shown in Figs. 2.2 and 2.3. As seen in Figs. 2.2 and 2.3, the gage length of the cyclic test specimen is shorter than monotonic test specimen to reduce the effect of buckling on the specimen during the cyclic test. Cyclic test specimens were also used to perform low cycle fatigue tests and CTE measurement tests.

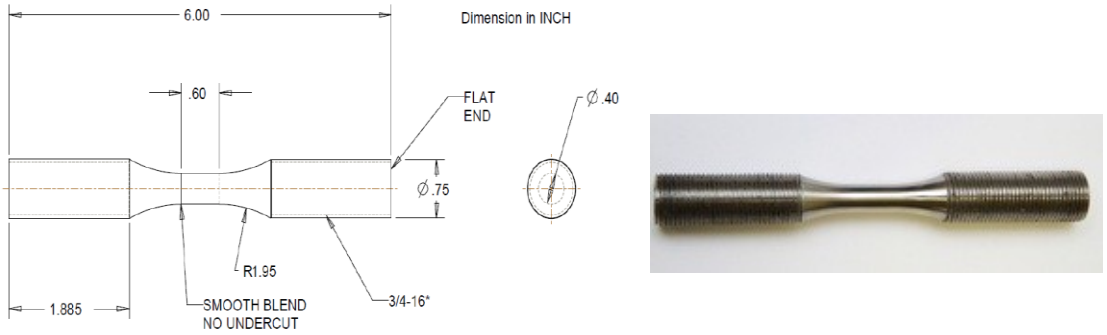

Figure 2.2: Cyclic test specimen [3].

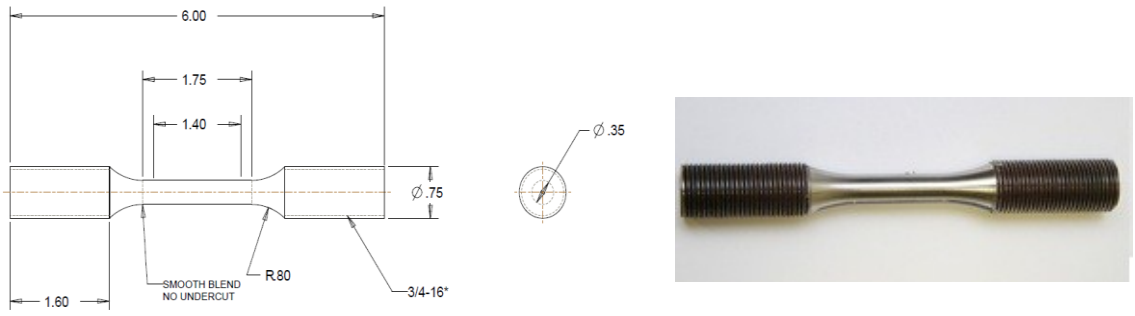

Figure 2.3: Monotonic test specimen [3].

2.3 Mechanical Properties

Monotonic stress-strain properties are reported in ASME database. In monotonic test, an increasing load is applied to the specimen until it fractures to obtain yield strength, modulus of elasticity and other properties. But in cyclic loading application, it is important to use the mechanical properties of cyclic stress-strain curve and the reasons behind it will be discussed later in this section. Under the guidance of ASTM standard E8 and E21 [15, 16], tension testing of the coke drum materials were performed at various temperatures.

2.3.1 Monotonic Test

Before beginning the monotonic test, a pair of dimples is punched on the specimen within the gage length at 1 inch distance to securely position the tips of the extensometer as shown in Fig. 2.4 (a). The arm of this modified MTS extensometer is made of quartz, which is stiff and capable to survive at very high temperature. The gripping fixtures are installed on the specimen, which primarily consists of two grips, two bolts and two grip adapters. A k-type thermocouple is carefully spot welded on the specimen to control the temperature of the specimen, which is recommended by ASTM E2368 [18]. Then the specimen with the gripping fixtures is mounted on the MTS testing system by connecting the upper and lower water cooled grip.

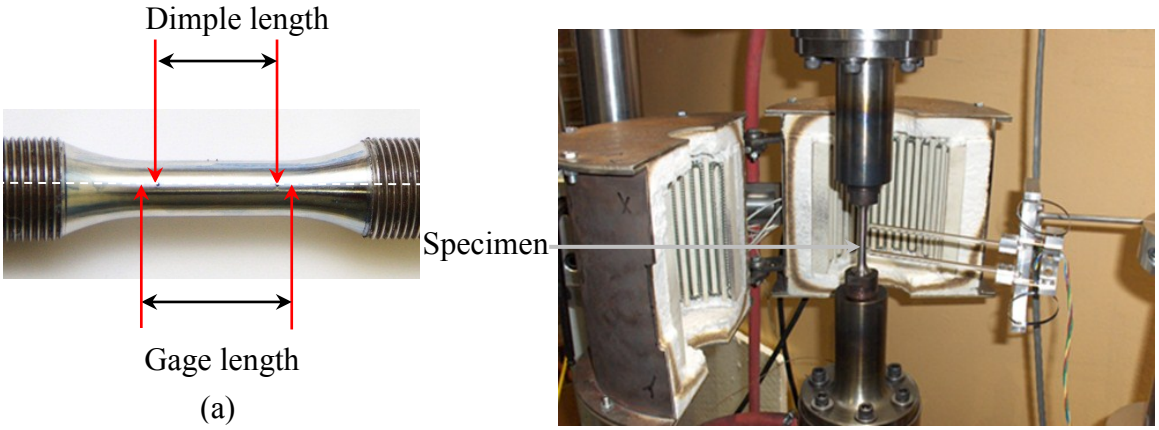

Figure 2.4: Picture of (a) a montonic test specimen; (b) experimental set-up.

Figure 2.4(b) shows the experimental set-up of a monotonic test at room temperature. At elevated temperature, a band heater is also attached at the bottom grips. The position of the band heater and the flow rate of the water can be adjusted to minimize the thermal gradient along the axial directions of the specimens' gage length. The temperature inside

the furnace can be controlled to set any desired value from ambient temperature to 500^{o} C. When the temperature of specimen reaches to a stable condition, strain is adjusted to zero by the control system to record only the mechanical strain (ε_{mecha}) of the specimen. Finally an increasing load is applied on the specimen until the failure of the specimen. The test data of load and strain are recorded by the data acquisition system.

Adjusted to zero

$$\varepsilon_{total} = \varepsilon_{mecha} + \varepsilon_{thermal}$$

$$\varepsilon_{total} = \varepsilon_{mecha}$$

where, ε_{total} and $\varepsilon_{thermal}$ are the total and thermal strain of the specimen respectively.

The mechanical properties of these materials were determined by the analysis of the obtained monotonic stress-strain curve as shown in Fig. 2.5. Due to the limitation of the extensometer of the machine, it was disengaged from the specimen after 10% of strain, while loads were recorded until the fracture of the specimen. For this reason, monotonic stress- strain curve was plotted up to 10% strain of the specimen. Modulus of elasticity (*E*) is obtained by the slope of the stress-strain curve within the proportional limit region. A straight dashed line is drawn parallel to the initial linear portion of the stress-strain curve. Then the yield strength is obtained from the point of intersection between the created straight dashed line and the stress-strain curve. Yield strength is the limit beyond which the material will not return to its original shape when the load is removed. Ultimate strength is the maximum stress in a stress-strain curve. To obtain the ultimate tensile strength, the variation of stress with time during a monotonic test was plotted as

shown in Fig. 2.6. The maximum peak value of the stress-time curve is the ultimate tensile strength.

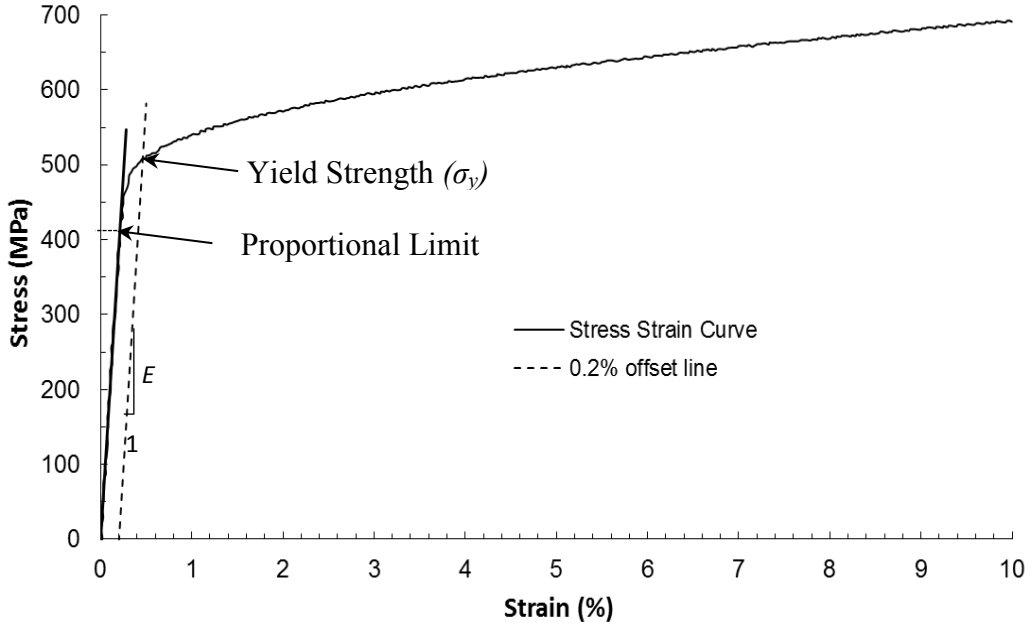

Figure 2.5: Monotonic stress-strain curve of N06625 at 100^{o} C.

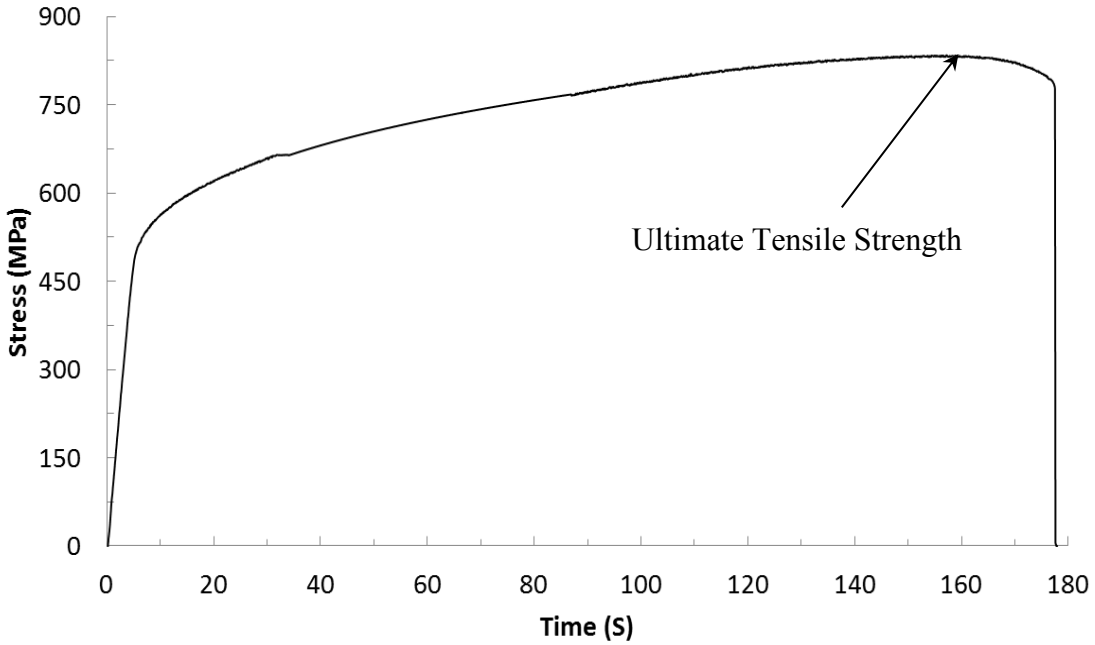

Figure 2.6: The variation of stress with time of N06625 at 100^{o} C.

Mechanical Properties of N06625 and SA302 Gr. B obtained from the monotonic stress-strain curve and their comparisons with ASME data [12] are listed in Table 2.2 and 2.3 respectively.

Table 2.2: Mechanical Properties of N06625 at various temperatures.

Materials	N06625 SB 443							
Temperatures	RT		100°C		250°C		480°C	
Data	*Test*	*ASME*	*Test*	*ASME*	*Test*	*ASME*	*Test*	*ASME*
Young's Modulus (GPa) - *E*	207.1	*207*	196.6	*202*	195.6	*194*	178.5	*180*
Yield Strength (MPa) – $\sigma_{0.2\%}$	548.7	*379*	506.1	*364*	448.4	*336*	425.4	*306*
Tensile Strength (MPa) - σ_{UTS}	876.0	*758*	833.2	*758*	786.4	*730*	750.7	*672*
Percentage Elongation-%	50.1	-	48.8	-	49.3	-	50.5	-

Table 2.3: Mechanical Properties of SA302B at various temperatures.

Materials	SA302 Gr. B							
Temperatures	RT		100°C		250°C		480°C	
Data	*Test*	*ASME*	*Test*	*ASME*	*Test*	*ASME*	*Test*	*ASME*
Young's Modulus (GPa) – *E*	202.1	*200*	198.2	*196*	193.2	*187*	172.5	*153.2*
Yield Strength (MPa) – $\sigma_{0.2\%}$	398.3	*345*	392.8	*323*	365.6	*299*	290.7	*238*
Tensile Strength (MPa) – σ_{UTS}	578.3	*552*	545.6	*552*	538.9	*552*	503.1	*496*
Percentage Elongation–%	43.5	-	38	-	35.3	-	36.4	-

From the above Tables 2.2 and 2.3, it can be seen that Young's modulus of both materials is consistent with the ASME data at four different temperatures. Yield strength of these materials is always greater than ASME data. For example, the minimum difference of yield strength between Test and ASME data for N06625 is around 33%, while for SA302B it is around 22%. Ultimate tensile strength (UTS) of N06625 is always greater than ASME data, while UTS of SA302B is greater than ASME data only at room temperature and 480^{o}C. Though ultimate tensile strengths of SA302B have lower value than ASME data at 100°C and 250°C, those values are still close to ASME data with a maximum difference of only 2.4%. Hence, it can be concluded that the mechanical properties of both materials satisfy the minimum requirement of section II of the ASME Boiler and Pressure Vessel Code [12]. High temperature results in lower mechanical properties of the materials as shown in Fig. 2.7, which is obvious for metals. Additionally, N06625 retains its excellent ductility since the percentage of elongation is slightly higher compared to the elongation of SA302B.

The mechanical properties of the optional material combinations N06625/ SA302B are compared with the currently used coke drum materials TP410S/SA387-22-2 as given in Tables 2.4 and 2.5. These comparisons are presented at temperatures of 100°C and 480°C. Stiffness and Strength (Yield and Ultimate Tensile) of SA387 Gr 22 CL 2 are higher than SA302B at both temperatures of 100°C and 480°C. As seen in Table 2.4, stiffness and strength (yield and ultimate tensile) of N06625 are much higher than TP410S at both 100°C and 480°C.

Though the base layer of the currently used coke drum possesses higher strength, because of the matching CTEs of the optional material combinations that results significant drop of the stress level in both clad and base layers, SA302B is still a better option as a base material that will be discussed thoroughly in chapter 3 and 4.

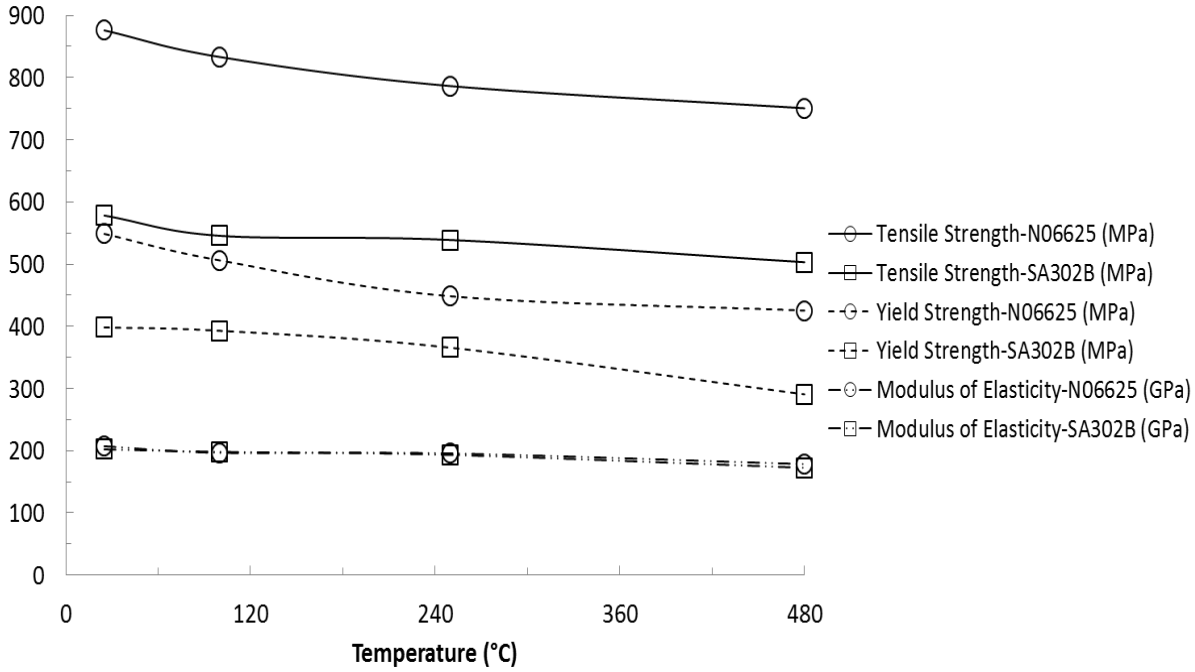

Figure 2.7: The variation of mechanical properties with the temperature.

Table 2.4: Comparison of the test results of the mechanical properties of the clad materials.

Materials	N06625		SA 240 TP410S	
Temperatures	100°C	480°C	100°C	480°C
Young's Modulus (GPa) – E	196.6	178.5	187.5	146.3
Yield Strength (MPa) – $\sigma_{0.2\%}$	506.1	425.4	244.3	164.4
Tensile Strength (MPa) – σ_{UTS}	833.2	750.7	394.5	275.6

Table 2.5: Comparison of the test results of the mechanical properties of the base materials.

Materials	SA302B		SA387 Gr 22 CL 2	
Temperatures	100°C	480°C	100°C	480°C
Young's Modulus (GPa) – E	198.2	172.5	202.7	157.6
Yield Strength (MPa) – $\sigma_{0.2\%}$	392.8	290.7	484.7	405.8
Tensile Strength (MPa) – σ_{UTS}	545.6	503.1	605.9	505.6

Jie et al [3] confirmed that mechanical properties of both base and clad materials are strain-rate insensitive after comparing the monotonic stress-strain curves at different strain rates of those materials at room and elevated temperatures. Hence, the effect of strain rate on the test results was neglected.

2.3.2 Cyclic Test

During cyclic tests, a pair of dimples is punched on the specimen within the gage length at 0.5 inch distance as shown in Fig. 2.8. The installation procedure of the specimen on the MTS testing system is same as the monotonic test [3]. Thermally induced strain is also adjusted to zero for this type of tests. Though the stroke control is maintained throughout the monotonic tests, the controlled parameter for cyclic tests is strain.

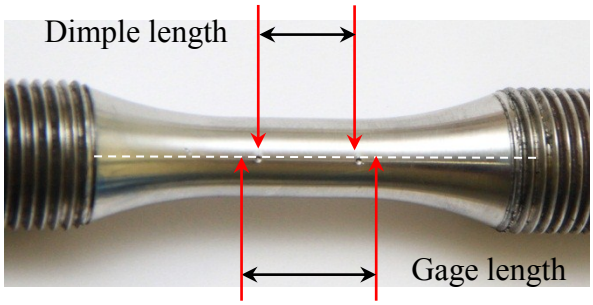

Figure 2.8: Cyclic test specimen with a pair of dimples.

Multiple step uniaxial cyclic test method was used to perform these cyclic tests. At the beginning, a fully reversed cyclic loading with lower constant strain amplitude is applied to the specimen until the cyclic stress-strain response (stress-strain hysteresis loop) becomes stable (if the maximum tensile stresses of the hysteresis loops fluctuate within ±2MPa) as shown in Fig. 2.9(b). Then the strain amplitude is increased to the next level as shown in Fig. 2.9(a). The period of the loading curve is kept constant with a value of 4 sec/cycle throughout the cyclic tests. This process is continued until sufficient number of stable hysteresis loops is obtained to draw a complete cyclic stress-strain curve.

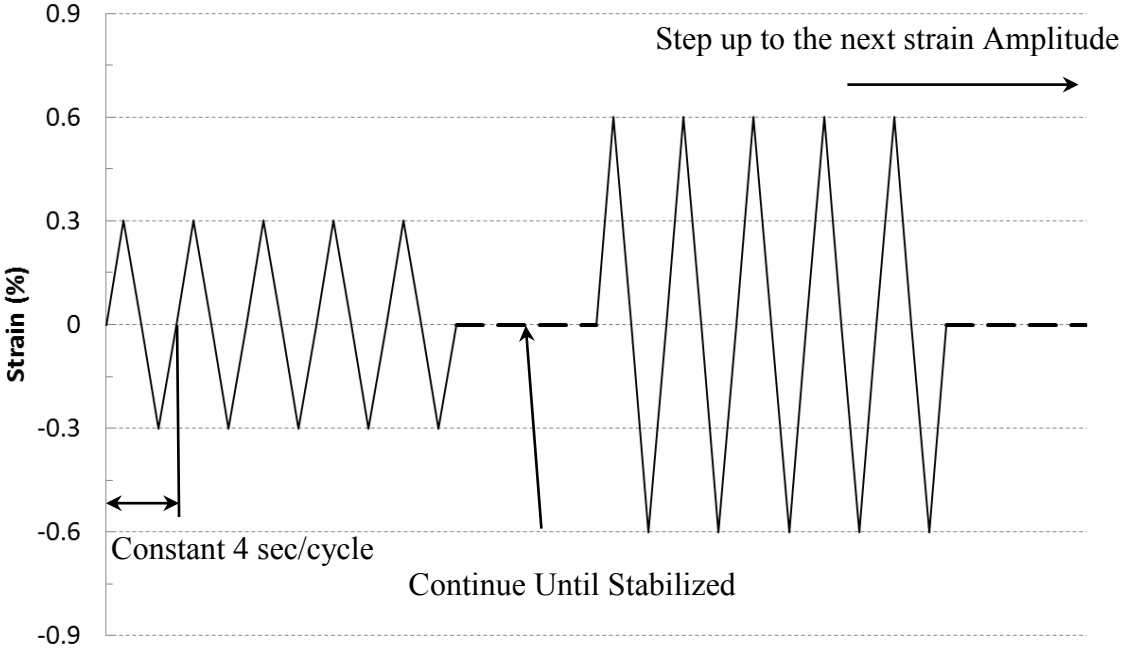

Figure 2.9 (a): Cyclic load.

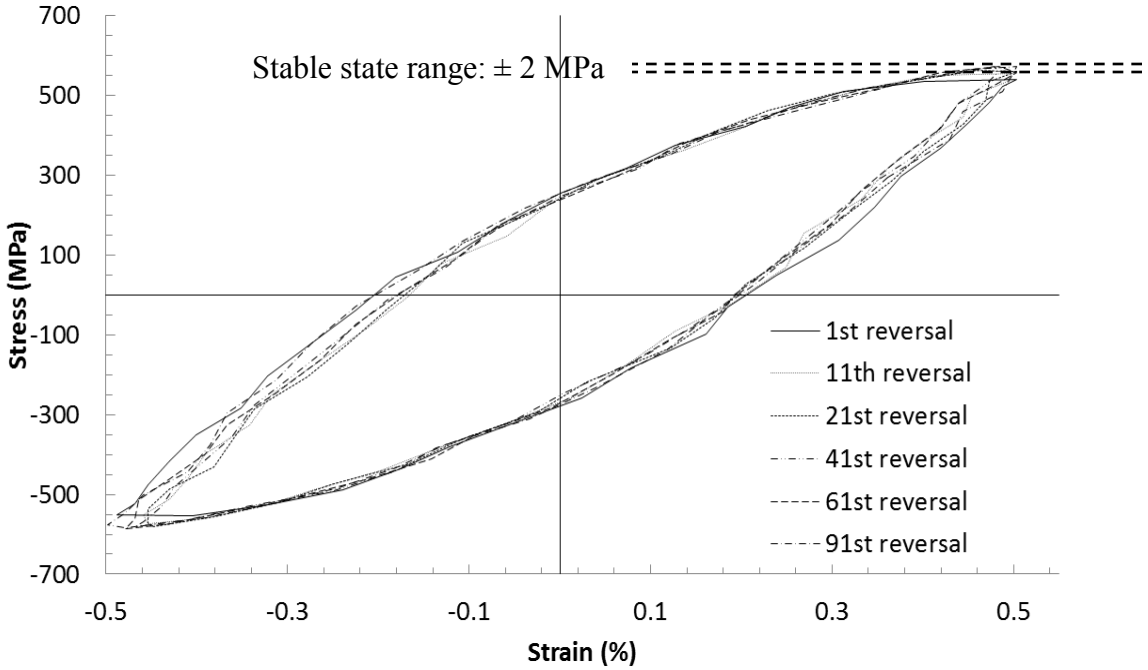

Figure 2.9 (b): Stress-strain behavior of N06625 subjected to cyclic load.

Cyclic stress-strain curve of a material is obtained by a family of stabilized hysteresis loops at different strain amplitudes. Figure 2.10 shows an isothermal cyclic stress-strain curve of N06625 at temperature 250^{o} C drawn by connecting the tips of the family of multiple loops.

The data obtained from the family of the hysteresis loops were fitted with the following relationship to acquire a smooth cyclic stress (σ) –strain (ε) curve.

$$\varepsilon = \frac{\sigma}{E} + \left(\frac{\sigma}{K'}\right)^{\frac{1}{n}}$$

Where, K' and n depends on the material deformation properties.

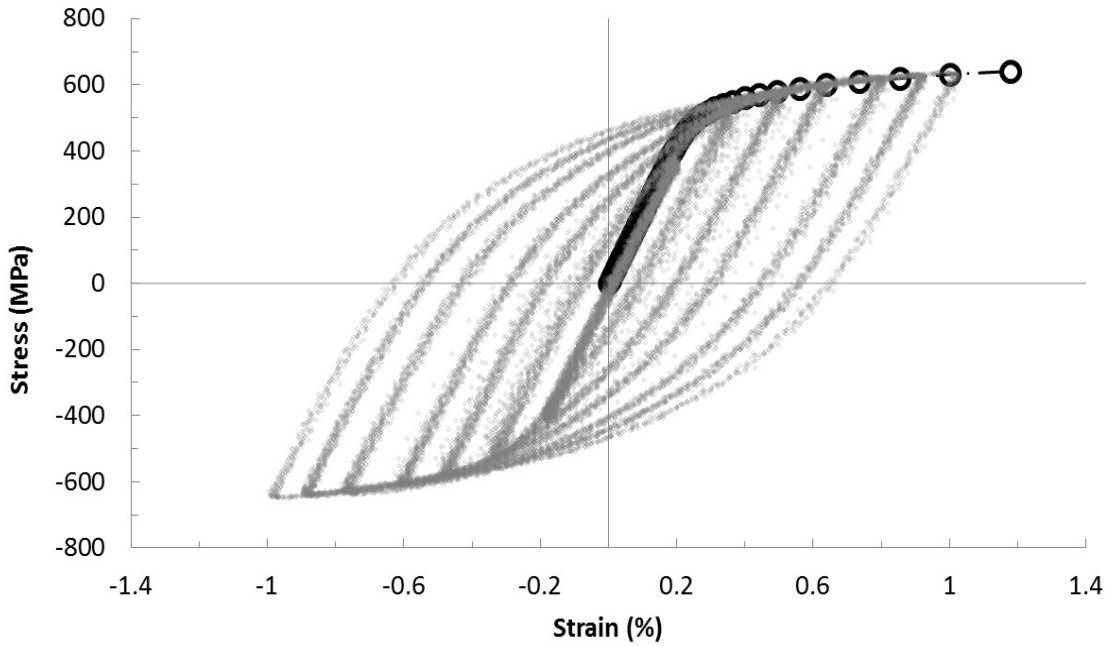

Figure 2.10: Cyclic stress-strain curve of N06625 at 250^{o} C.

Mechanical properties of the materials can be obtained by the cyclic stress-strain curves which are listed in chapter 4. But these mechanical properties may be different from the mechanical properties obtained from monotonic stress-strain curves. This is because after a single reversal of inelastic strain, the yield strength in tension and compression can be changed, which is known as Bauschinger effect. Since the coke drum is subjected to cyclic thermal and mechanical loadings, it is important to use the mechanical properties obtained from cyclic stress-strain curves in the finite element analysis in later chapters.

Total 16 specimens of N06625 and SA302B were prepared and tested for four different temperatures as shown in Table 2.6. Stepped fully reversed cyclic loading at a rate of 4 sec/cycle was applied during all the isothermal cyclic tests as discussed earlier. The

cyclic test results of TP410S and SA387-22-2 were obtained from Jie et al [17] who performed the cyclic tests on those materials.

Table 2.6: Number of specimens machined for cyclic testing of each coke drum material.

Temperature (^{o}C)	Number of Specimen
Ambient Temp.	2
100	2
250	2
480	2

The cyclic and monotonic stress-strain curves are generally compared to find the cyclically induced changes in mechanical properties of a material. A material may (a) cyclically soften, (b) cyclically harden, (c) stable or (d) show mixed behavior depending on the initial state of the material and test conditions [3]. A material may cyclically harden if the cyclic curve is above the monotonic curve, which means that material increases resistance to deformation. On the other hand, cyclical softening is present in a material if the cyclic curve is below the monotonic curve, which indicates that material decreases resistance to deformation. In cyclic loading application, using monotonic properties of a cyclically soften material may undervalue the problem. The cyclic and monotonic stress-strain curves of the base and clad materials will be compared at two temperatures of 100^{o}C and 480^{o}C, instead of comparing at all four temperatures, which are enough to show cyclic induced changes in mechanical properties of those materials.

The comparison of cyclic and monotonic stress-strain curves of N06625 are shown in Fig. 2.11. As seen in Fig. 2.11, cyclic curves at temperatures of 100°C and 480°C lie above the monotonic stress-strain curves after strains of 0.23% and 0.21% respectively. Therefore, N06625 mainly behaves cyclic hardening at both temperatures.

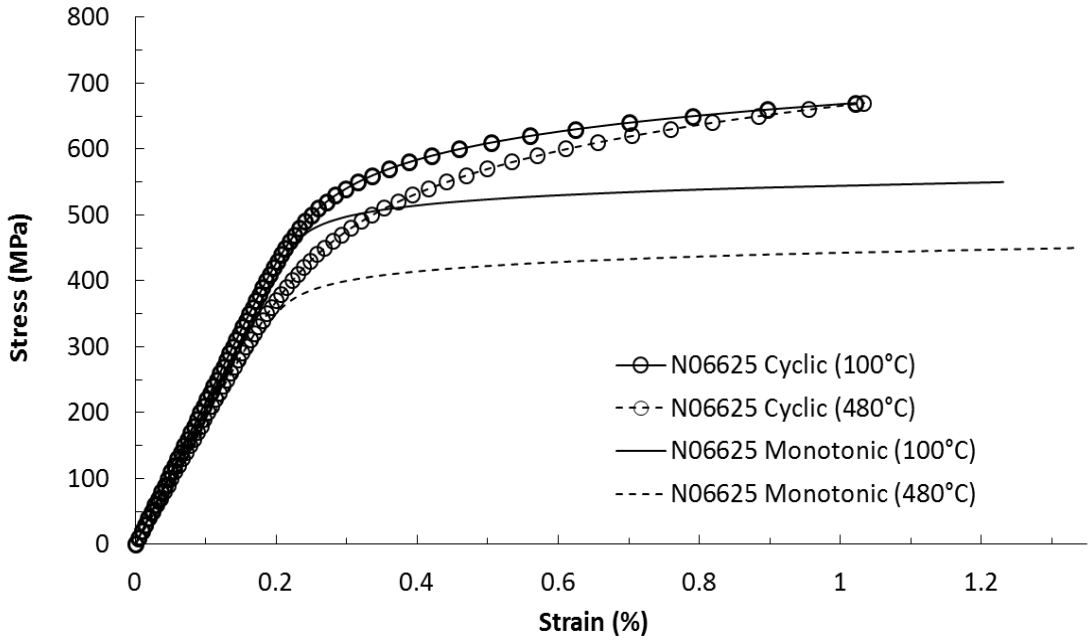

Figure 2.11: Monotonic and Cyclic stress-strain curves of N06625.

Figure 2.12 presents the comparison of monotonic and cyclic stress-strain curves of SA 302B. From Fig. 2.12, it is found that at temperatures of 100°C, the monotonic stress-stress curve is above the cyclic stress-strain curve between strains of 0.11% and 0.63% and the monotonic stress-strain curve is below the cyclic stress-strain curve after strain of 0.63%. That indicates that the base metal of the optional coke drum shows the mixed cyclic behavior at 100°C. But at 480°C, the cyclic stress-strain curve lies above the monotonic stress-strain curve after strain of 0.17%. Thus SA302B cyclically hardens at 480°C.

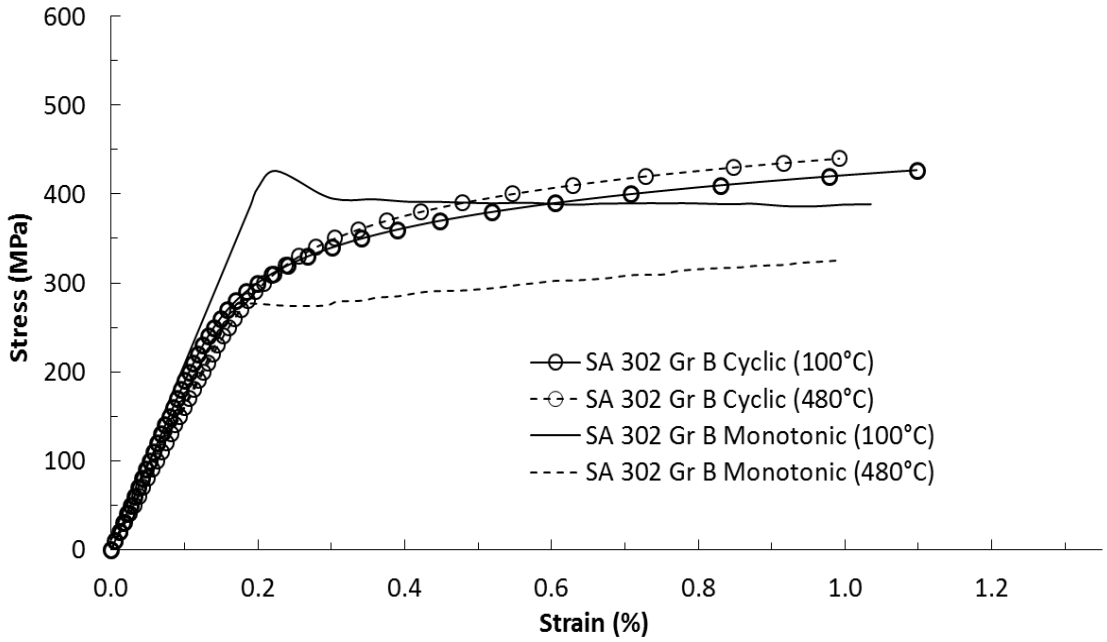

Figure 2.12: Monotonic and Cyclic stress-strain curve of SA302B.

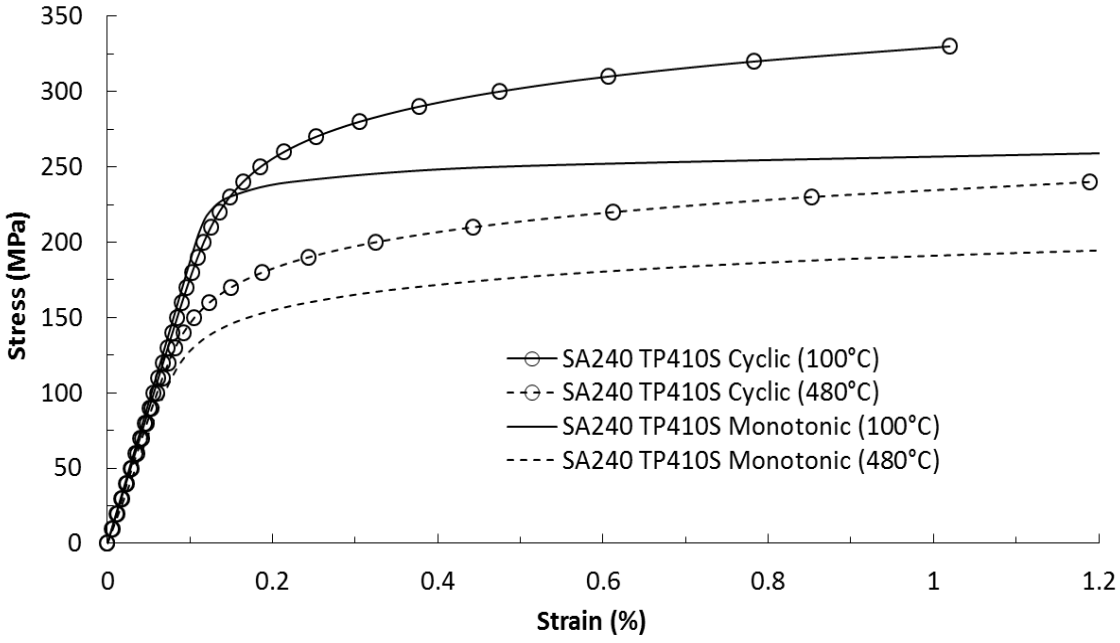

Figure 2.13: Monotonic and Cyclic stress-strain curves of TP410S.

The cyclic and monotonic stress-strain curves of TP410S are presented in Fig. 2.13. At both temperatures, cyclic stress-strain curves are above the monotonic stress-strain curves. Therefore, TP410S cyclically hardens at temperatures of 100°C and 480°C.

The cyclic and monotonic stress-strain curves of the base material (SA-387-22-2) of the currently used coke drum are demonstrated in Fig. 2.14. The monotonic stress-strain curve at both temperatures (100°C and 480°C) lies above the cyclic stress-strain curves after strains of 0.17% and 0.23% respectively. As a consequence, SA-387-22-2 demonstrates the behavior of cyclic softening at temperatures of 100°C and 480°C.

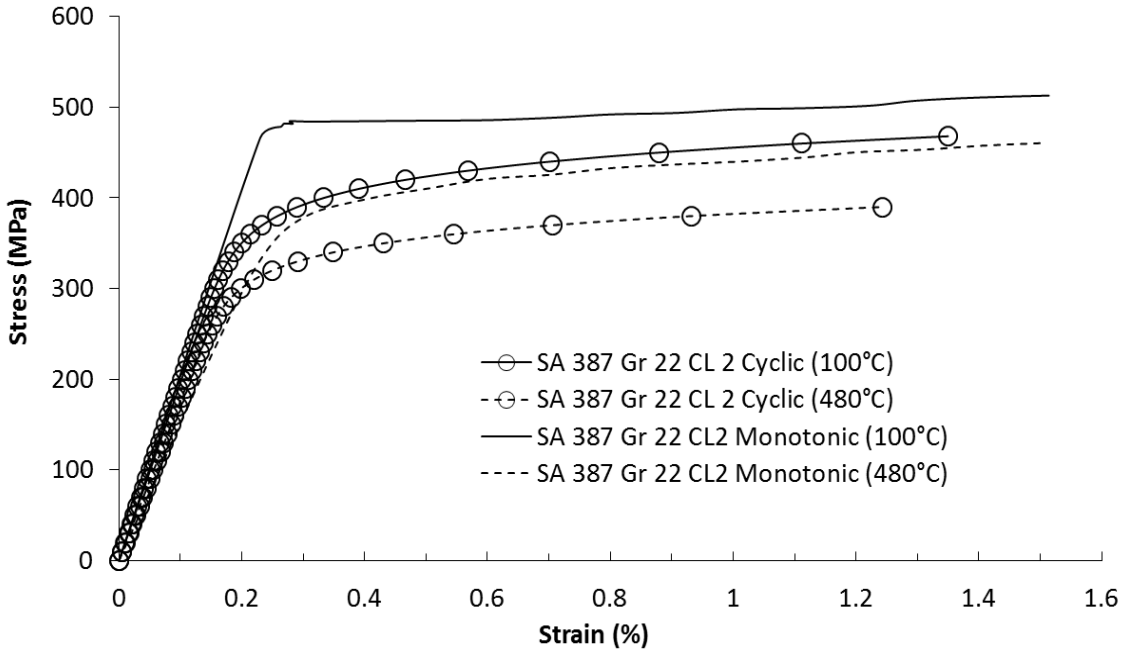

Figure 2.14: Monotonic and Cyclic stress-strain curves of SA387-22-2.

As seen in Fig. 2.14, cyclic softening lowers the monotonic yield strength of materials SA387-22-2. For this reason using monotonic material properties to model coke drum may cause error in prediction of the fatigue life of the coke drum materials.

2.4 Thermal Properties

Metals typically expand upon heating and contract when cooled. This response to temperature change is expressed as coefficient of thermal expansion (CTE). So the linear coefficient of thermal expansion can be defined as the fractional increase of length with the increase of temperature and it is a temperature dependent property [19]. During operations, coke drums have to go through severe thermal and mechanical loadings that cause stresses and strains in the drum shell. As explained earlier, the stress level in the clad layer of a coke drum can be reduced significantly by matching the coefficient of thermal expansion of both clad and base materials. That's why; test of measuring thermal expansion were conducted to determine the coefficient of thermal expansion of different coke drum's materials. There are several techniques available to measure thermal expansion such as mechanical dilatometry, optical imaging and x-ray diffraction method. Instead of using those methods, a method introduced by Xia at al. [17] had been used that requires MTS machine incorporated with a furnace, an extensometer etc. The validation of those experimental results is guaranteed by comparing with ASME data [12].

In this method, cyclic test specimens were utilized. The diameter of specimen within the gage length was reduced to 0.30 inch to obtain a uniform temperature along the axial direction of the specimen as shown in Fig. 2.15.

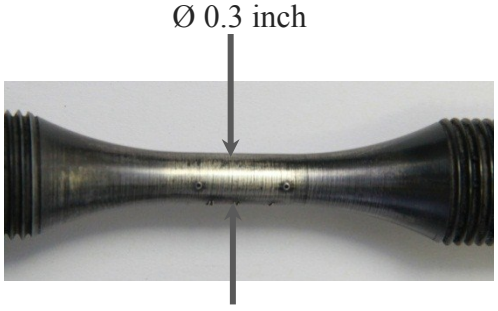

Figure 2.15: Specimen of CTE measurement test.

As seen in Fig. 2.16, three k-type thermocouples were spot welded on the specimen at three locations with a 0.25 inch space interval, while the extensometer was attached at two end locations (1 & 3). Then temperature inside the furnace was increased from arbitrary room temperature to 500^{o}C to carry out the CTE measurement test. The temperatures obtained from the middle thermocouples were always compared with the temperatures of thermocouples at other two locations (1 & 3) to maintain the uniformity of temperatures along the axial direction of the specimen.

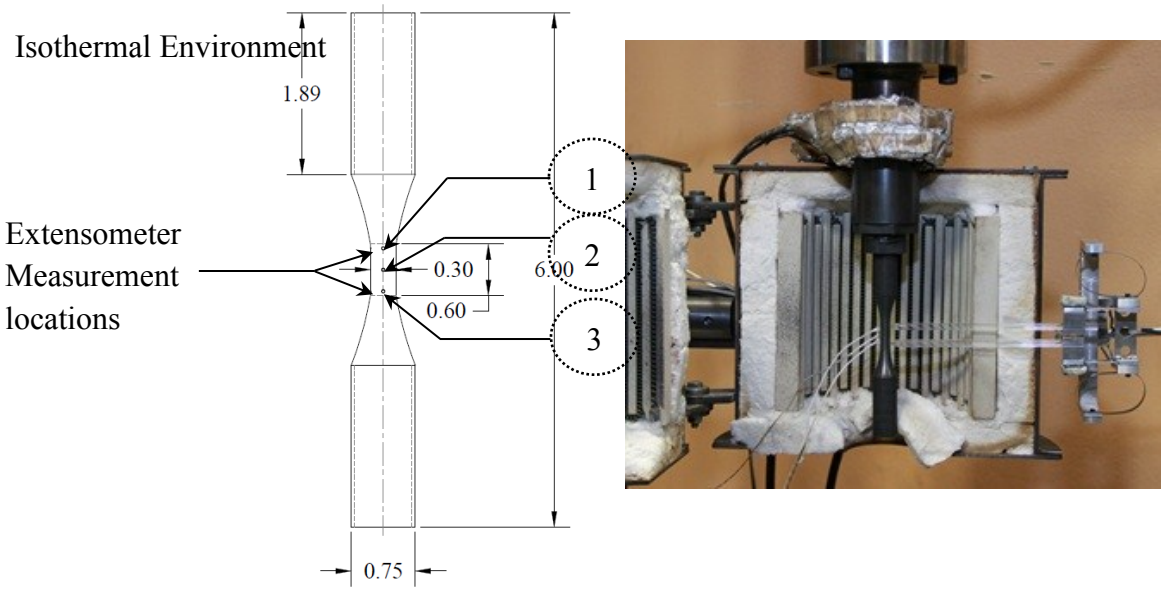

Figure 2.16: Experimental set-up of CTE measurement test.

The temperatures and strains were recorded and then plotted as shown in Fig. 2.17. The 4th order polynomial regression analysis was used to obtain a relationship between temperatures and strains (ε) of the material.

Finally, using the following equations, the coefficient of the thermal expansion (CTE) of the coke drum materials was determined at various temperatures.

$$CTE = \frac{d\varepsilon}{dT}$$

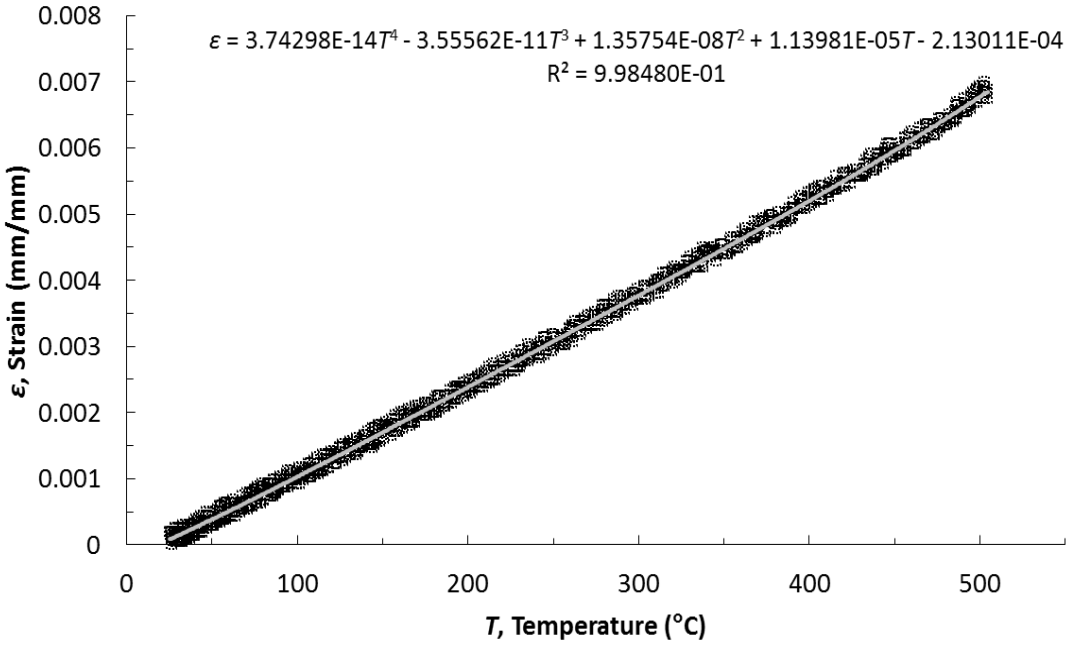

Figure 2.17: The variation of strain with temperature of N06625.

The test results and ASME data of CTE of N06625 and SA302B are shown in Fig. 2.18. ASME data are shown with solid line, while the test results are presented with dashed line. From Fig. 2.18, it is observed that the test results of the CTE of N06625 is very close to ASME data., while test results of the base material (SA302B) show a small difference with ASME data. The CTE of both materials are very close to each other without significant difference within any temperature range according to test results and ASME data.

Figure 2.19 presents the comparison between test data and ASME data of the CTEs of the currently used coke drum materials TP410S and SA387-22-2. These two materials show a large difference in CTE according to test and ASME data.

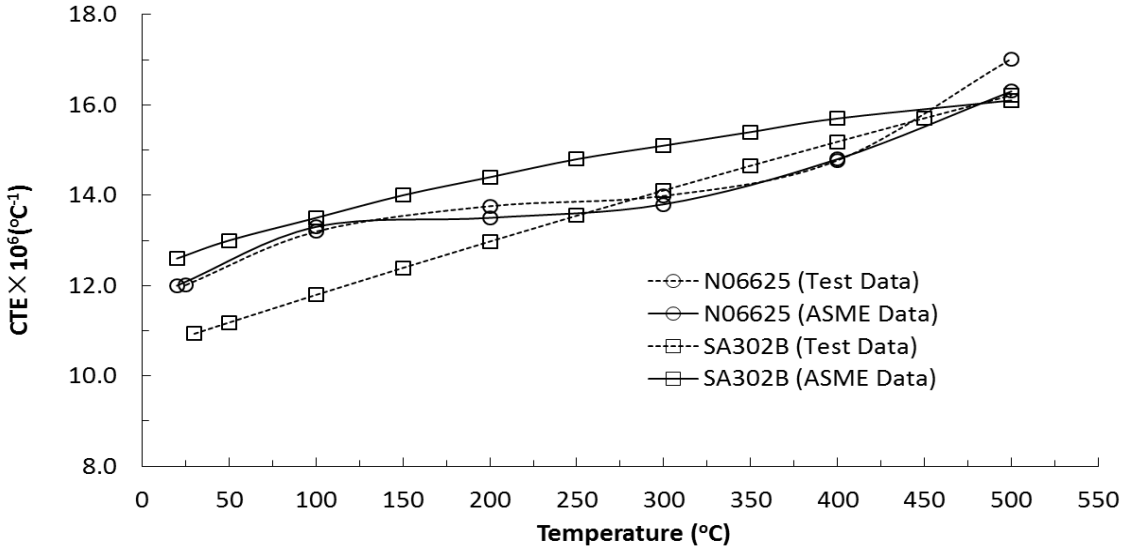

Figure 2.18: Comparison of the test results of CTE with ASME Data (N06625 and SA302B).

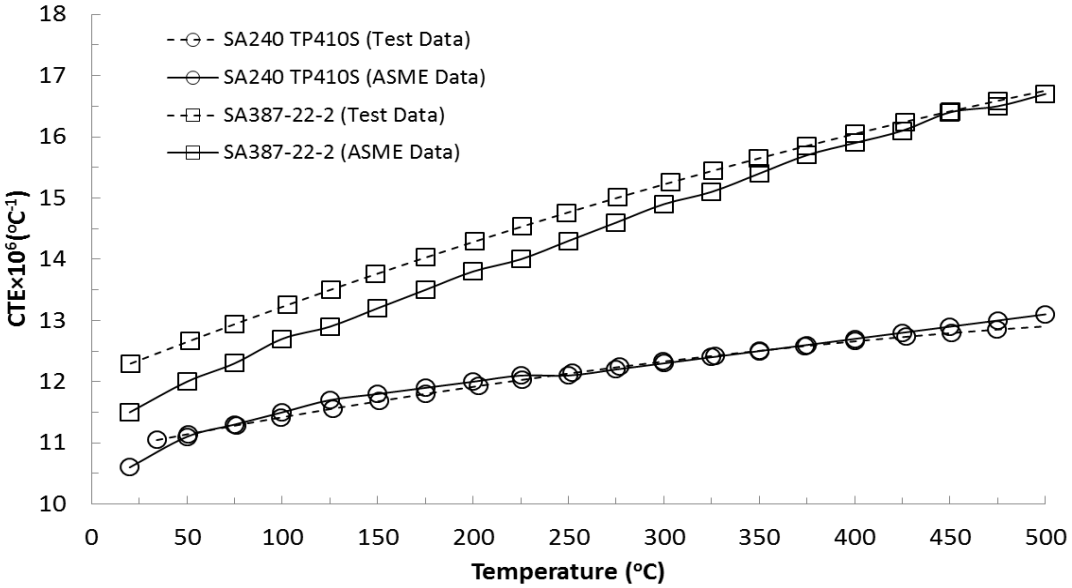

Figure 2.19: Comparison of the test results of CTE with ASME Data (TP410S and SA387-22-2).

2.5 Isothermal Low Cycle Fatigue

Coke drum experiences thermal-mechanical fatigue during operation. Jie et al [17] found that the life of the material according to thermal mechanical fatigue life is slightly higher than isothermal low cycle fatigue life. To model a coke drum based on isothermal low cycle fatigue life will be conservative to use in an application. Isothermal low cycle fatigue life will give a guidance to choose a suitable material that will remain in the operation for a long period of time.

Isothermal low cycle fatigue (ILCF) tests were carried out on the coke drum materials of N06625 and SA302B under four different strain amplitudes at temperature of 100^{o} C and 480^{o} C. The fatigue test specimens' geometry is same as the cyclic test specimen as shown in Fig. 2.2. Though the gage length of the specimen is 0.6 inch, for fatigue test, two dimples are punched at 1 inch distance outside the gage length of the specimen and used to set the extensometer as presented in Fig. 2.20.

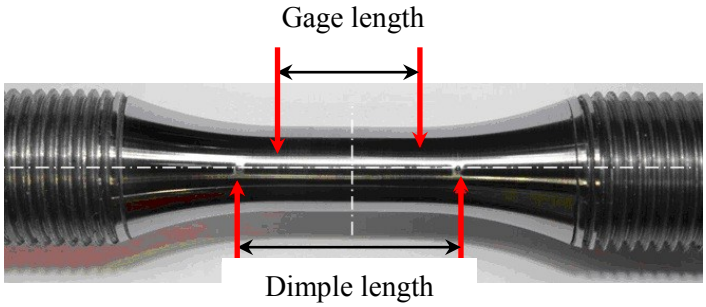

Figure 2.20: Isothermal fatigue tests specimen [17].

The procedure to install the specimen on the MTS testing system for fatigue tests is same as the cyclic tests. Then a fully reversed cyclic loading with the desired strain amplitude at a constant strain rate of 0.5%/sec is applied on the specimen until the failure of that

material as presented in Fig. 2.21. This isothermal low cycle fatigue tests were carried out according to ASTM E606 [20].

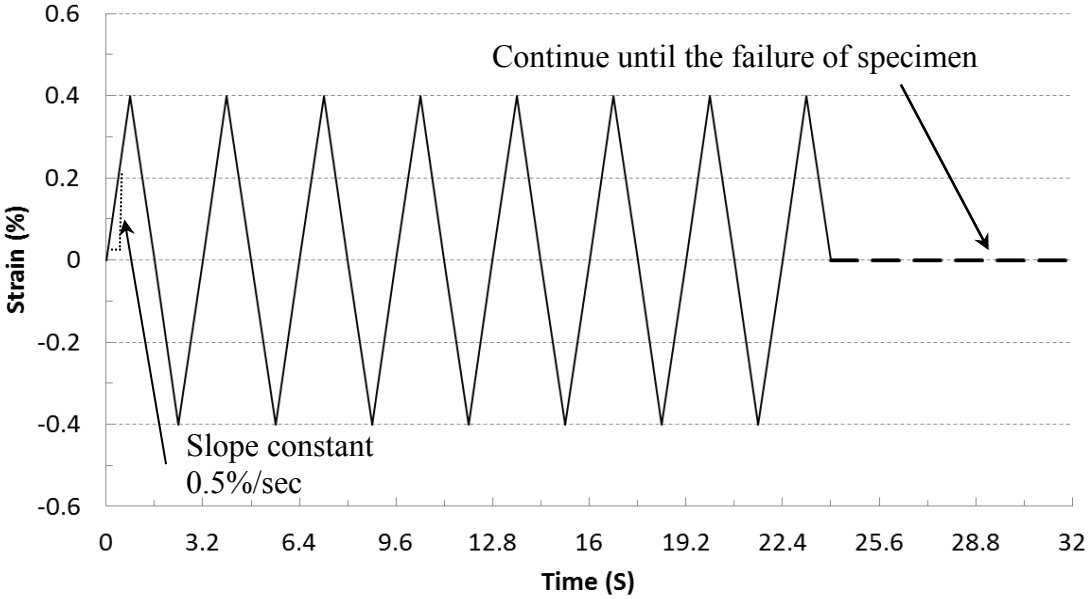

Figure 2.21: Fatigue Load.

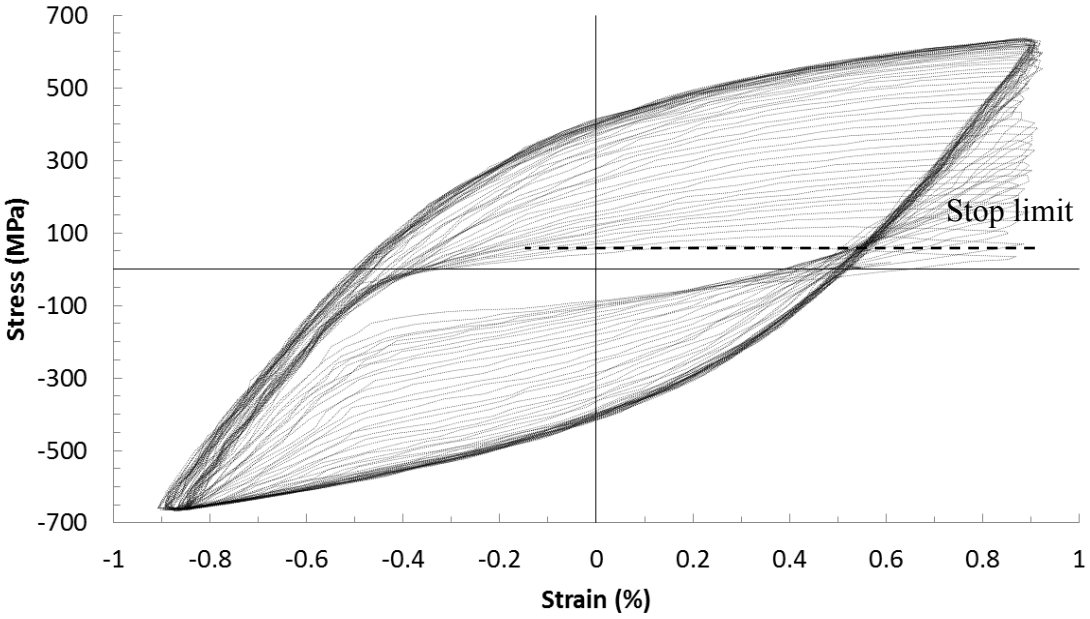

Figure 2.22: A family of hysteresis loops at the end of an ILCF test.

Figure 2.22 shows a family of hysteresis loops at the end of an isothermal low cycle fatigue test. When the tensile load amplitude of the specimen reaches to the stop limit (around 75 MPa), the experiment is ended for all fatigue tests. Therefore, failure criteria include life to decrease in load amplitude to 75 MPa.

In this fatigue test method, strain is measured between two dimples outside the gage length, where the cross-sectional area is larger compared to the cross-sectional area within the gage length. Jie et al introduced this alternative in-direct approach to prevent premature failure of the specimen initiated by dimples in gage sections [17]. According to this method, the increased cross-sectional area will help to avoid crack initiation on these dimples.

Jie et al [17] also developed a method to find out the direct strain correlation between gage section and dimple location using finite element analysis (FEA). This method was also verified by obtaining a strain correlation using analytical approach. Based on this method, an axisymmetric finite element model is created as shown in Fig. 2.23.

The boundary conditions considered for this FEA model are given as follows:

a. The top edge of the specimen grip is under plane-remain-plane condition and the load is also placed at this edge.
b. The bottom edge of the quarter of the specimen is constrained in Y-direction.

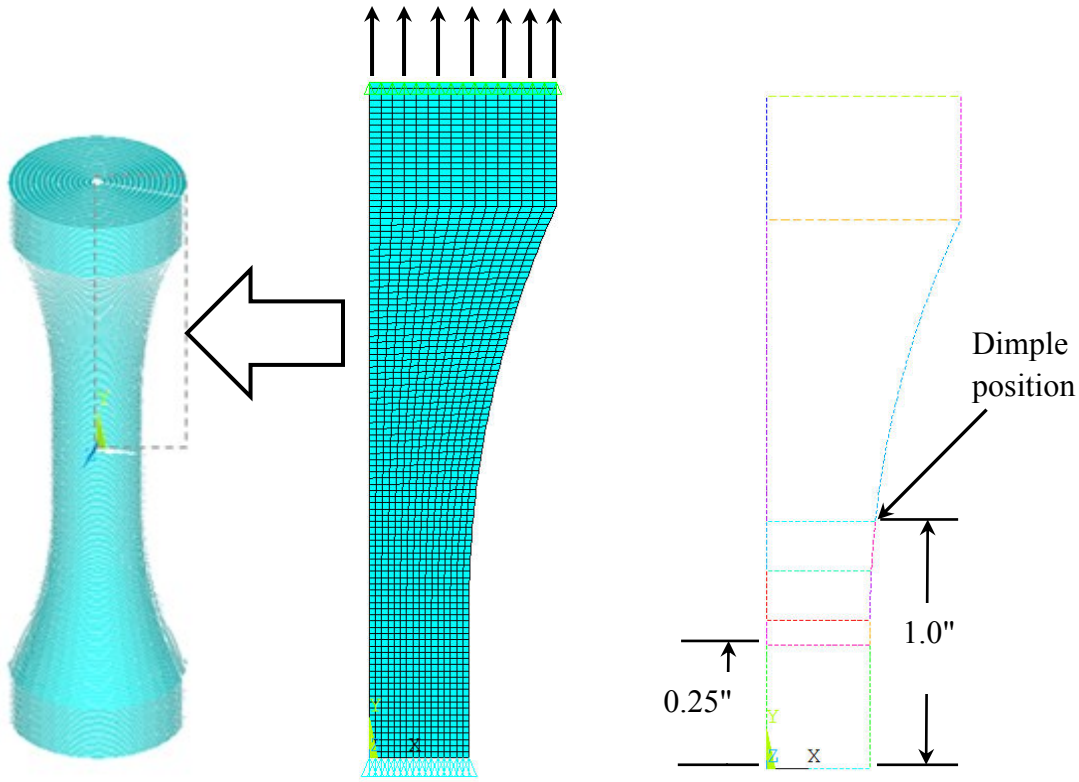

Figure 2.23: FE model and geometry of the quarter of a specimen [17].

The incremental displacements of gauge length (δ_{dimple}) and dimple length (δ_{length}) are found from the results of FEA. Then the engineering strains (ε) at these two locations can be found by [17]:

$$\varepsilon_{dimple} = \frac{\delta_{dimple}}{L_{dimple}} \text{ and } \varepsilon_{gage} = \frac{\delta_{gage}}{L_{gage}}$$

The corresponding correlation coefficient C_{in}, which is used to determine the strain in gage length, can be calculated using the following equation:

$$C_{in} = \frac{\varepsilon_{gage}}{\varepsilon_{dimple}}$$

Manson-coffin equation, a strain-based approach, was then utilized to find the relation between total strain ranges and fatigue life of the material. The Manson-coffin equation can be written in the following form [21, 22],

$$\frac{\Delta\varepsilon}{2} = \frac{\Delta\varepsilon^e}{2} + \frac{\Delta\varepsilon^p}{2} = \frac{\sigma_f'}{E}(2N_f)^b + \varepsilon_f'(2N_f)^c$$

where, $\Delta\varepsilon^e$ and $\Delta\varepsilon^p$ are the elastic and plastic ranges respectively, N_f is cycles to failure, σ_f' is the fatigue strength coefficient, ε_f' is the fatigue ductility coefficient and , b and c are the fatigue strength exponent and the fatigue ductility exponent respectively.

The total strain ranges is the summation of elastic and plastic strain ranges of the specimen. The elastic and plastic strain ranges can be determined from a "stabilized" hysteresis loop obtained from the isothermal fatigue test results as shown in Fig. 2.24.

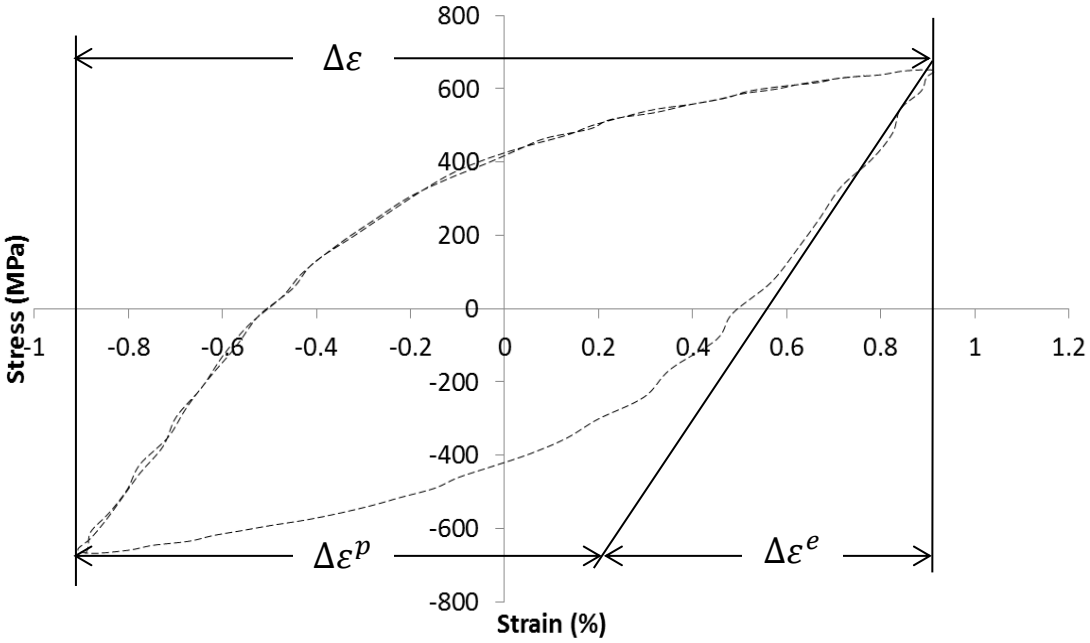

Figure 2.24: Hysteresis loop of N06625 during an isothermal fatigue test at ambient temperature.

The variation of elastic-, plastic-, and total-strain amplitude with the total number of reversals to failure for N06625 are shown in Fig. 2.25 and 2.26 at 100^o C and 480^o C respectively.

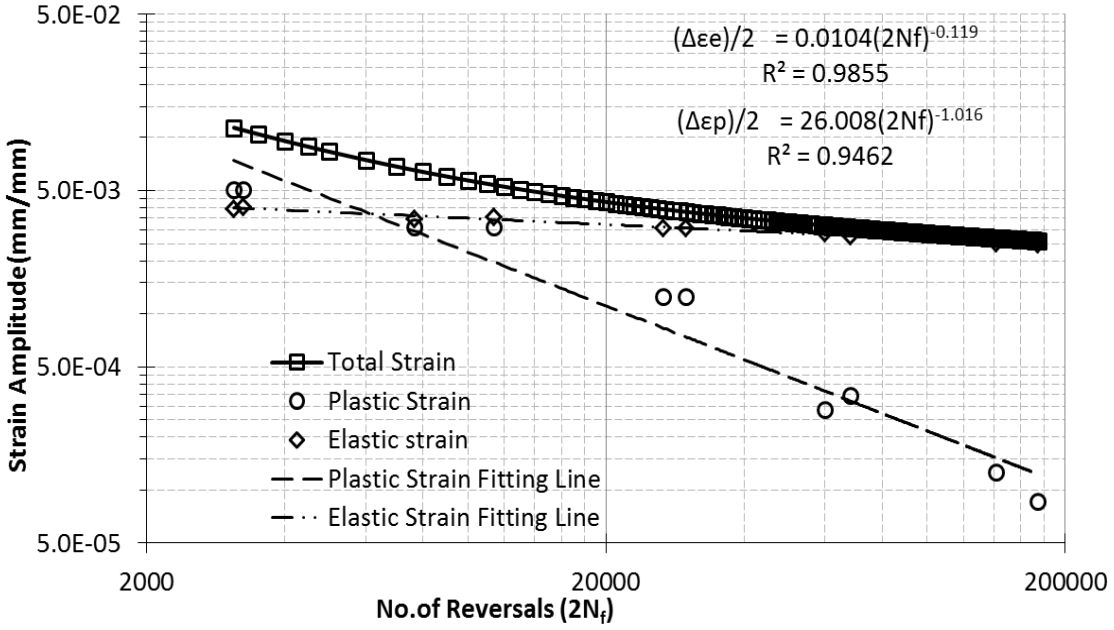

Figure 2.25: Low cycle fatigue Life of N06625 with the variation of strain amplitude at 100^{o} C.

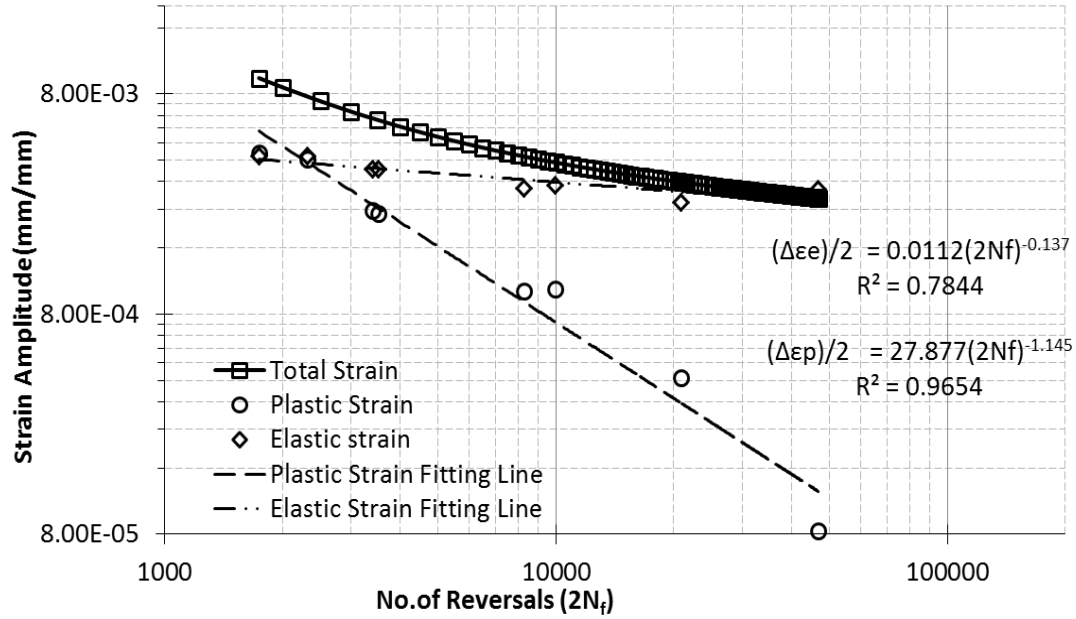

Figure 2.26: Low cycle fatigue Life of N06625 with the variation of strain amplitude at 480^{o} C.

Figure 2.27 and 2.28 represents the variation of strain amplitude with the number of reversal for material SA320B at 100^{o} C and 480^{o} C respectively.

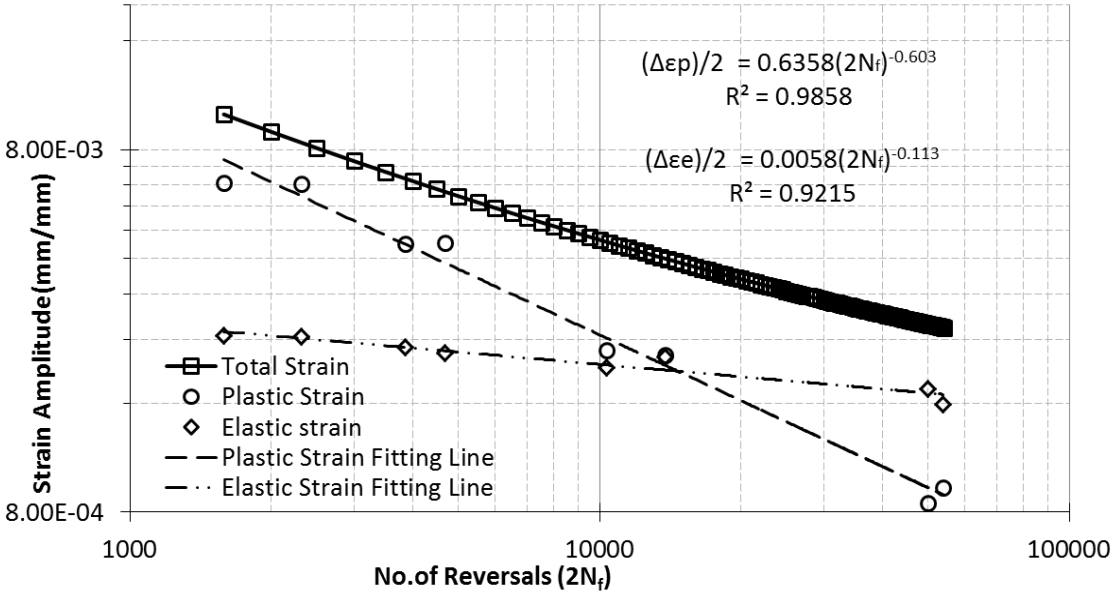

Figure 2.27: Low cycle fatigue Life of SA302B with the variation of strain amplitude at 100^{o} C.

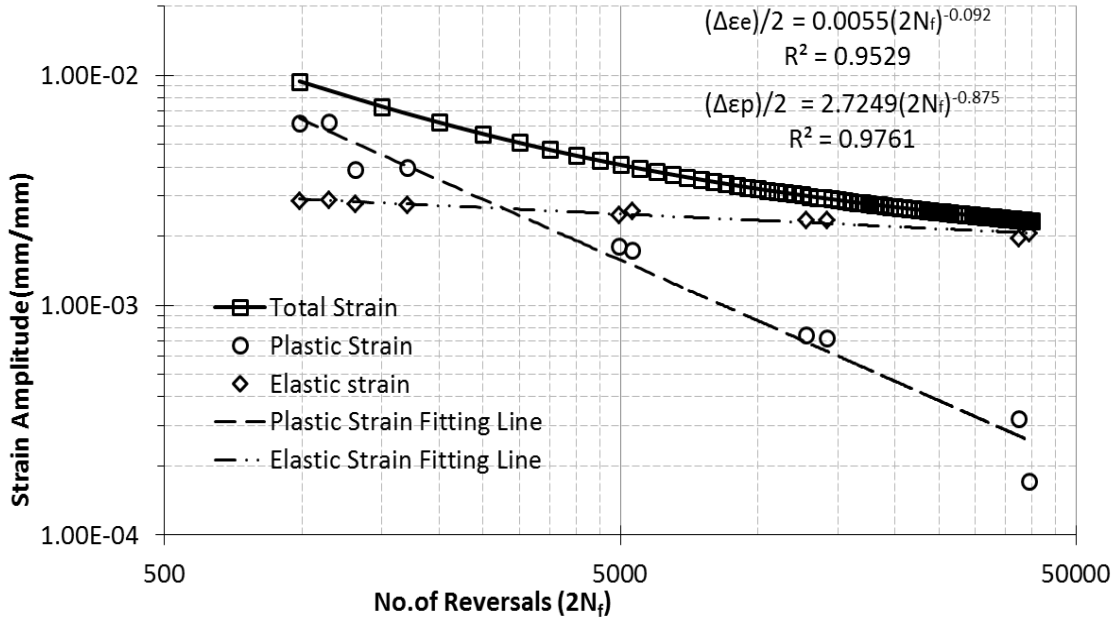

Figure 2.28: Low cycle fatigue Life of SA302B with the variation of strain amplitude at 480^{o} C.

It can be seen that higher temperature and strain results in lower fatigue life of both materials. Jie et al observed that ILCF life of N06625 is much higher than TP410S, while ILCF life of SA302B is comparable to the fatigue life of SA387-22-2 [17]. For example, as seen in Figs. 2.25 and 2.26, at 0.4% strain amplitude, N06625 survived around 40000 and 7000 number of cycles at 100^{o} C and 480^{o} C respectively, which indicates that N06625 has very high ILCF fatigue life to increase the performance of coke drum.

2.6 Summary

The mechanical and thermal properties of experimental results of the coke drum materials N06625 and SA302B satisfies the minimum requirement of ASME standard. High strength and outstanding isothermal fatigue strength are the properties of N06625. Coefficient of expansion of the optional material combinations is very close to each other, which makes these two materials as a good material combination for the coke drum. Both materials cyclically harden at the highest operating temperature of the coke drum. Though, SA302B shows the mix-behavior of softening and hardening at 100^{o} C, but N06625 cyclically hardens at the same temperature. N06625 has better ILCF fatigue life than TP410S based on strain amplitude of LCF analysis. Fatigue life of both material decreases noticeably with the increase of temperature and strain amplitude.

Chapter 3 Coupled Thermo-Elastic Analysis of the Coke Drum

3.1 Introduction

Coke drum in oil refineries are designed to perform delayed coking process and to upgrade heavy oil to gas product and petroleum coke. During delayed coking operation, it is subjected to not only the pressure of the operation but also the severe thermal loadings in the temperature range from arbitrary to 480^{o}C in each operational cycle including the processing stages of steam testing, vapor heating, oil filling , steam and water quenching and un-heading. Such cyclic thermal-mechanical loading causes high stress/strain in drum shell and eventually leads to the damage of the shell in the form of bulging and cracking.

The objective of this chapter is to analyze the stress/strain field in the shell of the coke drum during an entire operation cycle for two pairs of base and clad material combinations, one is base SA387-22-2 low alloy steel and clad SA240 TP410S stainless steel, which is currently used materials for the studied coke drum; another is base SA302B steel and clad N06625 super nickel alloy. The latter is considered as the optional material combination recommended by Nikic and Xia et al [10]. Finite element analysis codes ANSYS will be used to carry-out the coupled thermal-elastic analysis on the coke drum shell for an entire operation cycle. Coupled thermo-elastic analysis employs the sequential coupling method. Based on the thermal loads, it provides thermal results using

the heat transfer analysis. Then thermal results and structural boundary conditions are imposed on the structural model to get the final structural results. As will be seen later from the thermal-elastic stress analysis, the maximum stress for some materials will exceed their yield strength. It means that thermal-elasto-plastic analysis will give more practical results. However, the relative simple thermal-elastic analysis (ANSYS code provides the capacity of coupled thermal-elastic analysis but no coupled thermal-elasto-plastic analysis) could provide general features of the stress/strain distribution in the drum shell and give guidelines on the material selection, operating parameters, etc. In chapter 4, more accurate thermal-elasto-plastic analysis will be carried out by using temperature distribution history data from the current coupled thermal-elastic analysis.

3.2 Coke Drum Geometry

A typical coke drum is made with diameter of 7.92 m and height of the cylindrical part of coke drum is 20 m excluding drum head and skirt. Coke drum shell is fabricated with clad steel plate. The thickness of the base is 25.40 mm for courses 1-3, 22.225 mm for courses 4 and 5, and 19.05 mm for courses 6 and 7, respectively. The thickness of the clad is 2.54 mm. As shown in Fig. 3.1(a), the results of FE analysis from six different locations of the coke drum are examined.

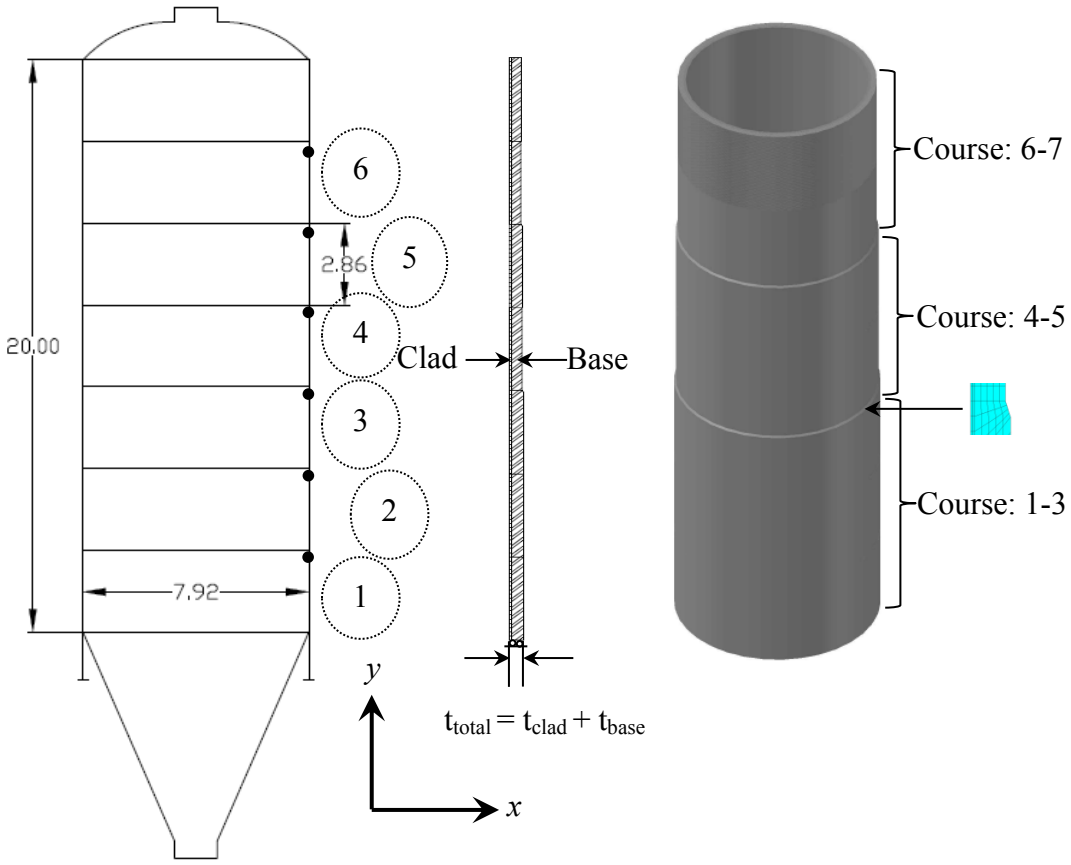

Figure 3.1: (a) Schematic view of full coke drum; (b) Axisymmetric model used in the FE analysis (thickness magnified); (c) 3D model of the cylindrical part of the coke drum;

3.3 Material Selection

Two pairs of base and clad materials are selected to pursue this finite element analysis. The common practice to select the materials for clad and base materials is SA240 TP410S and SA387-22-2 respectively. The clad N06625 and base SA302B recommended by Nikic and Xia et al. [10], has also been chosen mainly because of their matching coefficient of thermal expansions. The mechanical and thermal properties of materials TP410S and SA387-22-2 obtained from ASME are provided below.

Table 3.1: Physical and Thermal Properties of SA240 TP410S

Temperature (^oC)	Modulus of Elasticity E (GPa)	Density ρ (kg/m^3)	Poisson' ration v	Thermal Conductivity k (W/m. ^oC)	Thermal Expansion CTE ($1/^oC$)	Specific Heat c (J/kg.^oC)
20	201.4	7750	0.3	24.6	1.06×10^{-5}	445.81
100	195.0	7750	0.3	24.8	1.15×10^{-5}	478.33
200	189.0	7750	0.3	25.0	1.20×10^{-5}	515.30
300	182.0	7750	0.3	25.2	1.23×10^{-5}	562.56
400	173.0	7750	0.3	25.3	1.27×10^{-5}	617.11
500	157.0	7750	0.3	25.4	1.31×10^{-5}	677.15

Table 3.2: Physical and Thermal Properties of SA387-22-2

Temperature (^oC)	Modulus of Elasticity E (GPa)	Density ρ (kg/m^3)	Poisson' ration v	Thermal Conductivity k (W/m. ^oC)	Thermal Expansion CTE ($1/^oC$)	Specific Heat c (J/kg.^oC)
20	210.3	7750	0.3	36.30	1.15×10^{-5}	444.81
100	206.0	7750	0.3	36.90	1.27×10^{-5}	482.90
200	199.0	7750	0.3	37.20	1.38×10^{-5}	518.90
300	192.0	7750	0.3	36.70	1.49×10^{-5}	557.77
400	184.0	7750	0.3	35.40	1.59×10^{-5}	601.81
500	175.0	7750	0.3	33.70	1.67×10^{-5}	656.86

3.4 Thermo-Elastic Analysis of the Full Coke Drum

To reduce the complication in the FE model, skirt and head of the coke drum are removed from the model. Then the axisymmetric model is introduced to make the model much simpler. Since the coke drum is supported at skirt, the lower end is constrained by roller support that restricts the movement in vertical y-direction only. Plain remain plain conditions is considered at the top end because the head of the coke drum is free to move.

Weld zone in the coke drum are significantly prone to crack initiations. Since our main objectives in this study is to compare the two pairs of base and clad materials, the effect of weld is not considered in the current study. And perfect bonding between the clad and the base is also assumed. This model is developed using the same procedure developed by Xia et al [2].

All the loads and constrains as boundary conditions applied on the coke drum are discussed below:

1. The bottom of the coke drum is constrained on y-direction. This is because of that the coke drum is supported by skirt and details near the skirt area are not studied in the current thesis. This surface is also considered adiabatic that does not allow any heat transfer through this surface.
2. The movement of the top surface is allowed in y-direction under plain remain plain conditions as well as it is adiabatic. The axial pressure resulting from the internal pressure is also applied on the top surface in y-direction. Adiabatic boundary condition is also considered for the outer surface of the coke drum. In practice the outer surface is covered with insulation. Xia et al [2] found that the outer surface with adiabatic boundary conditions gave the similar thermal field as found from the model with insulator.
3. The boundary conditions at inner surface depend on different stages of a full operation cycle of the coke drum. The heat transfer coefficient, bulk temperature and pressure vary with the stages of the operation. And the boundary conditions depend on the height of the level and speed of the oil and water as shown in Figs

3.2 and 3.3. For this analysis, oil and water rising speeds of 3 mm/s is considered. The effect of the rising rate of water will be discussed later.

The values of the heat transfer coefficient, used in this analysis, are obtained from Xia et al [2]. They used inverse technique to obtain heat transfer coefficient values based on measured real coke drum temperature. The full boundary conditions imposed at inner surface during an 18-hour operation cycle are given below:

Table 3.3: Boundary conditions at inner surface of the coke drum during a complete operation cycle.

Stages	Boundary Conditions			
	Time (hr)	h (W/m^{2o}C)	T_b (^{o}C)	P (MPa)
Steam Testing	2	113.4	142	0.276
Vapor Heating	2	54.9	316	0.276
Oil Filling	10	141*	482*	0.276
Water Quenching	2	345*	93*	0.276 + P_w**
Un-heading	2	63.7	38	0.12

*Surfaces that are in direct contact with water and oil experiences these film coefficients and bulk temperatures.

**P_w is the pressure due to the weight of the water that varies with the height of the water.

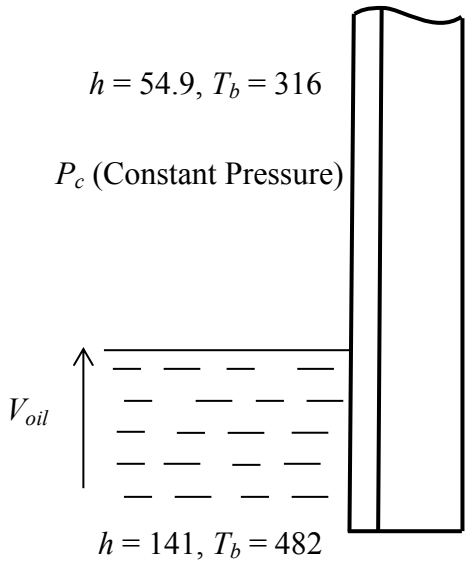

Figure 3.2: Oil Filling Stage

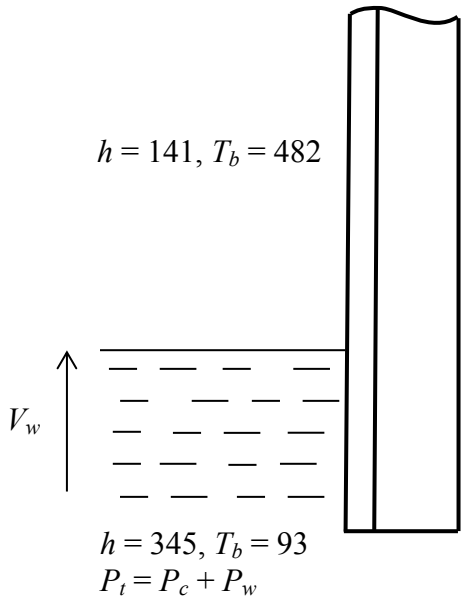

Figure 3.3: Water Quenching Stage

3.5 Verification of Mesh Dependency of the FE Model

To investigate the dependency of FE model on the mesh density, different mesh density (N) of 150 and 300 per one course are considered. Along the thickness of the clad and base, the number of division is constant as shown in Fig. 3.4.

That makes the total no. of nodes in two different models are 9459 and 18909 respectively. Plane 13 elements were chosen to carry out this analysis. Plane 13 is a 2D-coupled field solid element defined by four nodes with four degree of freedoms (DOF) per node. The four DOFs are: displacements in x and y direction (UX & UY), temperature and magnetic vector potential (AZ). That means the total degree of freedom (TDOF) is four times of the corresponding no. of nodes in each model.

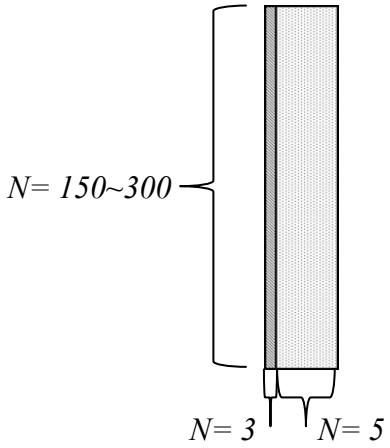

Figure 3.4: Single Course of a coke Drum

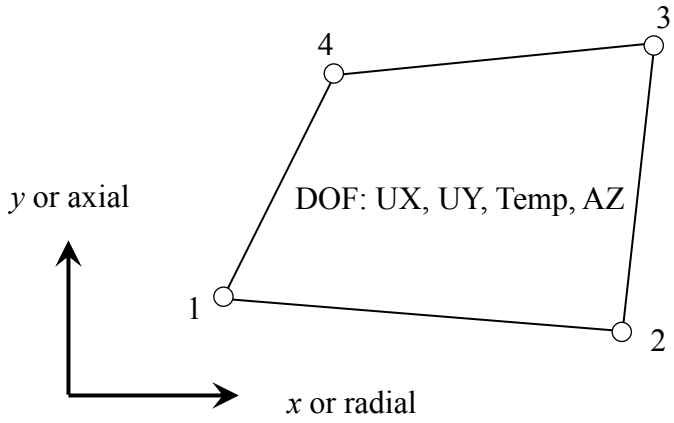

Figure 3.5: Plane 13 element.

The results from the two meshes are compared. The maximum difference of the maximum stress/strain components are within 3%. As an example, von Mises stresses over a complete operation cycle of the two models are compared at both inner and outer surface of the coke drum as shown in Figs. 3.6 and 3.7. Therefore, the first mesh will be adopted in the future analysis to save cost and time.

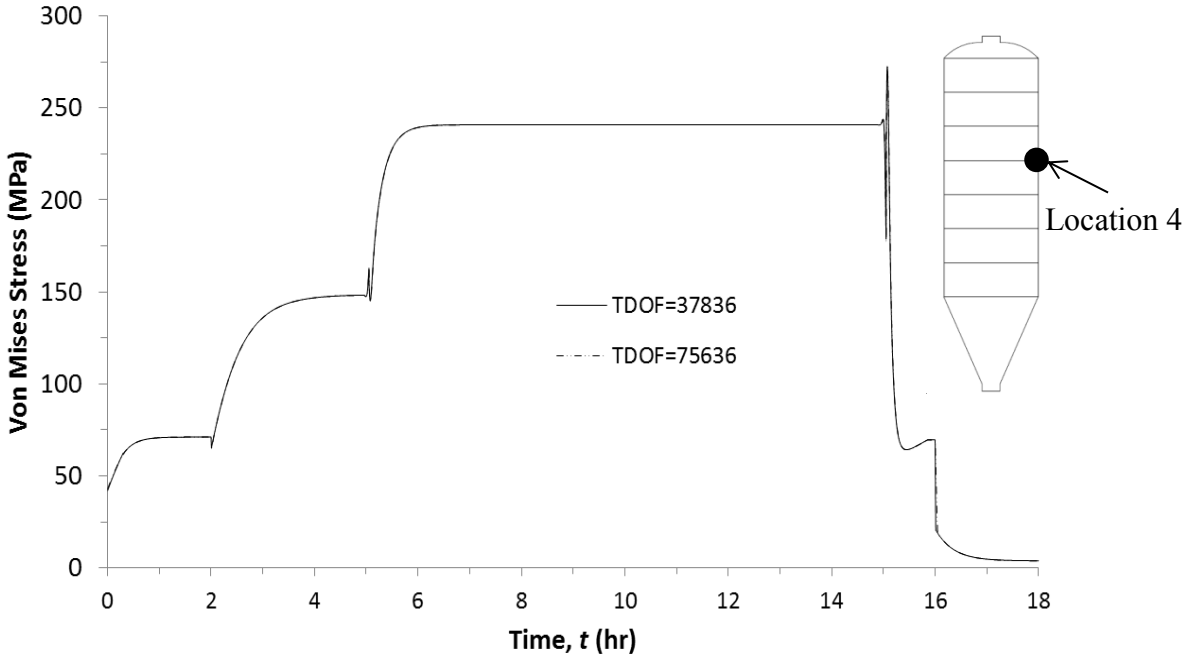

Figure 3.6: Von Mises stress at inner surface of the coke drum in the process cycle.

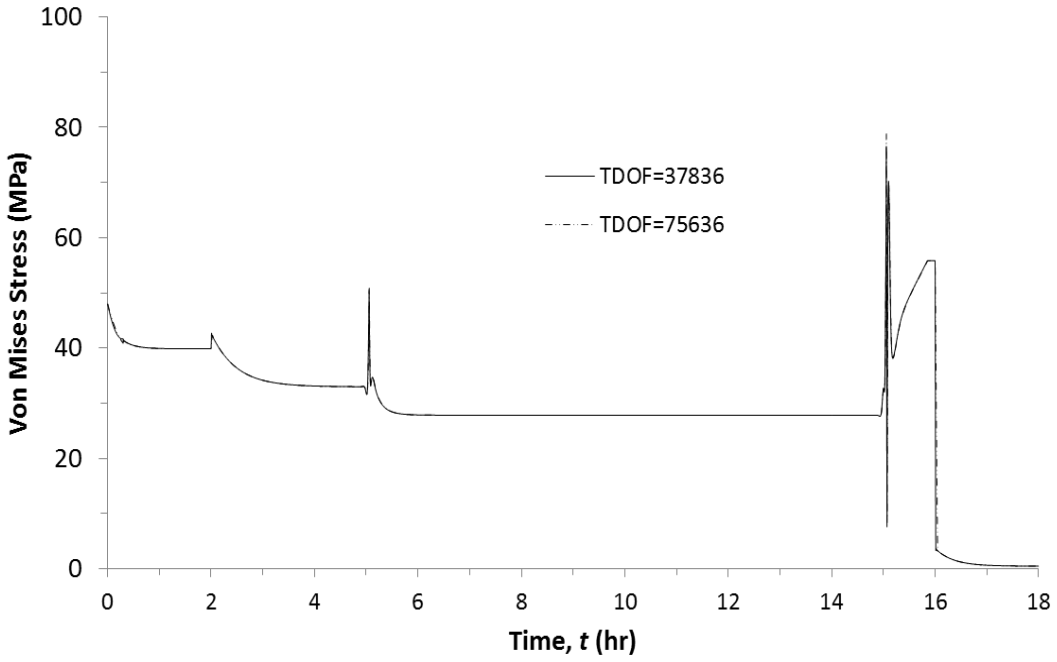

Figure 3.7: Von Mises stress at outer surface of the coke drum in the process cycle.

3.6 Analysis Results

All the stresses and mechanical strain components induced by the combined thermal and mechanical loading for an entire operation cycle are given in Fig. 3.9 to Fig. 3.20 at six different locations for both inner and outer surfaces of the coke drum. These six locations are chosen as shown in Fig. 3.1(a). Temperature curves in a process cycle are given in Fig. 3.8. These calculated results are in agreement with measured results as provided by Xia et al [2]. The effect of oil filling and water quenching stage on temperature is visible initially at the bottom reference point of location 1 and finally at the top point of location 6. The level of oil and water requires some time to move from bottom position to top of the coke drum. Since the diameter of the coke drum is very large compared to the thickness, radial stress developed in the shell is very small compared to the other two stress components. Hence radial stress is not included in this discussion.

It can be seen from all the graphs of stresses and strain that there is a fluctuation of stresses and strains at the beginning of oil charging and water quenching stage due to the severe bending effect which will be discussed-later in details in this chapter. Strain and stress developed in the coke drum due to the internal pressure is very small. Therefore, the major contribution of induced stress and strain is because of the thermal loading. Xia et al. [2] already verified that the main source of the stress is developed due to thermal loading compared to mechanical loading. The main reason of the included thermal stress is due to the mismatch of the coefficient of thermal expansion (CTE) between clad and base materials. Due to larger CTE of SA387 than that of TP410S and much smaller thickness of TP410S than that of SA387, larger tensile hoop and axial stresses are induced in the clad and smaller compressive hoop and axial stresses are in the base material.

Summary of the stresses and mechanical strains in coke drum in a complete operation cycle under the temperature and internal pressure loadings are in Table 3.4 and Table 3.5.

Table 3.4: Summary of stresses in an 18-hr operation cycle of the coke drum at location 4.

	Stress at inner surface (MPa)				Stress at outer Surface (MPa)			
	Maximum	Minimum	Amplitude	Mean	Maximum	Minimum	Amplitude	Mean
σ_{zz}	252.9	3.7	124.6	128.3	75.4	-69.9	72.6	2.7
$\sigma_{\theta\theta}$	312.7	3.8	154.5	158.2	67.4	-24.4	45.9	21.5
σ_{Mises}	283.2	3.8	139.7	143.5	81.6	0.40	40.7	41.1

Table 3.5: Summary of mechanical strains in an 18-hr operation cycle of the coke drum at location 4.

	Mechanical strain at inner surface ($\times 10^{-3}$)				Mechanical strain at outer surface ($\times 10^{-3}$)			
	Maximum	Minimum	Amplitude	Mean	Maximum	Minimum	Amplitude	Mean
ε_{zz}	0.955	0.007	0.474	0.481	0.445	-0.37	0.4075	0.0375
$\varepsilon_{\theta\theta}$	1.403	0.013	0.695	0.708	0.306	-0.216	0.261	0.045
ε_{rr}	-0.011	-0.955	0.472	-0.48	-0.125	-0.156	0.141	-0.016

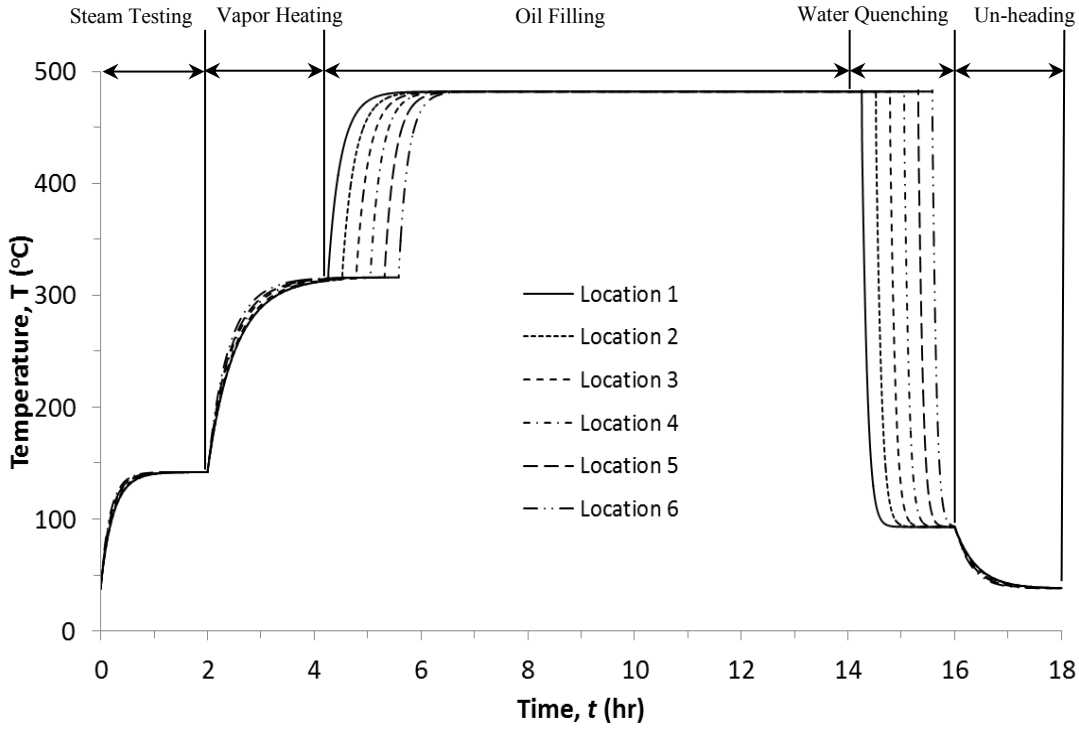

Figure 3.8: Temperature profile of the coke drum in the process cycle.

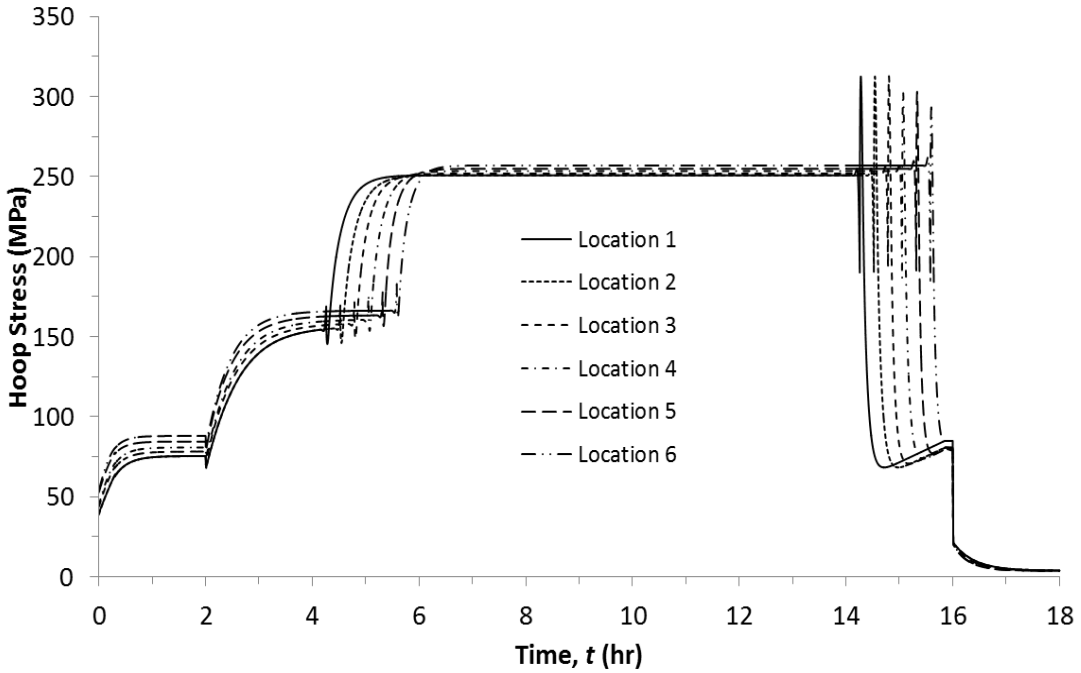

Figure 3.9: Hoop stress at the inner surface of the coke drum in the process cycle.

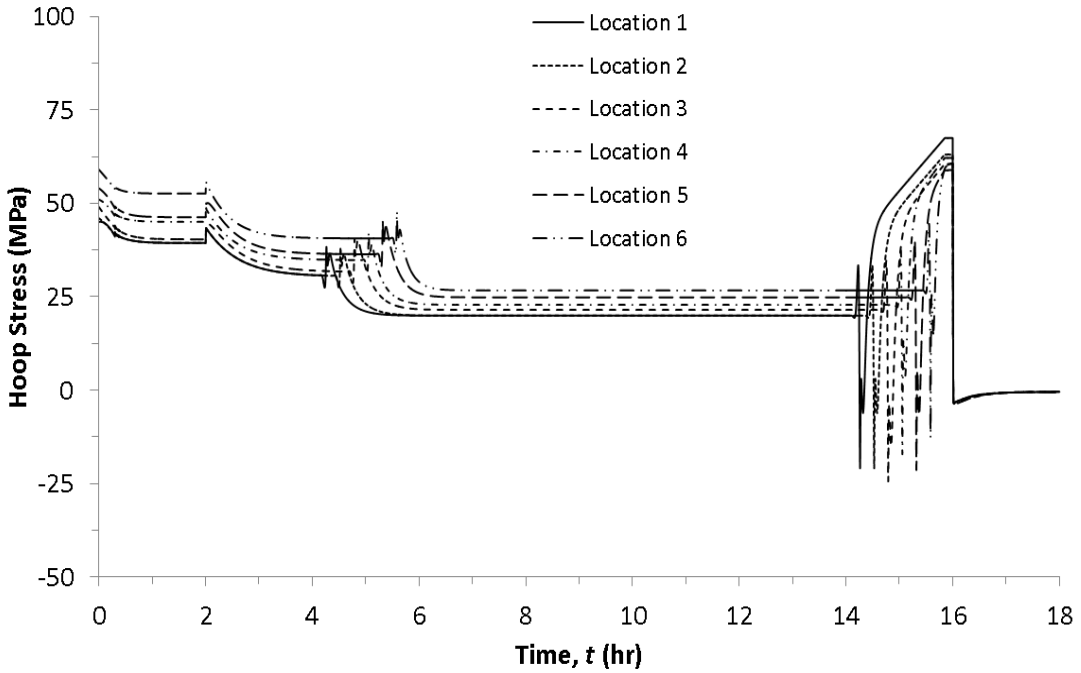

Figure 3.10: Hoop stress at the outer surface of the coke drum in the process cycle.

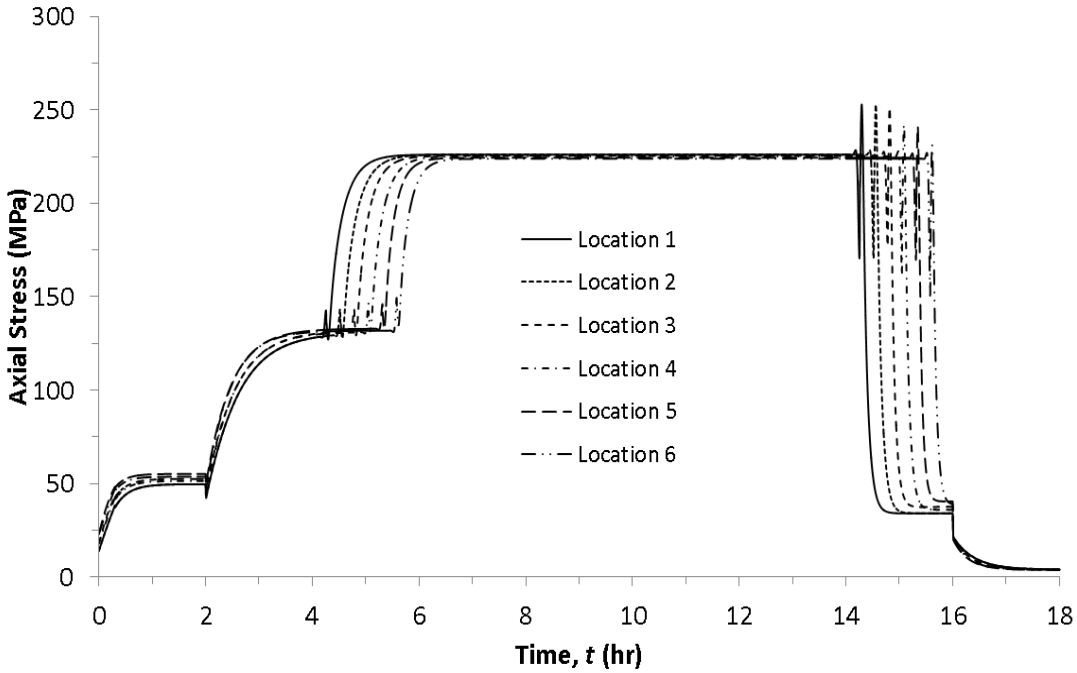

Figure 3.11: Axial stress at the inner surface of the coke drum in the process cycle.

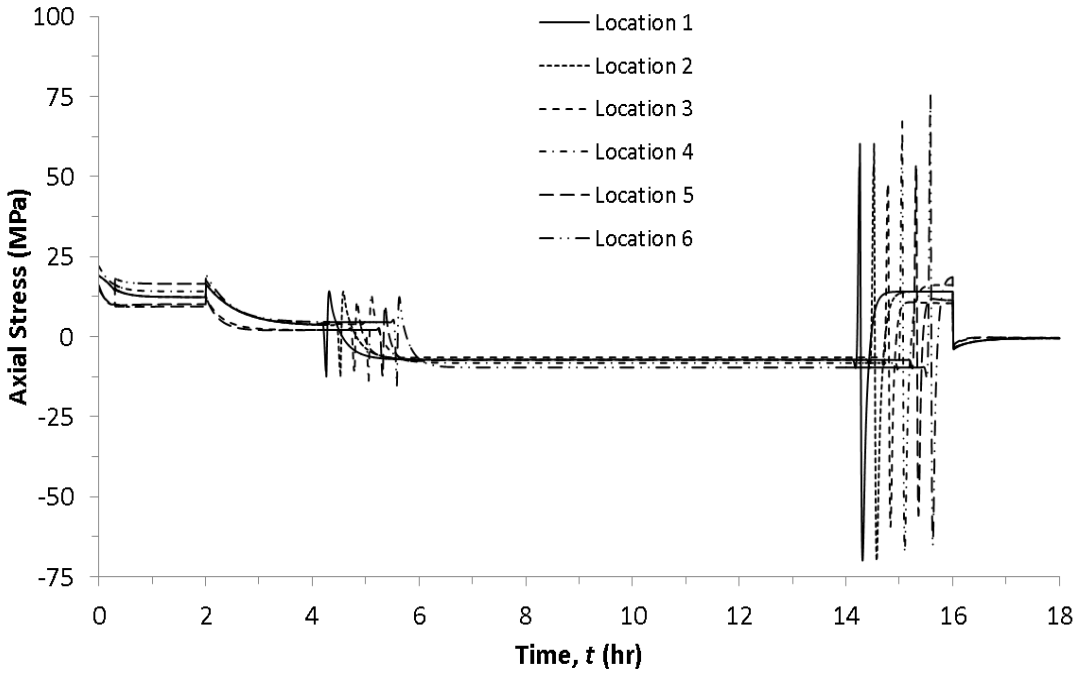

Figure 3.12: Axial stress at the outer surface of the coke drum in the process cycle.

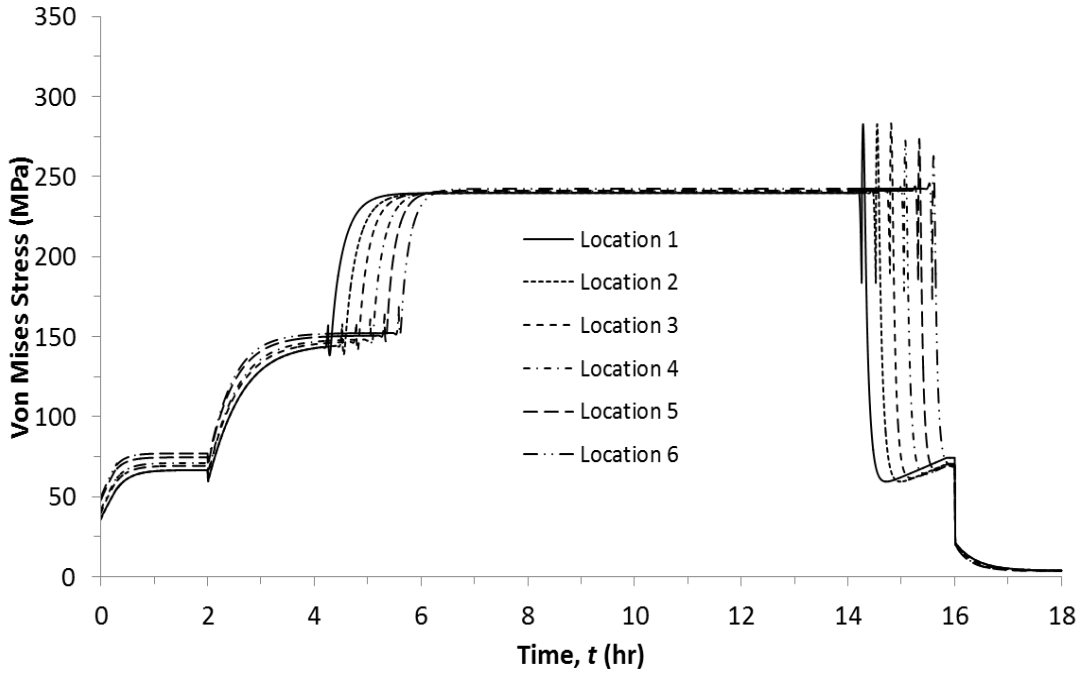

Figure 3.13: Von Mises stress at the inner surface of the coke drum in the process cycle.

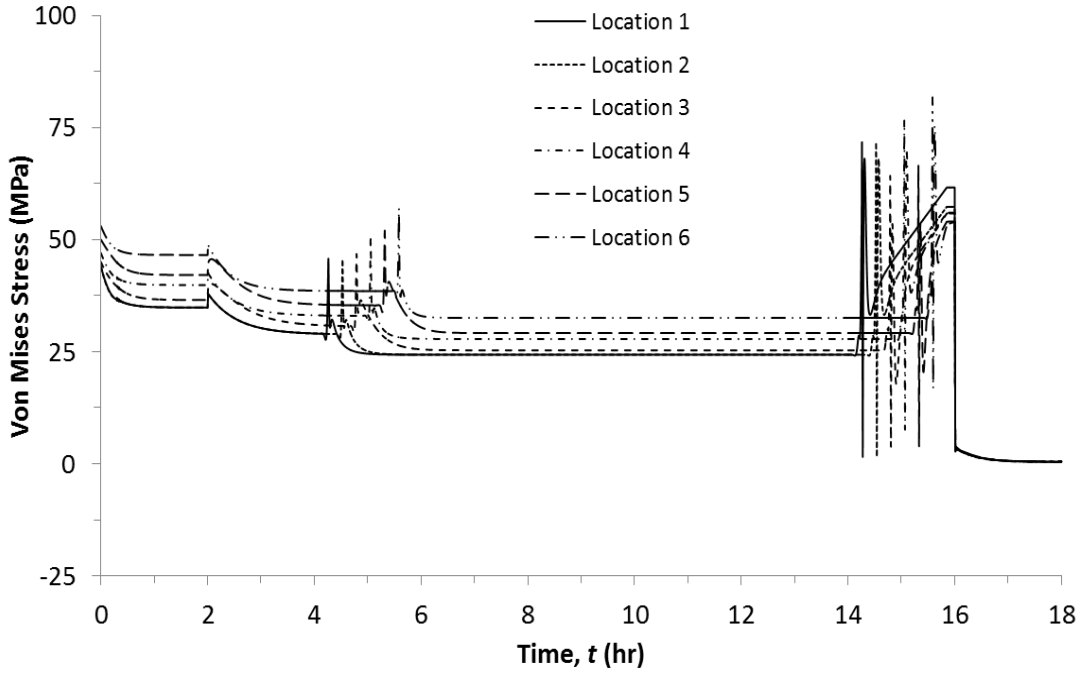

Figure 3.14: Von Mises stress at the outer surface of the coke drum in the process cycle.

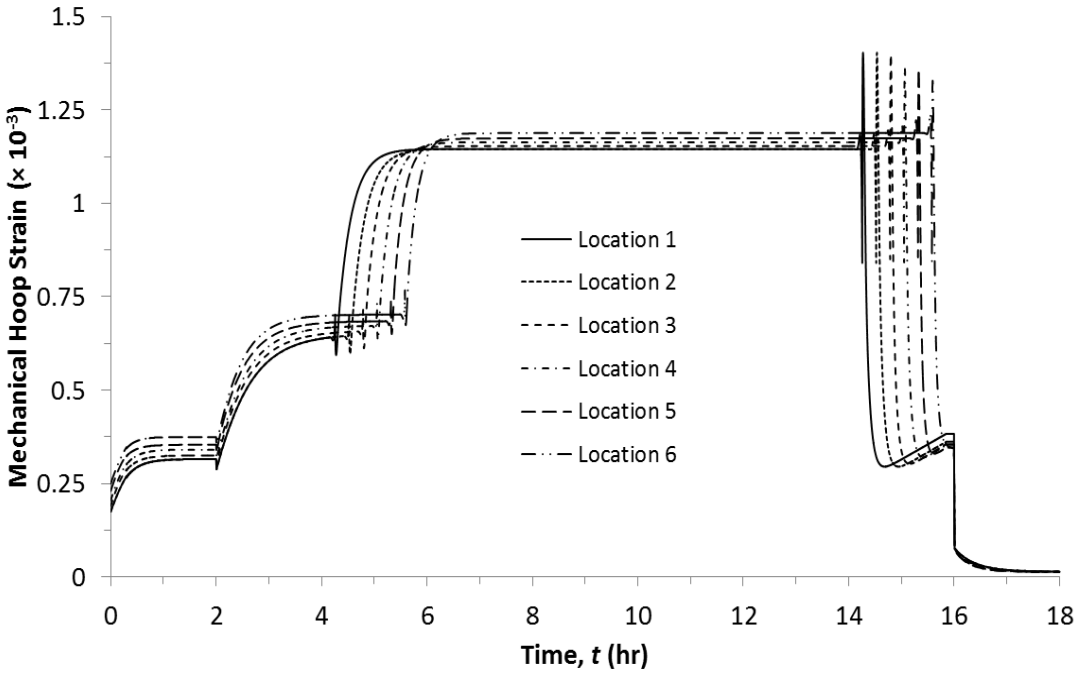

Figure 3.15: Mechanical hoop strain at the inner surface of the coke drum in the process cycle.

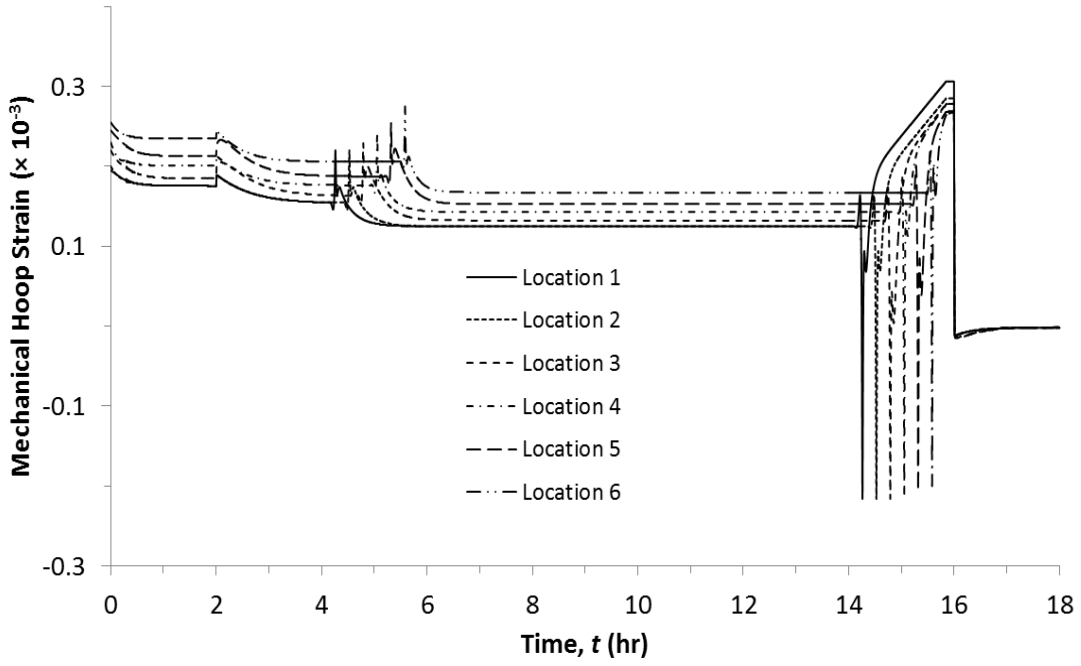

Figure 3.16: Mechanical hoop strain at the outer surface of the coke drum in the process cycle.

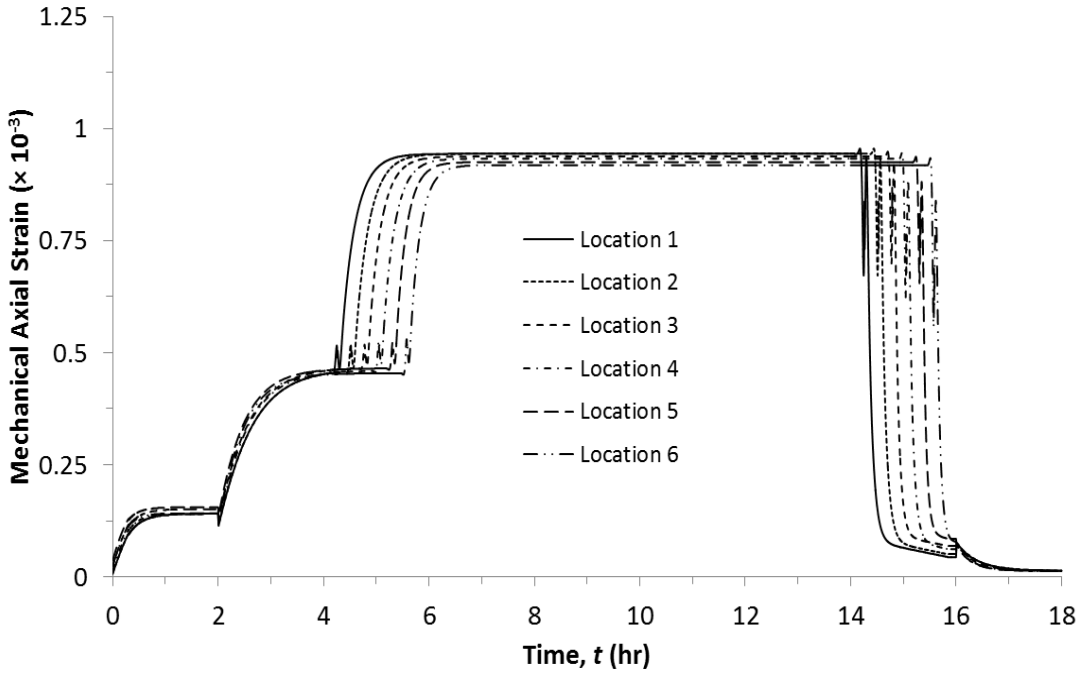

Figure 3.17: Mechanical axial strain at the inner surface of the coke drum in the process cycle.

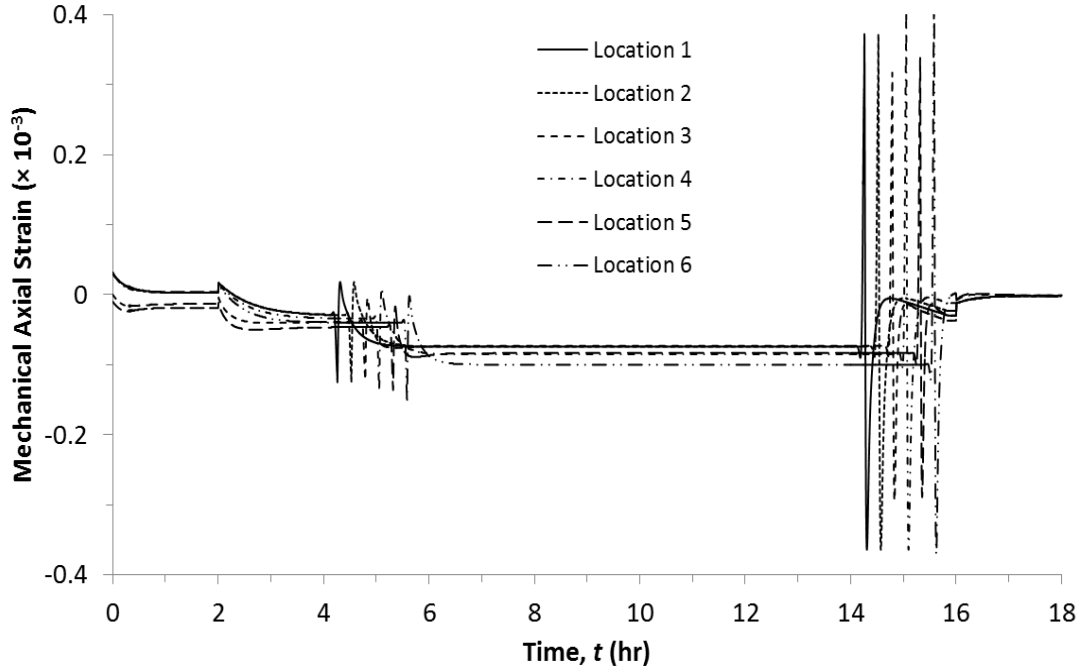

Figure 3.18: Mechanical axial strain at the outer surface of the coke drum in the process cycle.

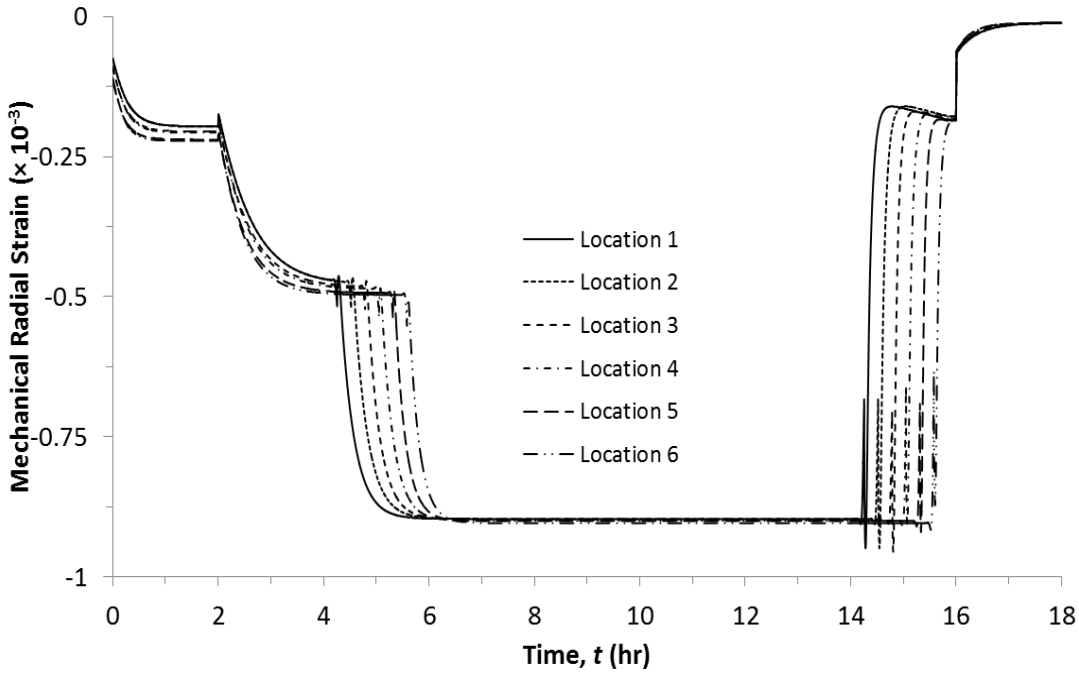

Figure 3.19: Mechanical radial strain at the inner surface of the coke drum in the process cycle.

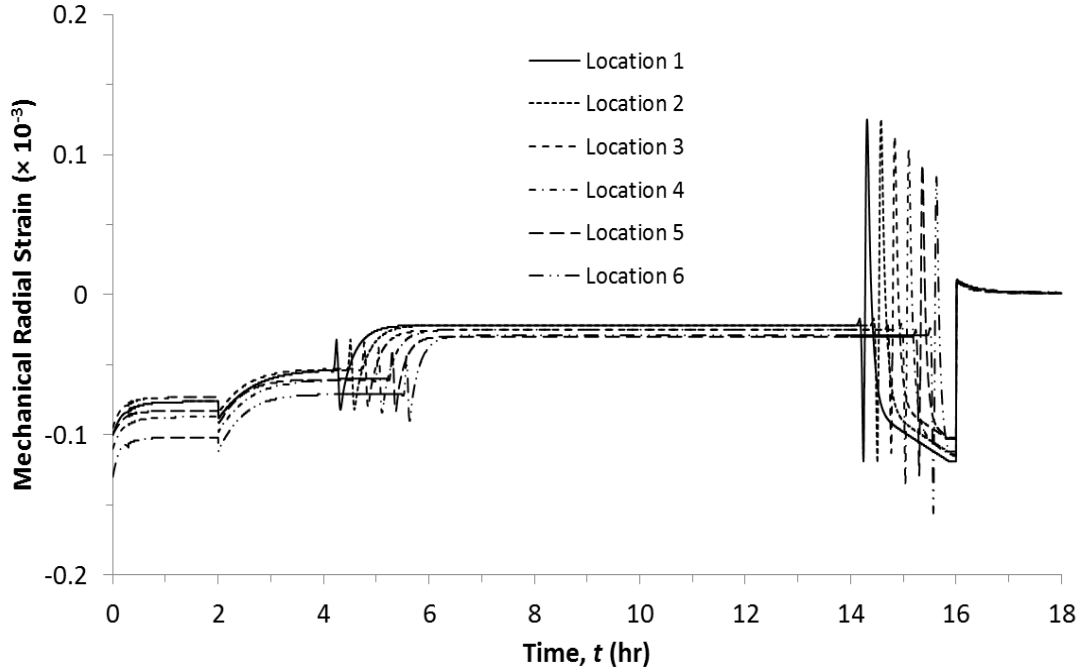

Figure 3.20: Mechanical radial strain at the outer surface of the coke drum in the process cycle.

3.7 Explanation of Fluctuation of Stresses on Oil filling and Quenching Stage

During quenching stage, cold water is directly injected into the bottom of the coke drum that cools down coke drum shell where the water reached while the shell above the water level remains hot [10]. Hot oil is injected during oil filling stage that also results the temperature difference too. This temperature difference causes bending effect on the shell and induces bending stresses and strains in the shell. However, the temperature difference at oil filling stage is not as severe as happened in quenching stage. Because the temperature of the vapor above the hot oil very quickly becomes hot due to the heat radiation effect. Except the radiation, one more possible factor is the convection heat transfer between the hot oil and the vapor above the hot oil, which is already considered during the imposition of the boundary conditions on the FE model.

The effect of bending stress can be explained by comparing the induced von Misses stress and axial stress at inner and outer surfaces at location 4 (see Fig. 3.1) of the coke drum during quenching stage as shown in Fig. 3.21 and 3.22. The rising rate of water is 3mm/s. As shown in Fig. 3.21 and 3.22, the stress variation during quenching stage can be divided in the following four steps:

Step i: When the quenching water level is low and far away from the location, still the stresses level in this step is same as in the oil filling stage. The stresses induced in this step are because of the difference of CTEs of clad and base materials as explained earlier.

Step ii: In this step the water level is getting closer to the location 4 and the von Misses' and axial stresses at the inner surface are decreasing drastically whereas at outer surface both stresses are increasing as shown in Fig. 3.21 and Fig. 3.22. This happens because the shell that was directly in contact with water shrinks but the hot shell above the water level was still in its previous shape as shown in Fig 3.23 (a). This deformation causes tensile bending axial stress at the outer surface and compressive bending stress at the inner surface.

Step iii: In this step the water level already passes the location 4 as shown in Fig 3.23(b). The inner and outer surfaces experience increasing tensile and compressive axial bending stresses, respectively.

Step iv: Finally due to cooling effect of water, induced stress level is decreasing at the inner and outer surfaces. But from Fig. 3.21, it can be seen that there is a sudden rise of von Mises stress in this step at outer surface. This is because of the temperature difference between inner and outer surface of the drum shell as shown in Fig. 3.24. The temperature at the outer surface is higher than that at the inner surface that causes additional thermal stresses. At the end, all the stresses are going down due to the cooling effect of the quenching water.

From the above explanation it can be seen that the rising quenching water is more critical in terms of induced strain and stress in the drum shell. In the following section the effect of water filling rate is further explored.

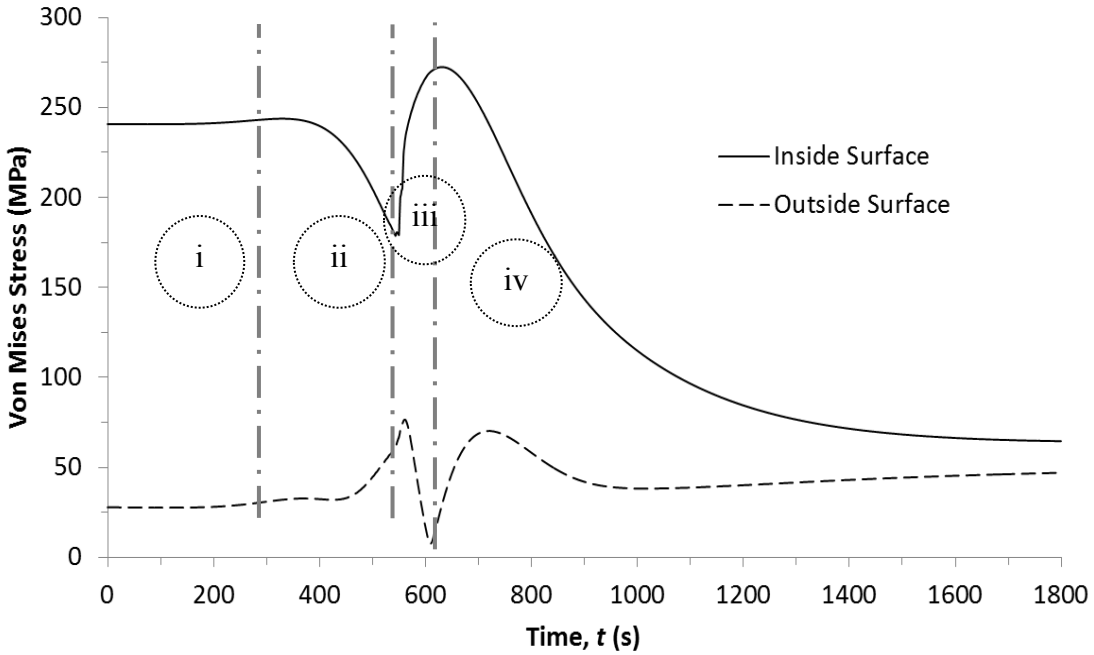

Figure 3.21: Variation of von Mises stress at location 4 during water quenching stage.

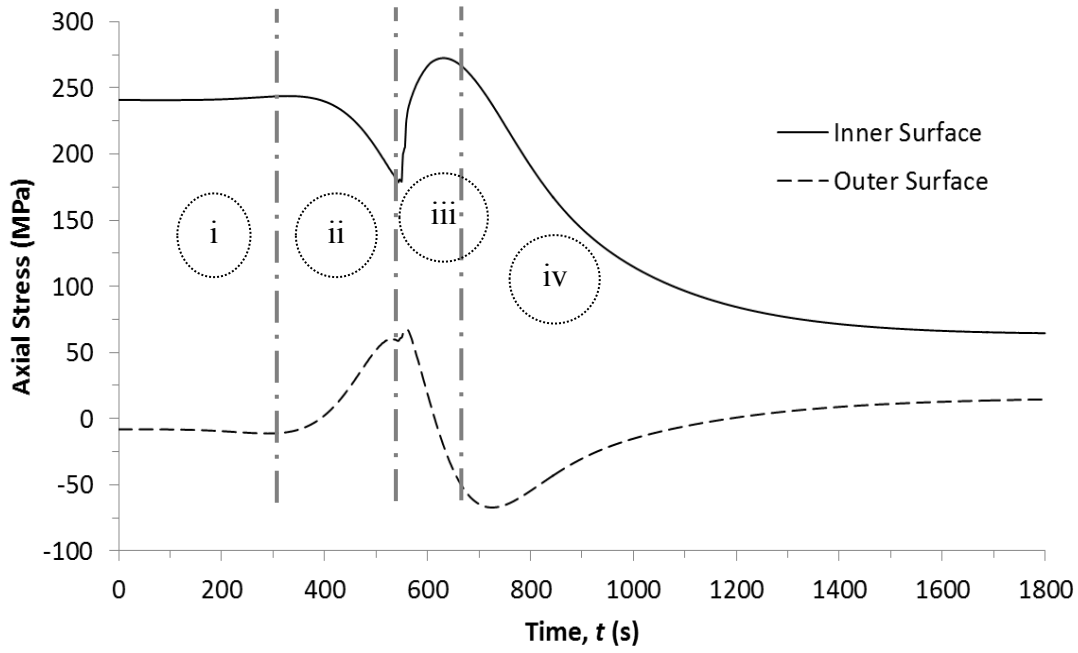

Figure 3.22: Variation of axial stress at location 4 during water quenching stage.

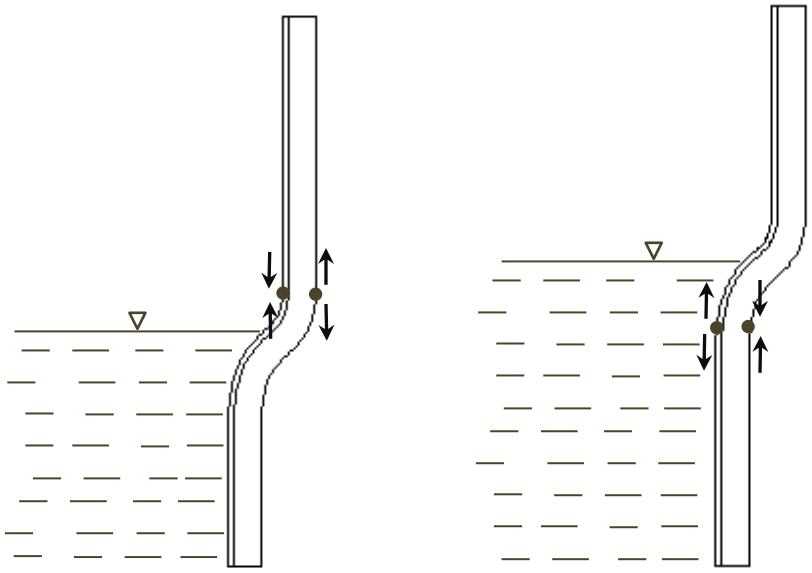

Figure 3.23: Bending effect on inner and outer surfaces during quenching stage when the water level is (a) below the reference points and (b) above the reference points.

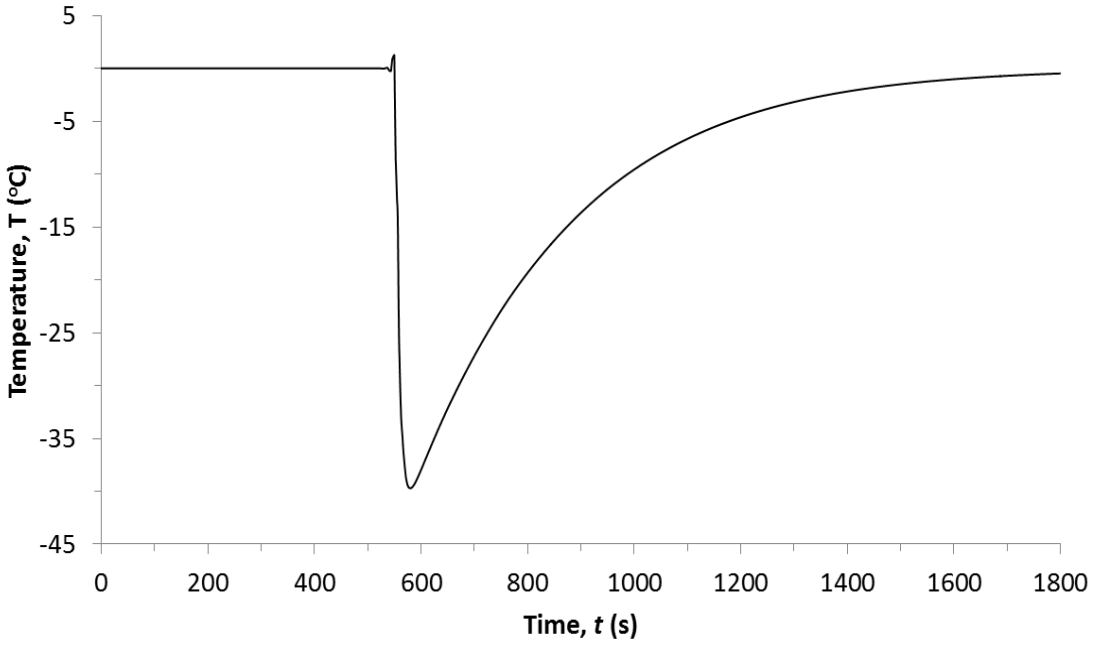

Figure 3.24: Temperature difference between inner and outer surfaces at quenching stage.

3.8 Effect of Rising Rate of Water during Quenching Stage on Coke Drum

Since severe stress fluctuation occurs in the water quenching stage, the influence of different cooling water rising rates in the quenching process were employed in the analysis. So far in the previous analyses water rising speed $V_c = 3\ mm/s$ was assumed. This rate is adopted for a practical coke drum in Suncor Energy Inc. A second water rising speed $V_c = 1\ mm/s$ was also considered in the analysis to investigate the effect of different water charging rates on the coke drum.

The heat transfer coefficient between cooling water and inner surface of the coke drum is dependent on the rising rate of water. As a result the boundary conditions on inner surface may vary with the variation of water speed. But there is no analytical method to determine the heat transfer coefficient in multiphase environment. Besides that field temperature with different quenching rates are not available. Since level of water with rising speed of 1 mm/s requires long time to reach to the top of a coke drum, the duration of water quenching stage was increased from 2 hours (within which only one-third of the coke drum will be filled up with water) to 6 hours. The results of the model for water rising speed $V_c = 3\ mm/s$ are shown in solid lines while the results at 1mm/s are shown in dashed lines.

Fig. 3.25 presents the temperature difference during quenching stage between inner and outer surfaces at location 4 for those two water rising speeds. The maximum temperature differences are almost same for both speeds with a difference within 0.7%. Therefore,

there is no significant influence of the variation of water rising rates on temperature difference between inner and outer surfaces of the coke drum.

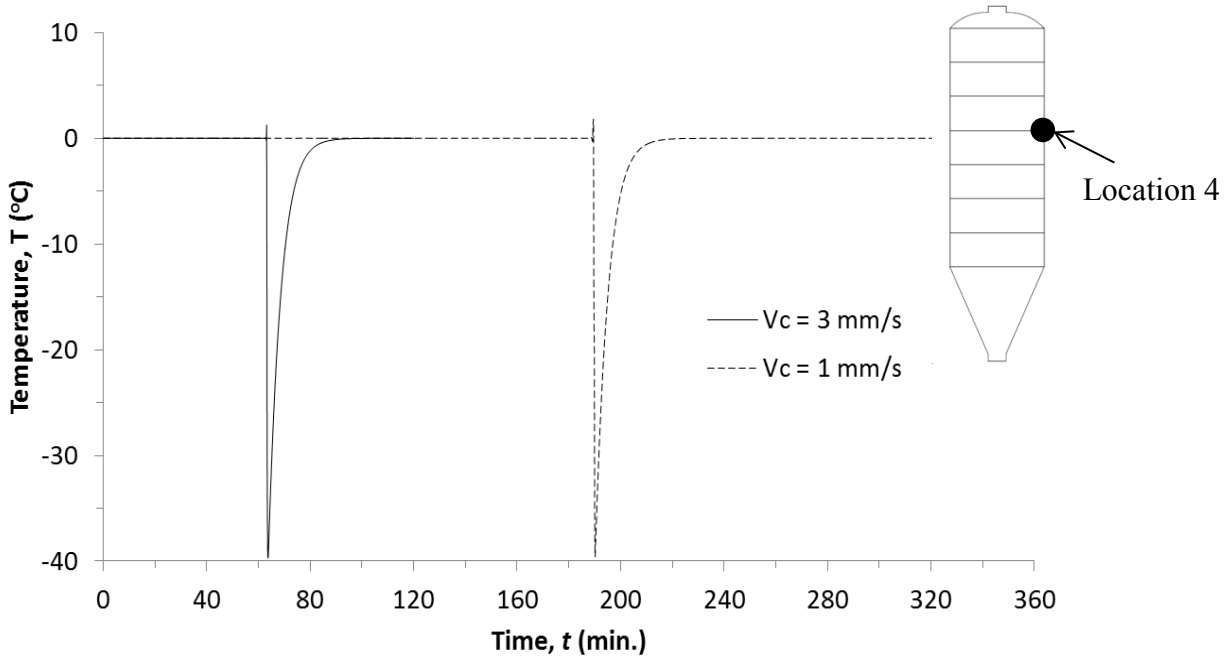

Figure 3.25: Temperature difference between inner and outer surfaces during quenching stage at location 4.

Figures 3.26 and 3.27 show the variation of von Mises stress with the water rising rates during the quenching stage at location 4. It is found that the difference of maximum von Mises stresses at the inner surface is within 7.5%, while at the outer surface that difference is significant with a value of 172%. That clearly indicates that with the decrease of the water rising rate, very high stress is induced at the base layers of the coke drum. Summary of the maximum von Mises stresses during the quenching stage at the hot and cold end of clad and base layers are listed below in Table 3.6.

Table 3.6: Maximum von Mises stresses during the quenching stage at location 4.

Rising Rate	3 mm/s				1 mm/s			
Location	Hot End		Cold End		Hot End		Cold End	
	Base	Clad	Base	Clad	Base	Clad	Base	Clad
Temperature (^{o}C)	480	482	338	380	478	482	214	251
Von Mises Stress (MPa)	73	244	68	272	200	249	167	249
Yield Strength (MPa)	331	192	383	253	324	192	380	249
Von Mises/Yield ratio in %	22.1	127	17.8	108	61.7	130	43.9	100

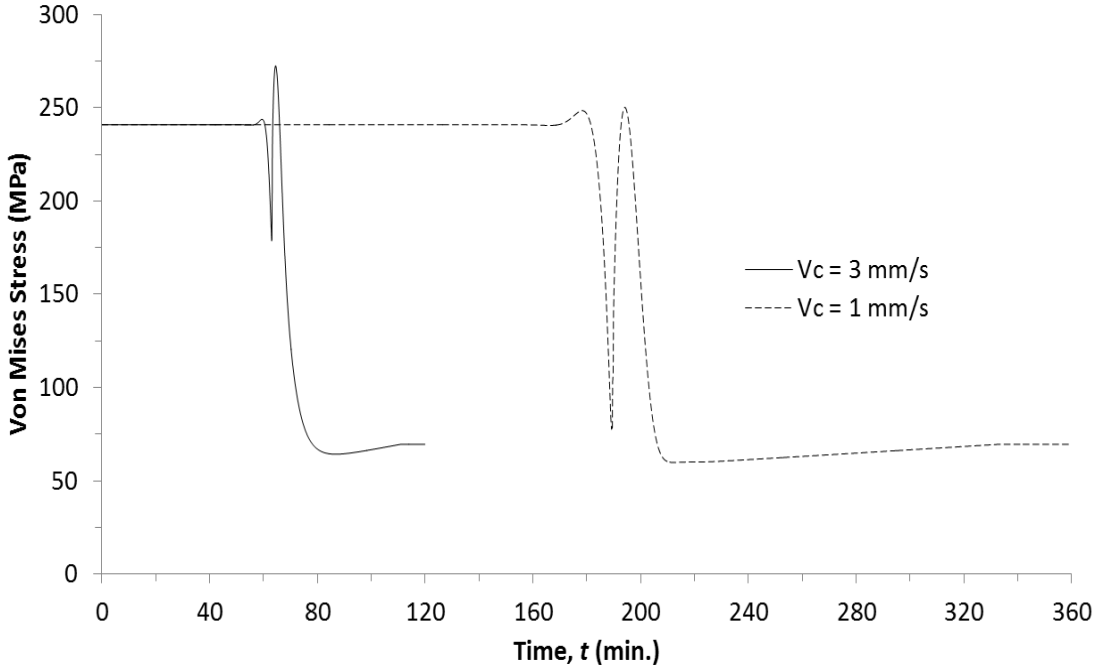

Figure 3.26: Variation of von Mises Stress at the inner surface of Coke Drum for different water rising rates.

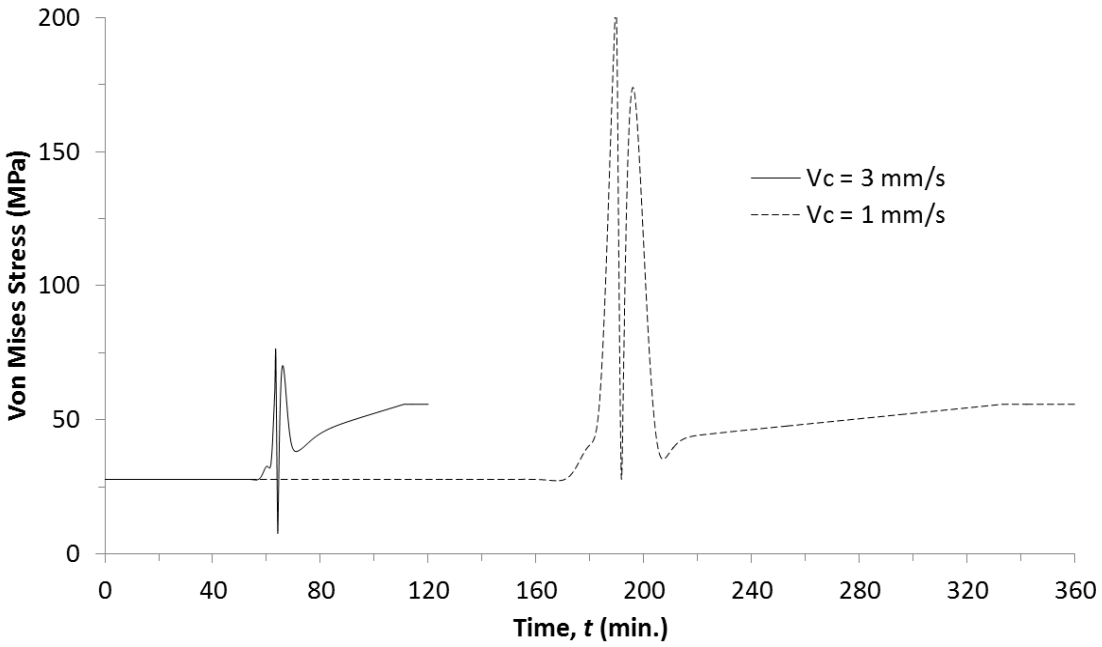

Figure 3.27: Variation of von Mises Stress at the outer surface of Coke Drum for different water rising rate.

This analysis can be explored in more details by investigating temperature distributions along axial directions along course 4 and radial directions at location 4. When the water level reached at location 4, the solutions were obtained along the two lines (A-A' and B-B') as shown in Fig. 3.28. Ning et al. [23] found that axial temperature distribution varies with the variation of water rising speed as shown in Fig. 3.28. Figure 3.29 presents the temperature distributions along the inner surface, of course 4 for two water rising speeds. And it is found that the smooth temperature gradient happens with the water rising speed $V_c = 3\,mm/s$, while the slower rising speed $V_c = 1\,mm/s$ gives the steep temperature gradient. Due to the steep temperature gradient in short distance of course 4, deflection in the coke drum occurs in a small region that contributes severe bending stress at both inner and outer surfaces. As a consequence high bending strain is induced at the outer surface with lower water rising speed $V_c = 1\,mm/s$ as shown in Fig. 3.30. Figure 3.31

also confirms that von Mises stress at the outer surface is high compared to the water rising rate $V_c = 3\,mm/s$. But at $3\,mm/s$, low bending stress is induced in both inner and outer surfaces due to the smooth temperature gradient over a long distance. But a major portion of the inner surface of coke drum during water rising rate $3\,mm/s$ is still in direct contact with the very hot water as can be seen from Fig. 3.28(b). For this reason, at a higher water rising rate, Stresses in the base and clad materials are still induced due to the mismatch of CTEs.

Figure 3.32 shows that the temperature variation in the radial direction is not linear. And the temperature gradient along a radial direction is almost similar for both water rising speeds as shown in Fig. 3.33. That is in agreement with the temperature differences between inner and outer surfaces for two different water rising speeds. It can be concluded that the radial temperature gradient has a very negligible effect on the induced stress-strain of the coke drum shell compared to the axial temperature gradient.

From this analysis, it seems that higher water rising rates are better in terms of induced stresses and strains in the base layers of the coke drum. Note that in this analysis the quenching water is assumed uniformly arising. But in reality, due to existence of porous solid cokes, channel water flows are formed which result in formation of random hot or cold spots on the drum shell. Further increase of water rising rate (more than 3mm/s) would result extreme hot and cold spots, which may cause excessive local stresses in the shell of the coke drum [24]. Therefore, very high water rising rate is also not favorable for the operation of the coke drum.

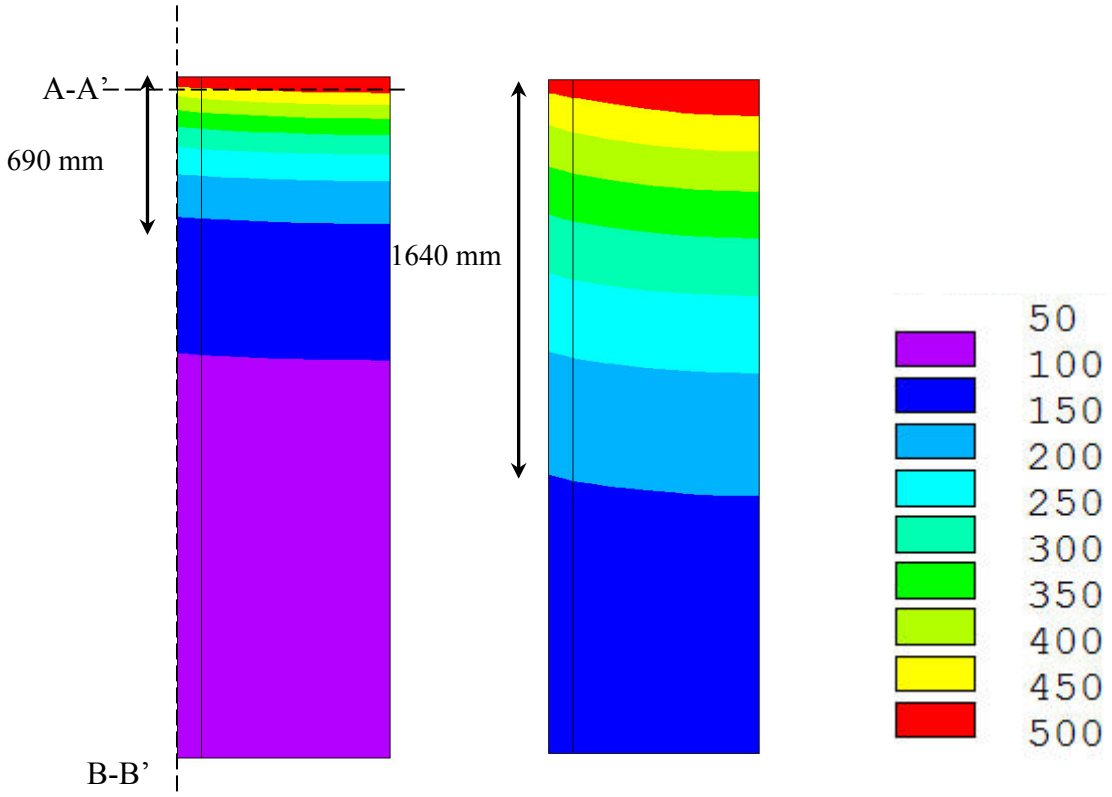

Figure 3.28: Temperature distribution of course 4 when the cooling water reached at A-A' (a) for 1 mm/s and (b) for 3 mm/s (Radial dimension×40).

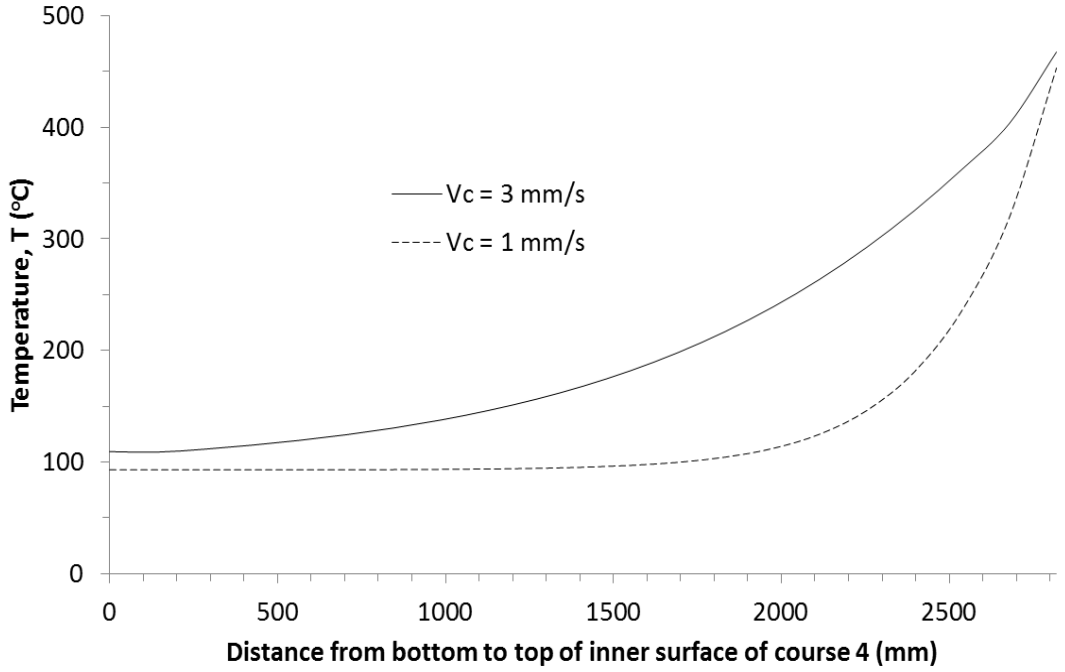

Figure 3.29: Axial temperature distribution at the inner surface of course 4.

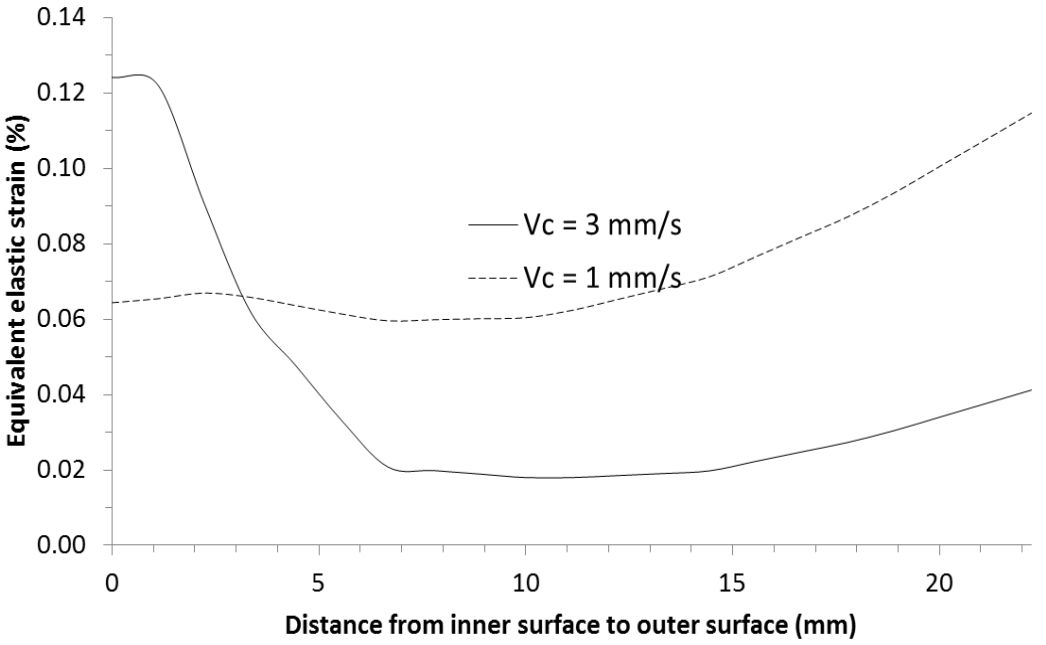

Figure 3.30: Effect of water rising speeds on equivalent elastic strain at location A-A'.

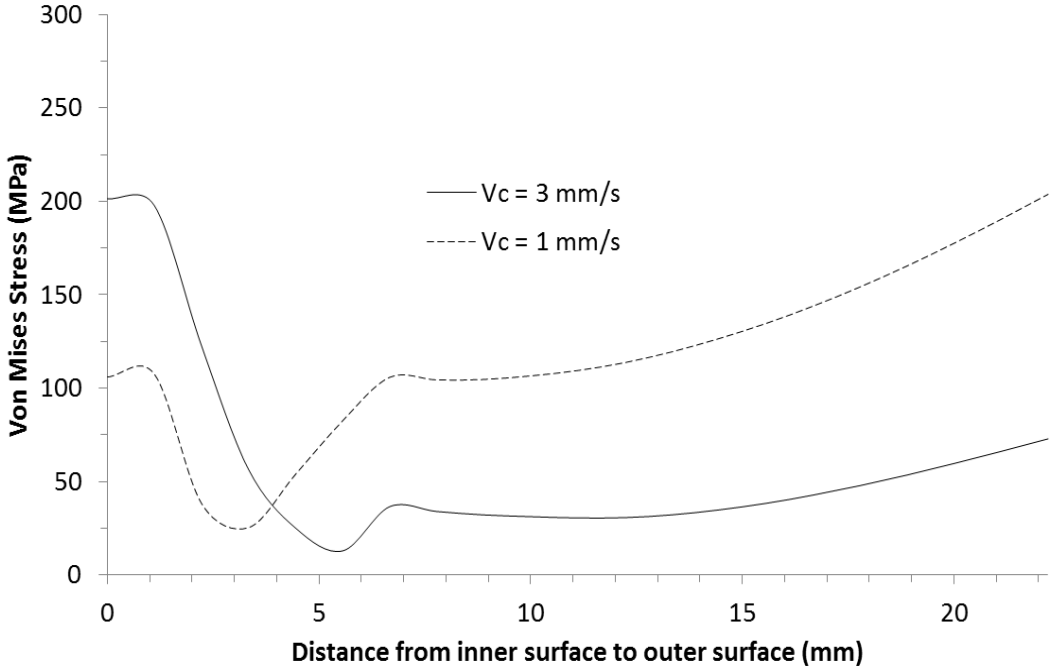

Figure 3.31: Effect of water rising speeds on von Mises stress at location A-A'.

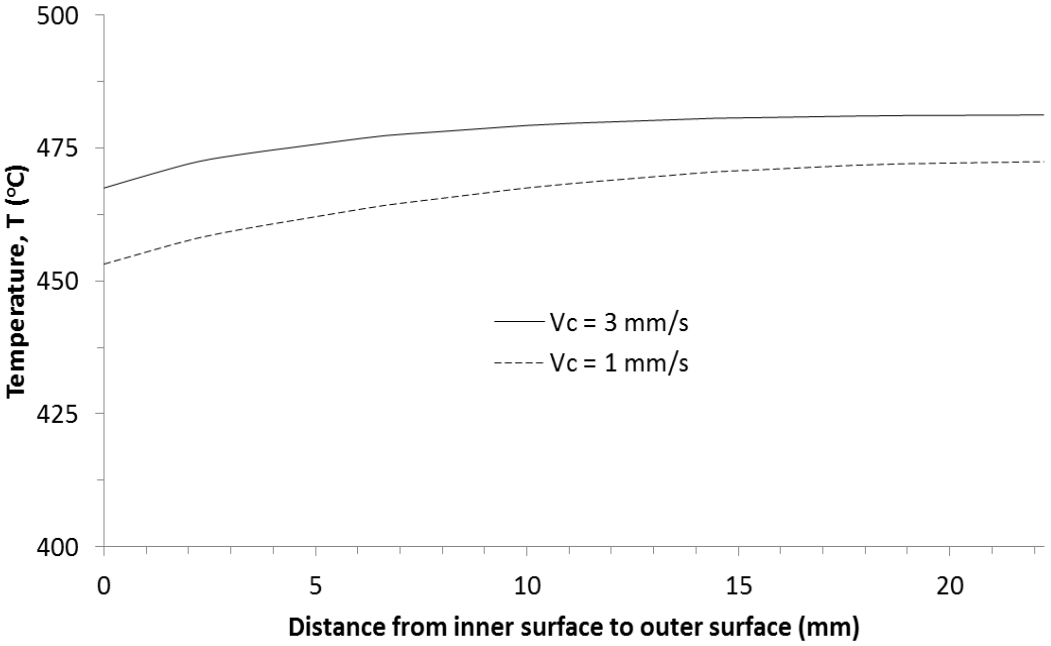

Figure 3.32: Effect of water rising speeds on radial temperature distributions at location A-A'.

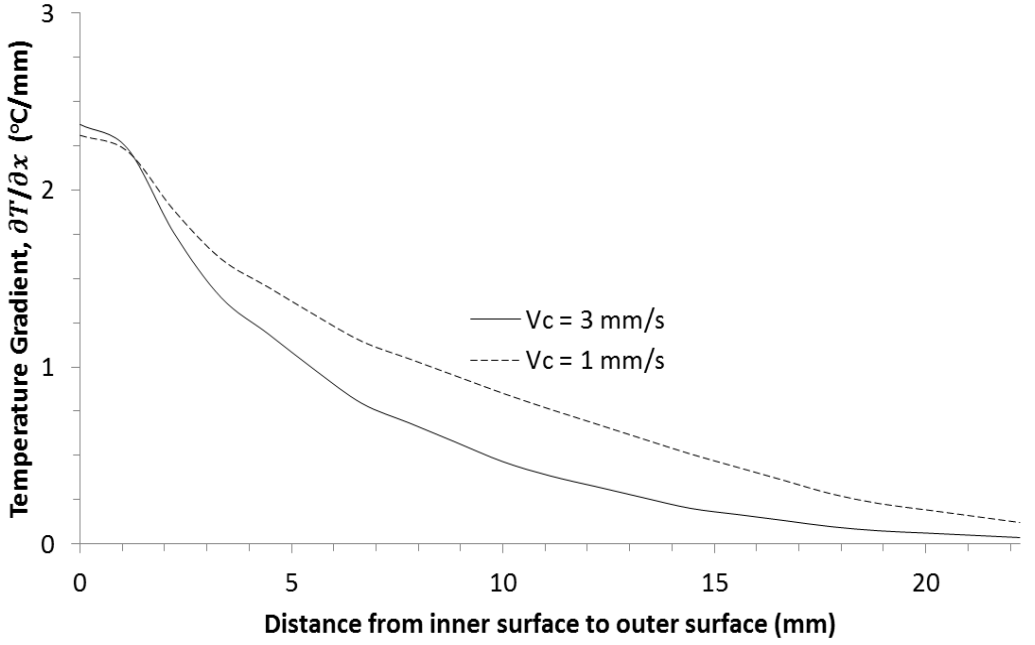

Figure 3.33: Effect of water rising speeds on the temperature gradient at location A-A'.

Through the above comparison it can be seen that the clad material at both cases yields, however, the ratio of maximum von Mises yield stress to yield strength is lower for the case of $V_c = 3\,mm/s$; Stresses at base layers can be significantly reduced by adopting higher water rising rate of $V_c = 3\,mm/s$ as found in Table 3.6, but the stresses in the base layer are still within the elastic range (the maximum von Mises stress to yield strength ratio is 61.7%) for the lower water rising rate of $V_c = 1\,mm/s$. Furthermore, the higher water rising speed saves the operation time. Therefore, the water rising speed $V_c = 3\,mm/s$ will be used in the future analysis.

3.9 Alternative Selection of Base and Clad Materials of the Coke Drum

Optimal selection of base and clad material combinations for coke drums is very important to increase the reliability and performance. As explained in the previous chapter, by matching the coefficient of coefficient of thermal expansion of base and clad material von misses stress in base and clad layer can be reduced significantly. Nikic et al [10] found that the combination of SA302C as a base material with N06625 as clad material had low maximum von Mises to yield strength ratio for both clad and base materials. Due to unavailability of material SA302C in market, SA302B was chosen as a base material. In addition, all the thermal and mechanical tests were performed on SA302B as mentioned in chapter 2.

The physical and thermal properties of SA302 B and N06625 are obtained from the database" 2007, ASME Boiler and Pressure Vessel Code II, Part D Properties". These properties are listed below in Table 3.7 and Table 3.8.

Table 3.7: Physical and Thermal Properties of SA302B

Temperature (^oC)	Modulus of Elasticity E (GPa)	Density ρ (kg/m^3)	Poisson' ration v	Thermal Conductivity k (W/m. ^oC)	Thermal Expansion CTE ($1/^oC$)	Specific Heat c (J/kg.^oC)
20	200.0	7750	0.3	41.0	1.26×10^{-5}	445.69
100	196.0	7750	0.3	40.6	1.35×10^{-5}	481.50
200	190.0	7750	0.3	40.1	1.44×10^{-5}	526.90
300	183.0	7750	0.3	38.7	1.51×10^{-5}	566.16
400	170.0	7750	0.3	36.8	1.57×10^{-5}	607.99
500	149.0	7750	0.3	34.8	1.61×10^{-5}	663.27

Table 3.8: Physical and Thermal Properties of N06625

Temperature (^oC)	Modulus of Elasticity E (GPa)	Density ρ (kg/m^3)	Poisson' ration v	Thermal Conductivity k (W/m. ^oC)	Thermal Expansion CTE ($1/^oC$)	Specific Heat c (J/kg.^oC)
20	207.3	8440	0.31	9.80	1.20×10^{-5}	407.42
100	202.0	8440	0.31	10.90	1.33×10^{-5}	419.31
200	197.0	8440	0.31	12.40	1.35×10^{-5}	446.56
300	191.0	8440	0.31	13.90	1.38×10^{-5}	474.62
400	186.0	8440	0.31	15.40	1.48×10^{-5}	498.54
500	180.0	8440	0.31	16.90	1.63×10^{-5}	518.75

The results of FE-analysis of Coke drum with the new material combination have been compared and analyzed with the conventional material combination TP410S/SA387-22-2. The time history of temperature profile is given in Fig. 3.34. The temperature profiles are almost the same for both cases as shown in Fig. 3.34 except that there is slight difference of the temperature history in the range of around 1^o to 3^oC during quenching stage.

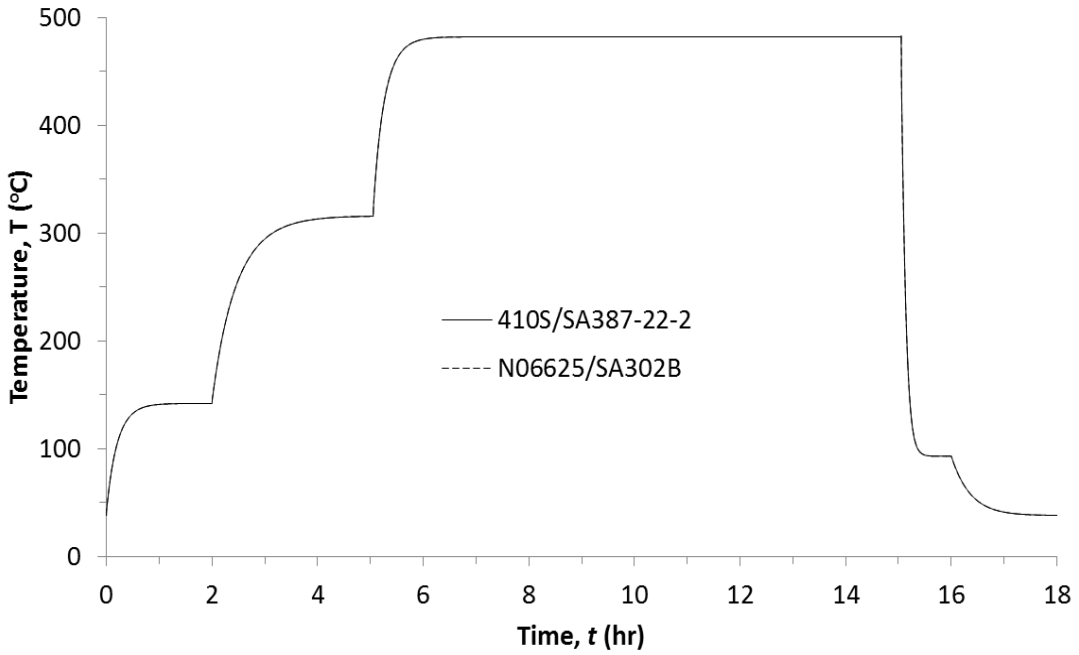

Figure 3.34: Temperature profile at inner surface of the coke drum in the process cycle at location 4.

It can be found that from Fig. 3.35 that the von Mises stress at the inner surface of TP410S/SA387-22-2 combinations is much higher than the combination of N06625/SA302B. The main reason is the very large difference of coefficient of thermal expansions of TP410S and SA387-22-2, while the difference of coefficient of thermal expansions is very small for the combination of N06625/SA302B. On the other hand, in the base materials the stress values are quite low for both cases although it is a little higher for the combination of N06625/SA302B as found in Fig. 3.36.

The maximum von Mises stresses occurred during quenching stage at the hot and cold end of clad and base layers are listed below in Table 3.9.

Table 3.9: Maximum von Mises stress over a complete operation cycle at location 4.

	TP410S/SA387-22-2				N06625/SA302B			
Location	Hot End		Cold End		Hot End		Cold End	
	Base	Clad	Base	Clad	Base	Clad	Base	Clad
Temperature (^{o}C)	480	482	338	380	480	482	334	355
Von Mises Stress (MPa)	73	244	68	272	71	126	63	226
Yield Strength (MPa)*	331	192	383	253	291	425	332	443
Von Mises/Yield ratio in %	22.1	127	17.8	108	29.8	19.5	18.7	24.8

For the combination of SA387-22-2 with TP410S as the clad material, the base material remains in the elastic range while the clad material exceeds the yield strength. But for the combination N06625/SA302B both clad and base materials remain in the elastic range. Therefore, the combination of materials N06625/SA302B seems better than the combinations of TP410S/SA387-22-2.

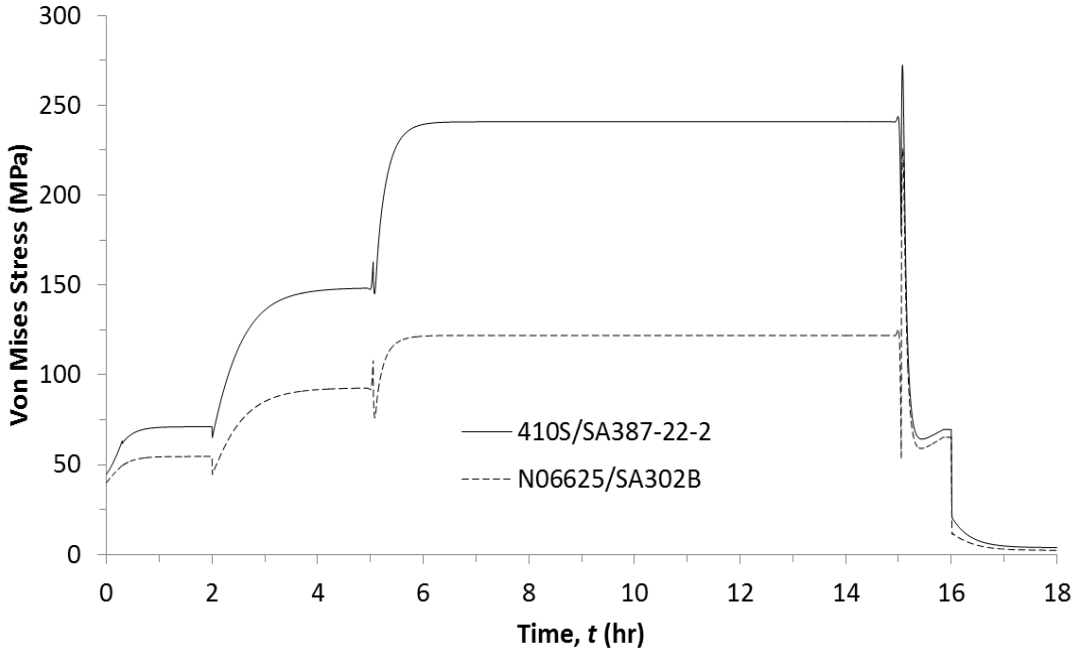

Figure 3.35: Von Mises stress at inner surface of coke drum in the process cycle for two different material combinations.

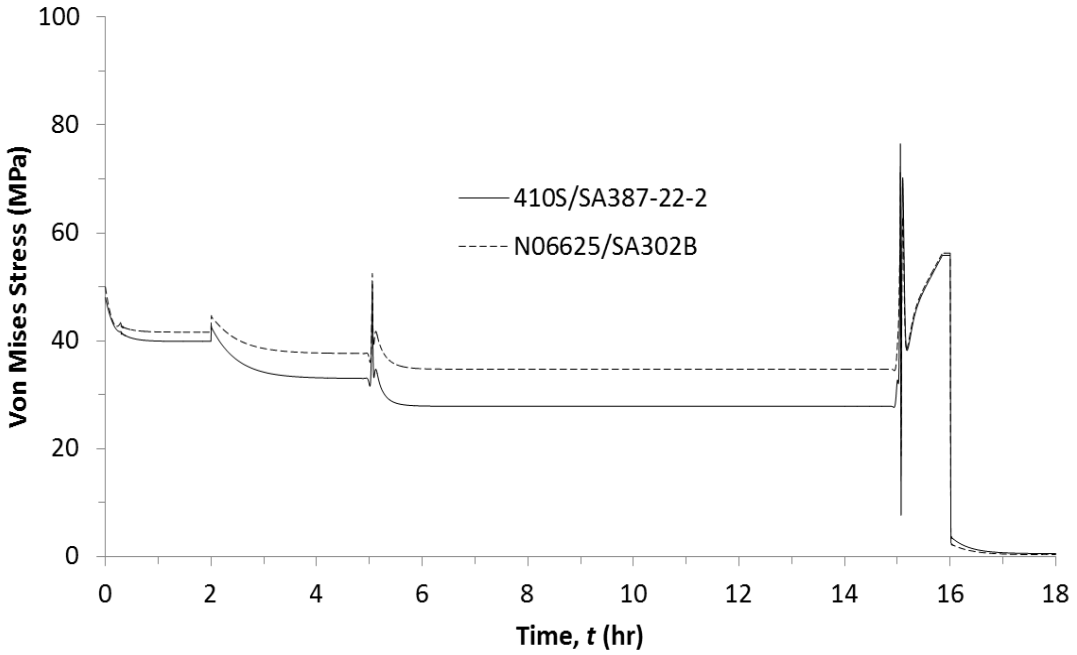

Figure 3.36: Von Mises stress at outer surface of coke drum in the process cycle for two different material combinations.

Hoop stress and axial stress at inner and outer surface for the two material combinations are presented in Fig. 3.37 to Fig. 3.40. In all cases, all stress components at the inner surface is much higher for the material combinations TP410S/SA387-22-2.

The same trend has been found in mechanical strain components of the two material combinations as shown in from Fig. 3.41 to Fig. 3.46. The mechanical strains drop significantly in the optional material combinations due to the matching of CTEs. Total radial strain is still negative at the inner surface for the optional combination of materials but absolute value of the radial strain is much lower compared to the currently used material combinations. Since all the analysis have been done in the elastic range, the mechanical strains developed in the coke drum shell are not that much high as expected. The accurate results will be explored in the next chapter using thermal elastic-plastic analysis in more details.

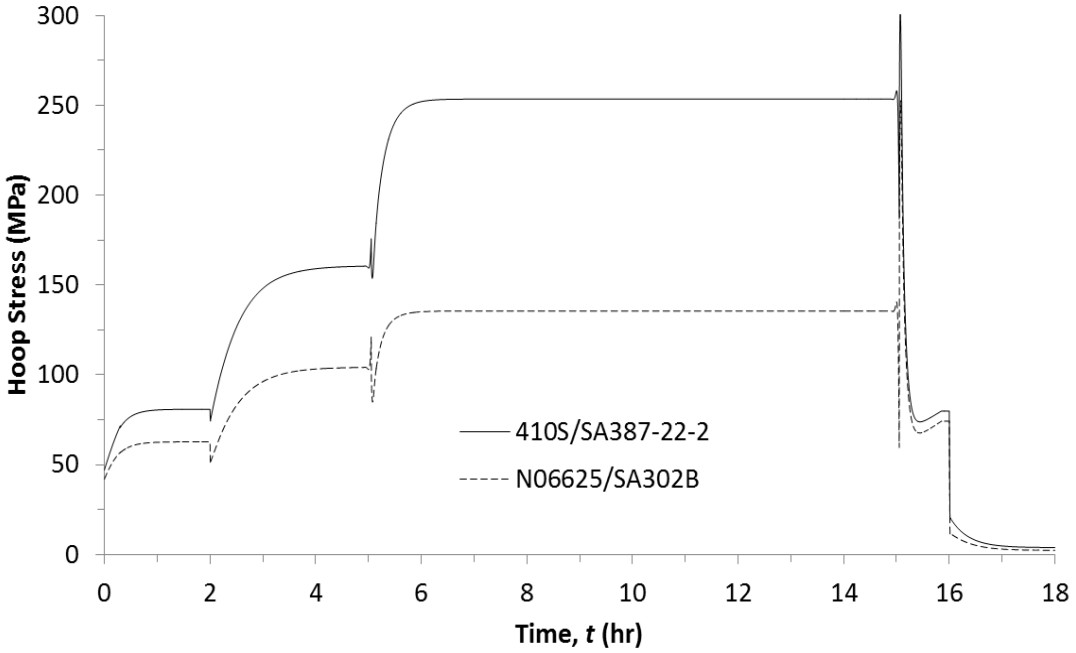

Figure 3.37: Hoop stress at inner surface of coke drum in the process cycle for two different material combinations.

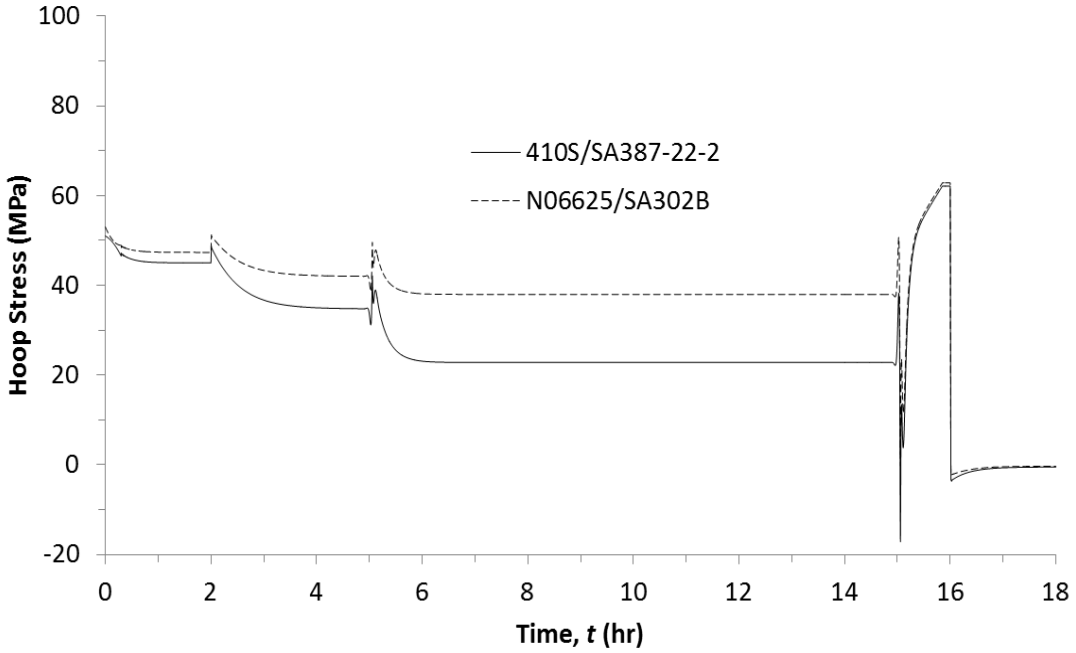

Figure 3.38: Hoop stress at outer surface of coke drum in the process cycle for two different material combinations.

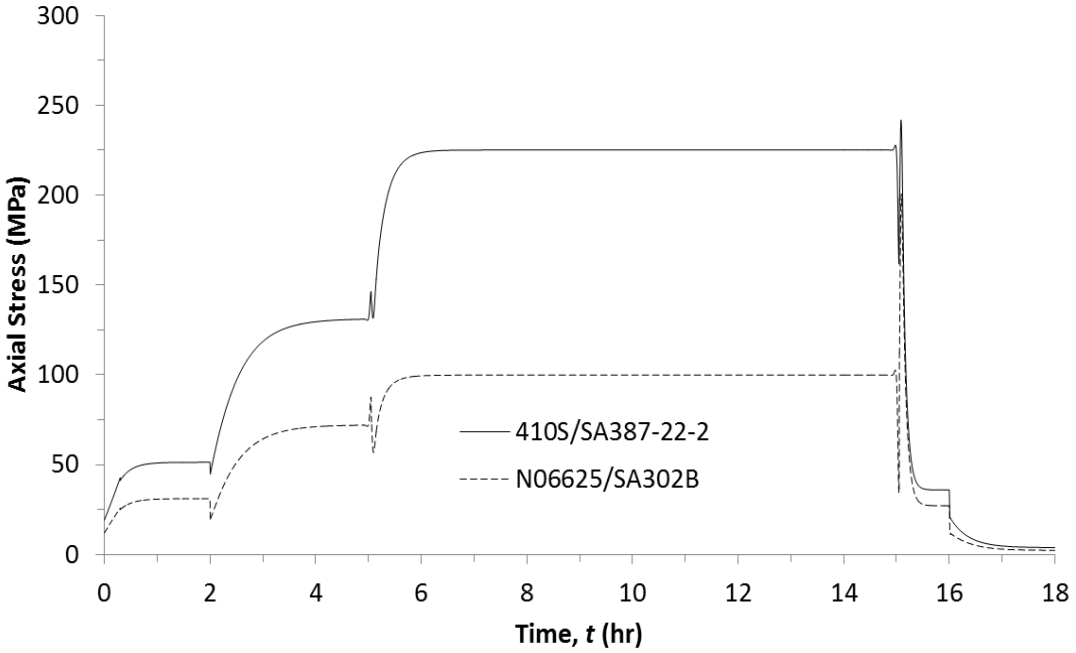

Figure 3.39: Axial stress at inner surface of coke drum in the process cycle for two different material combinations.

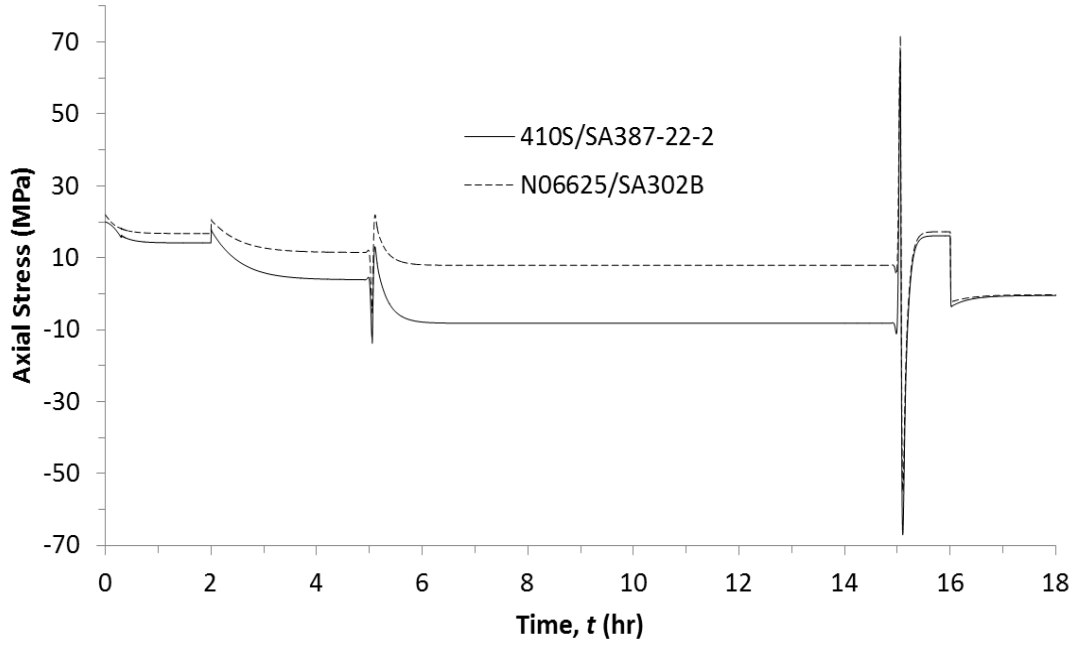

Figure 3.40: Axial stress at outer surface of coke drum in the process cycle for two different material combinations.

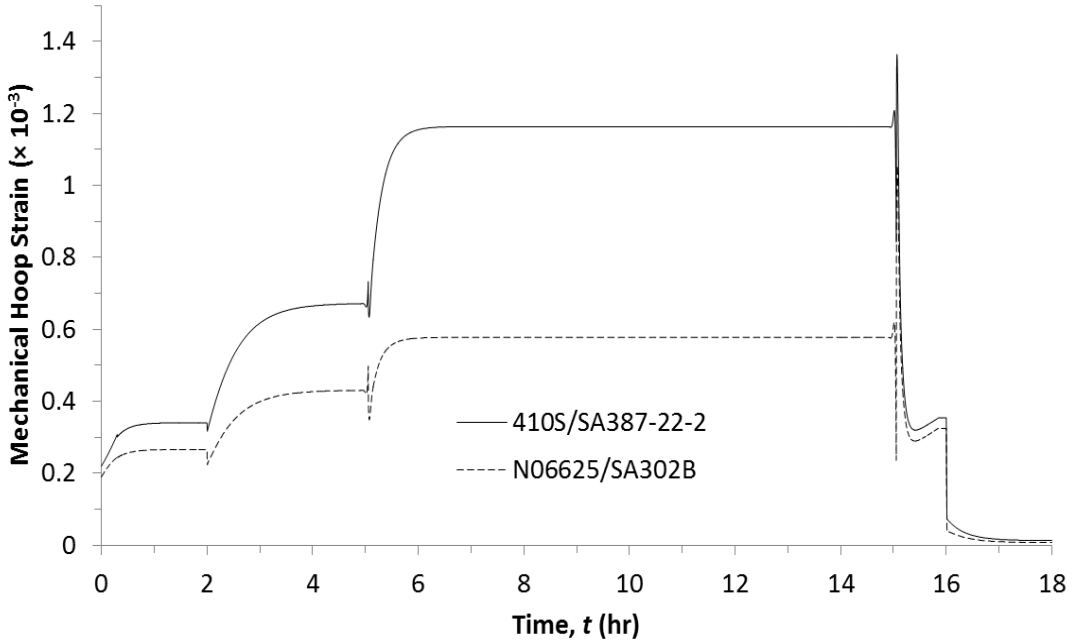

Figure 3.41: Mechanical hoop strain at inner surface of coke drum in the process cycle for two different material combinations.

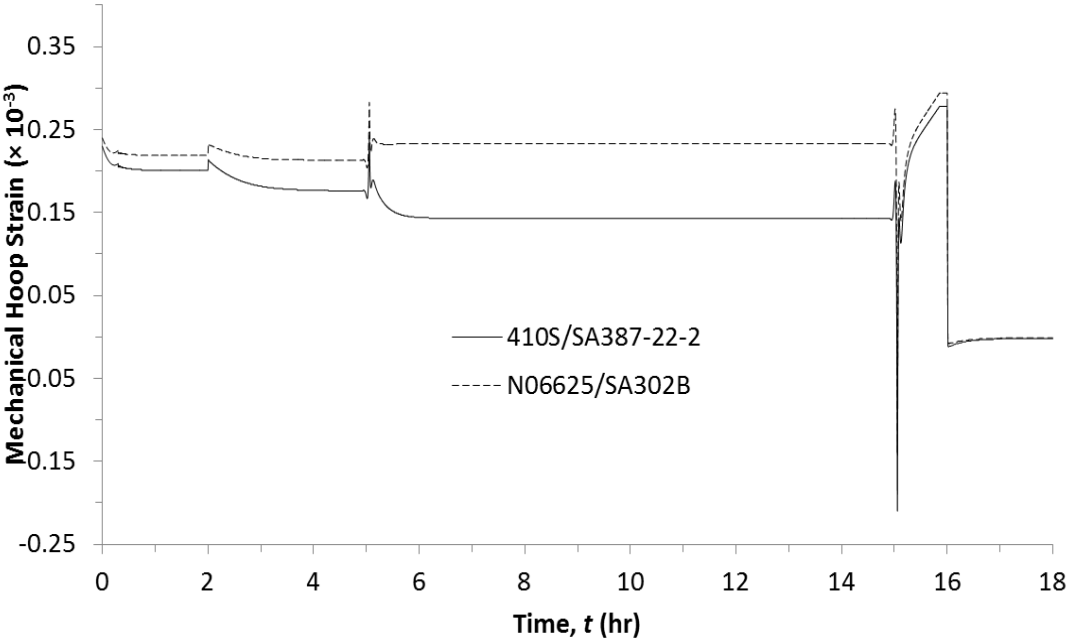

Figure 3.42: Mechanical hoop strain at outer surface of coke drum in the process cycle for two different material combinations.

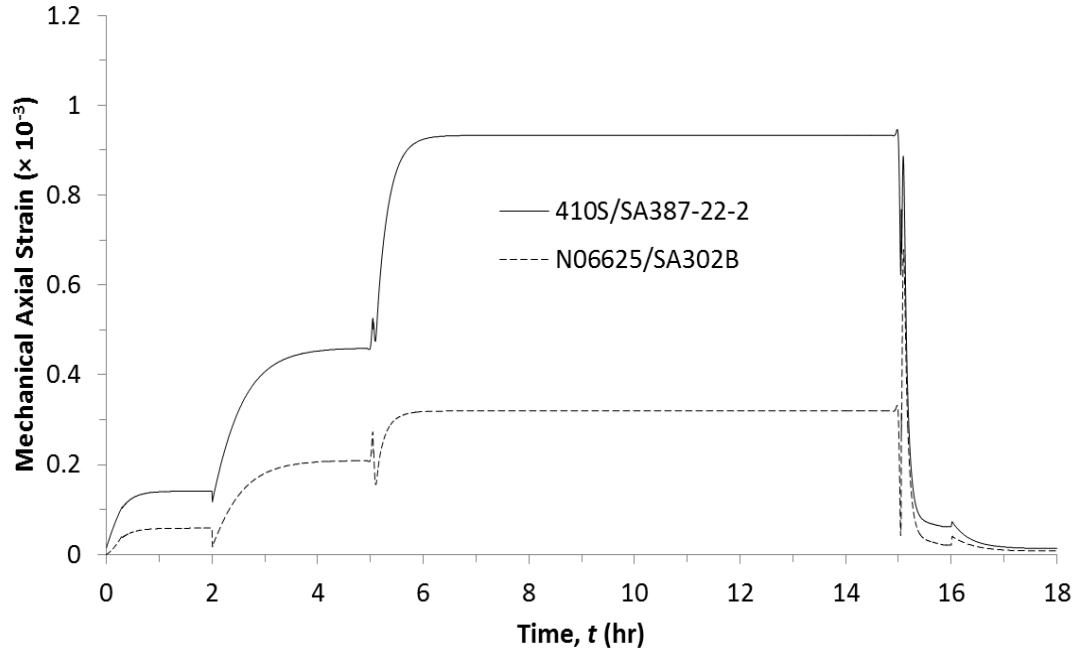

Figure 3.43: Mechanical axial strain at inner surface of coke drum in the process cycle for two different material combinations.

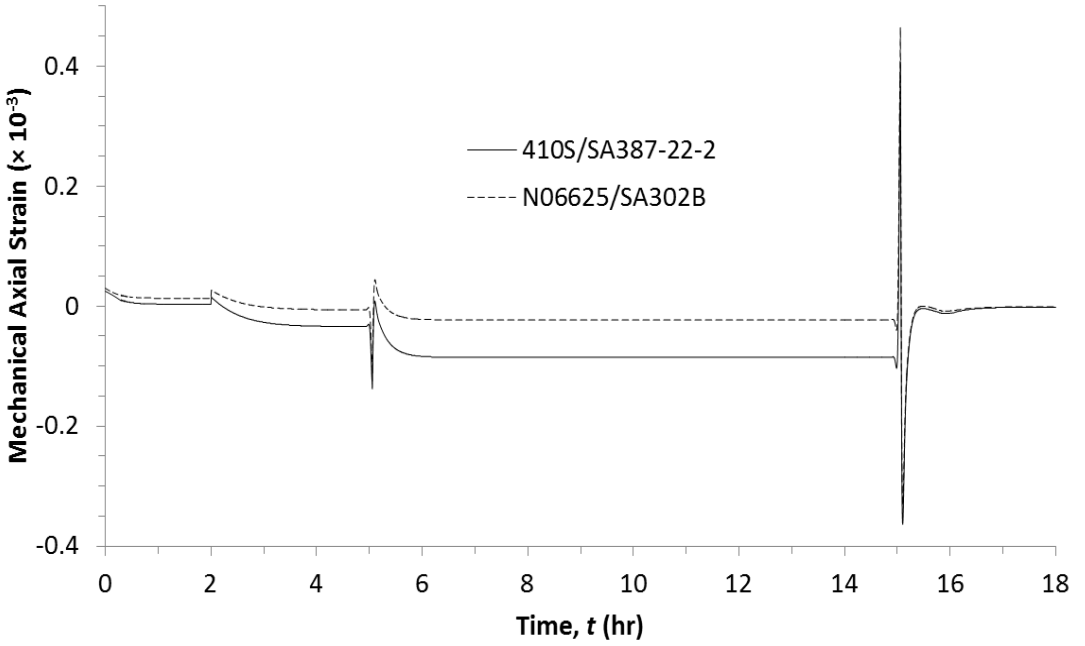

Figure 3.44: Mechanical axial strain at outer surface of coke drum in the process cycle for two different material combinations.

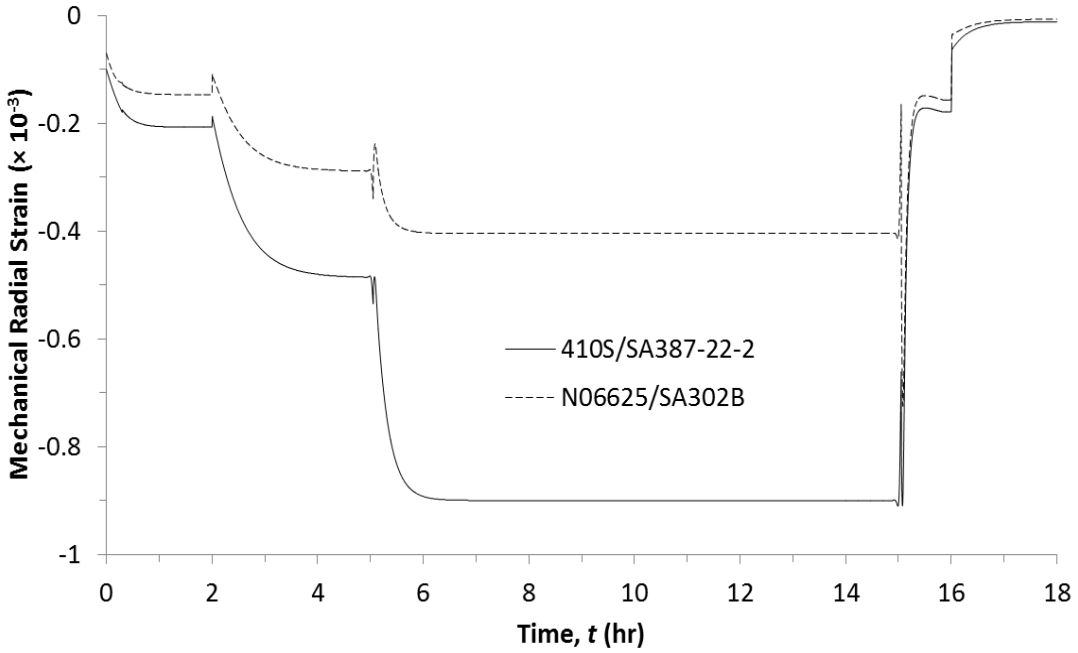

Figure 3.45: Mechanical radial strain at inner surface of coke drum in the process cycle for two different material combinations.

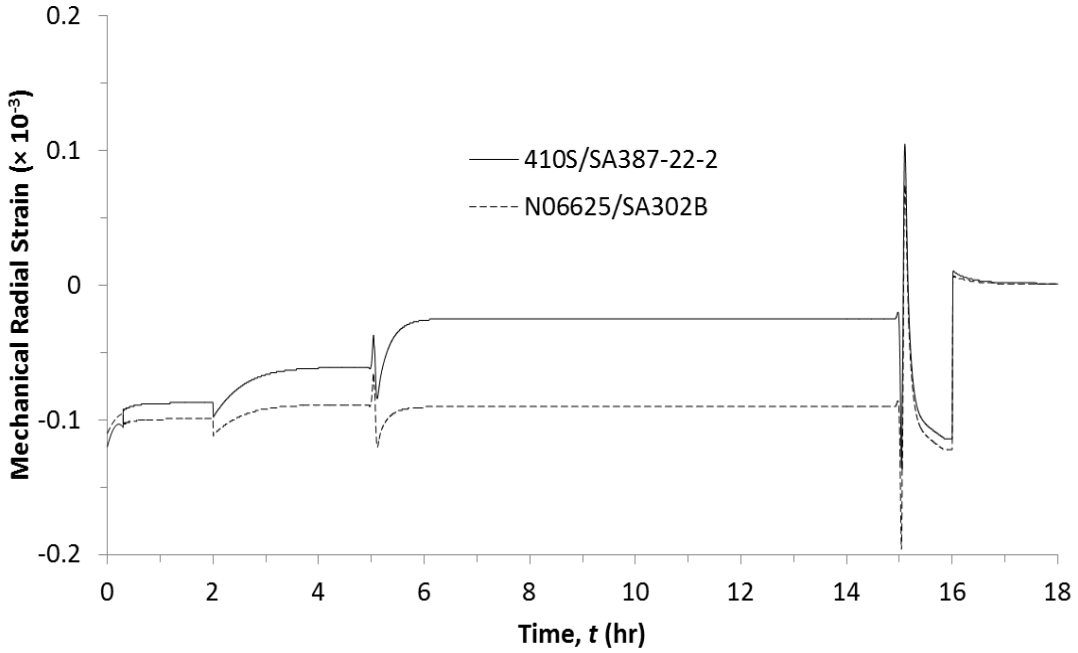

Figure 3.46: Mechanical radial strain at outer surface of coke drum in the process cycle for two different material combinations.

3.10 Analysis of Coke Drums with Practical Experimentally Determined Material Properties

ASME provides minimum specific value of yield strength and tensile strength, etc. as mentioned in the previous chapter. Hence it is important to test the corresponding materials to characterize more accurate mechanical and thermal properties and incorporate those practical material properties in the FE analysis. In the section, results obtained by using AMSE and test data in the analysis will be compared and analyzed. The tests results of the coefficient of thermal expansion and modulus of elasticity of N06625 and SA302B are listed below in Table 3.10.

Table 3.10: Test results of CTE and Modulus of Elasticity of N06625 and SA302B.

Modulus of Elasticity, *E* (GPa)			Thermal Expansion, *CTE* ($1/^oC$)		
Temperature (^oC)	N06625	SA302B	Temperature (^oC)	N06625	SA302B
20	207.1	202.1	20	1.20×10^{-5}	1.10×10^{-5}
100	196.6	198.2	100	1.32×10^{-5}	1.18×10^{-5}
250	195.6	193.2	200	1.38×10^{-5}	1.30×10^{-5}
480	178.5	172.5	300	1.40×10^{-5}	1.41×10^{-5}
			400	1.48×10^{-5}	1.52×10^{-5}
			500	1.70×10^{-5}	1.62×10^{-5}

It can be seen from the above table and Fig. 3.47 that the test results of the CTE of N06625 is higher than the CTE of SA302B. Compressive hoop and axial stresses occurs in the clad materials, while tensile hoop and axial stresses induces in the base materials. As a result all the stress components in the clad materials drop significantly as shown in Figs. 3.48 and 3.50. The maximum differences of the hoop and axial stress in the clad layers between the two cases of ASME data and test data are within 130 MPa and 140

MPa. On the other hand, all the stress components are slightly increased in the base layer as shown in Figs. 3.49 and. 3.51. Figures 3.52 and 3.53 show the variation of von Mises stress over a complete operational cycle at the inner and outer surface for both ASME and test data. Maximum von Mises stress at the hot and cold end for both cases are listed in Table 3.11. From Table 3.11, it is found that the ratio between maximum von Mises stress to yield strength in the clad materials can be reduced significantly form 70% to 19% by including the test data in the analysis. Hence in the next chapter, thermal elastic-plastic analysis will be conducted using the test data of the material properties.

The trend of the graphs of mechanical hoop and axial strain are almost same as shown in from Fig. 3.54 to Fig. 3.57. In this analysis the mechanical radial strain at the inner surface became positive as shown in Fig 3.58.

Table 3.11: Maximum von Mises stress over a complete operation cycle at location 4.

	Test Data				ASME Data			
Location	Hot End		Cold End		Hot End		Cold End	
	Base	Clad	Base	Clad	Base	Clad	Base	Clad
Temperature (^{o}C)	480	482	339	361	480	482	334	355
Von Mises Stress (MPa)	86.7	82.9	62	110	71	126	63	226
Yield Strength (MPa)	291	425	332	443	245	305	281	322
Von Mises/Yield ratio in %	29.8	19.5	18.7	24.8	30.0	41.3	22.4	70.2

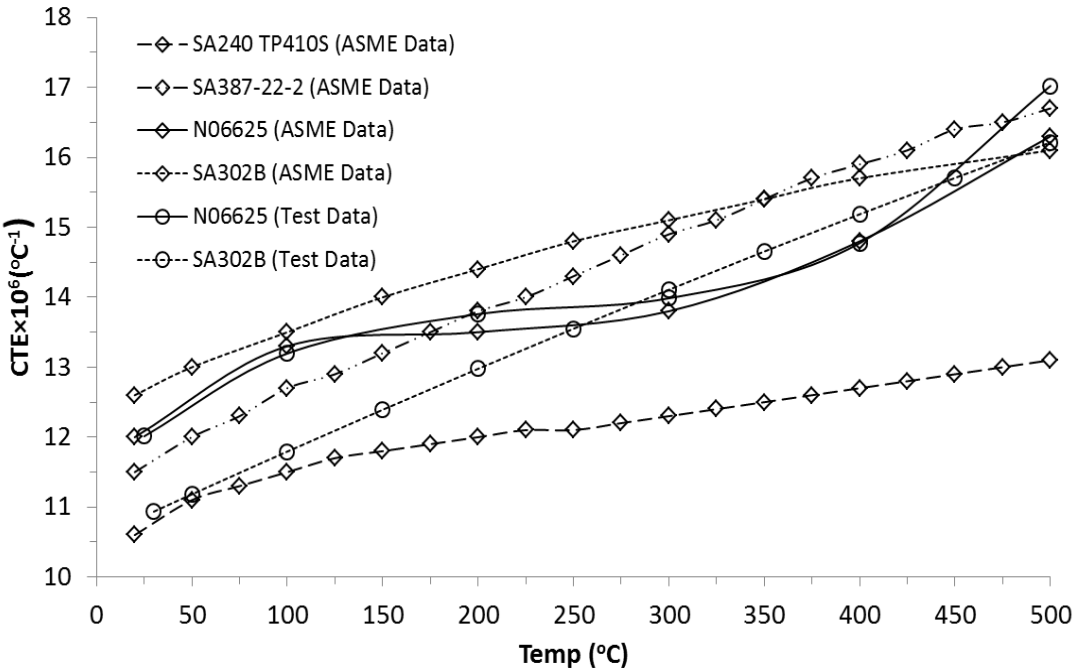

Figure 3.47: Coefficient of thermal expansions of the base and clad materials.

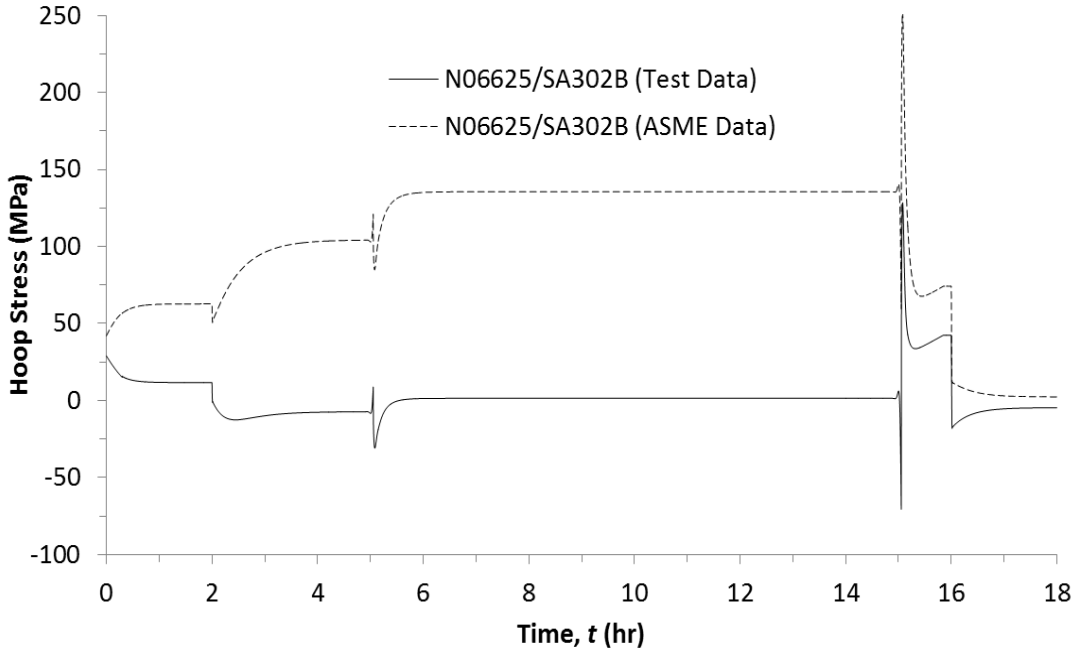

Figure 3.48: Hoop stress at location 4 on the inner surface of coke drum in the process cycle.

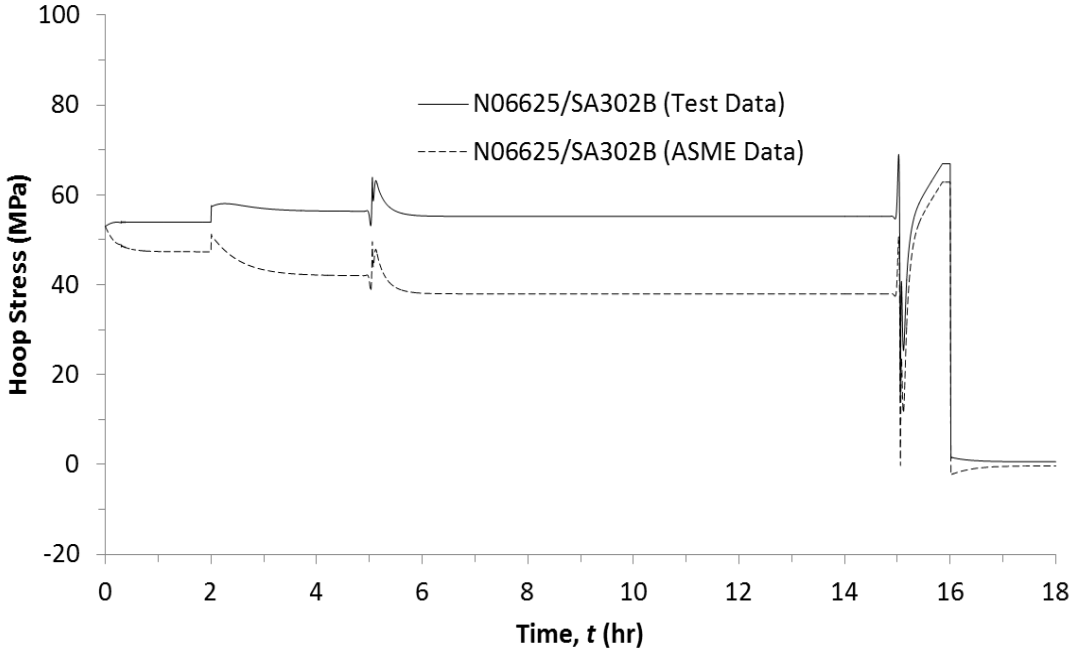

Figure 3.49: Hoop stress at location 4 on the outer surface of coke drum in the process cycle.

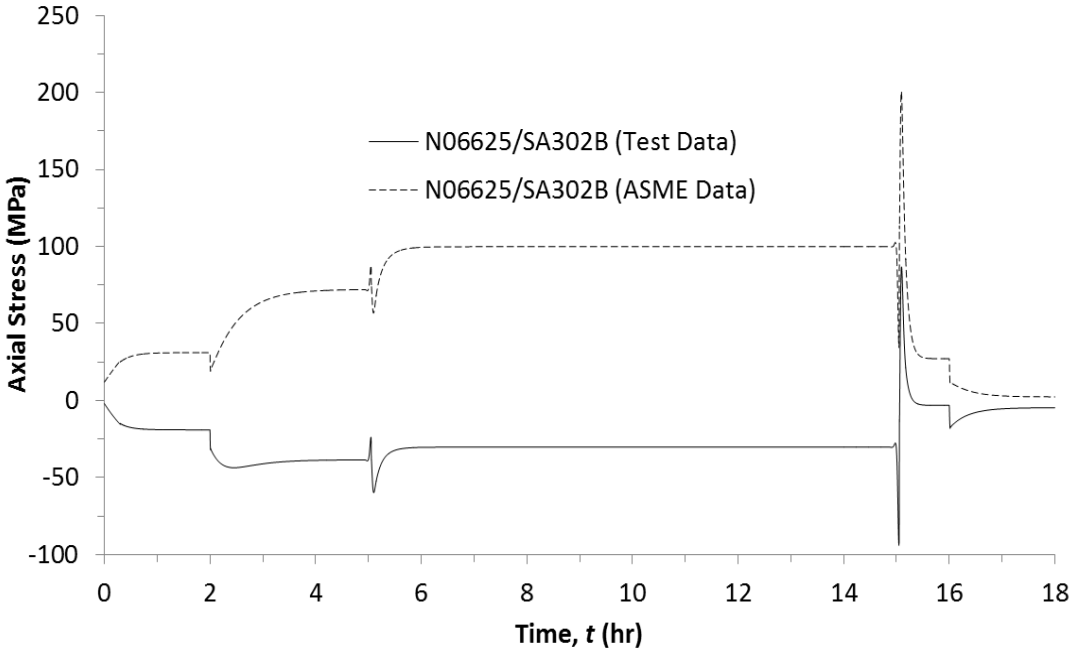

Figure 3.50: Axial stress at location 4 on the inner surface of coke drum in the process cycle.

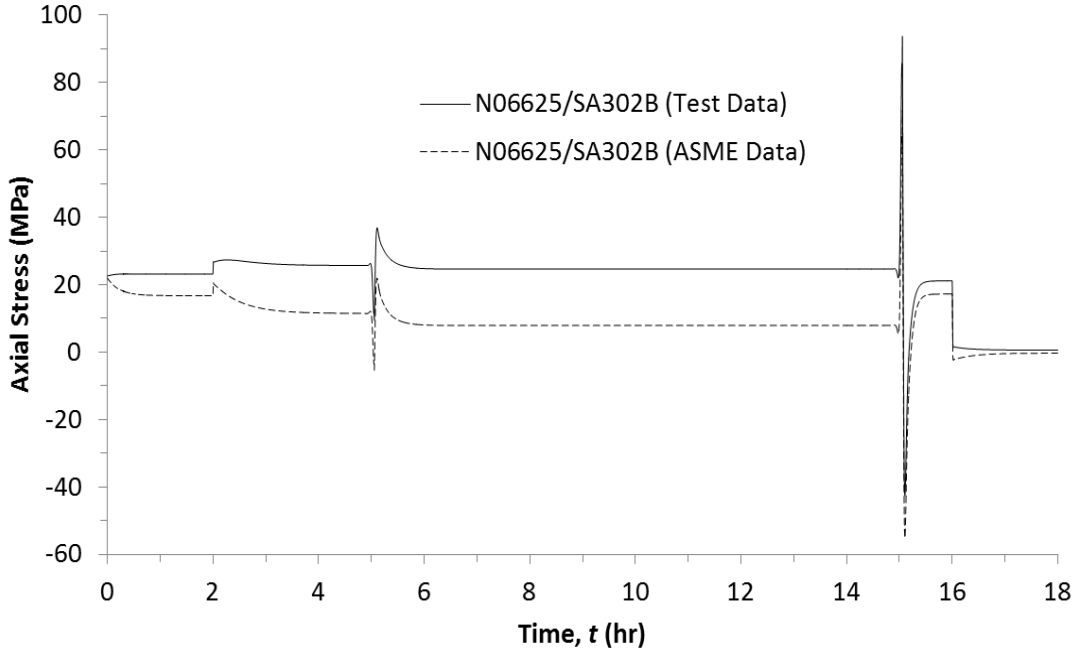

Figure 3.51: Axial stress at location 4 on the outer surface of coke drum in the process cycle.

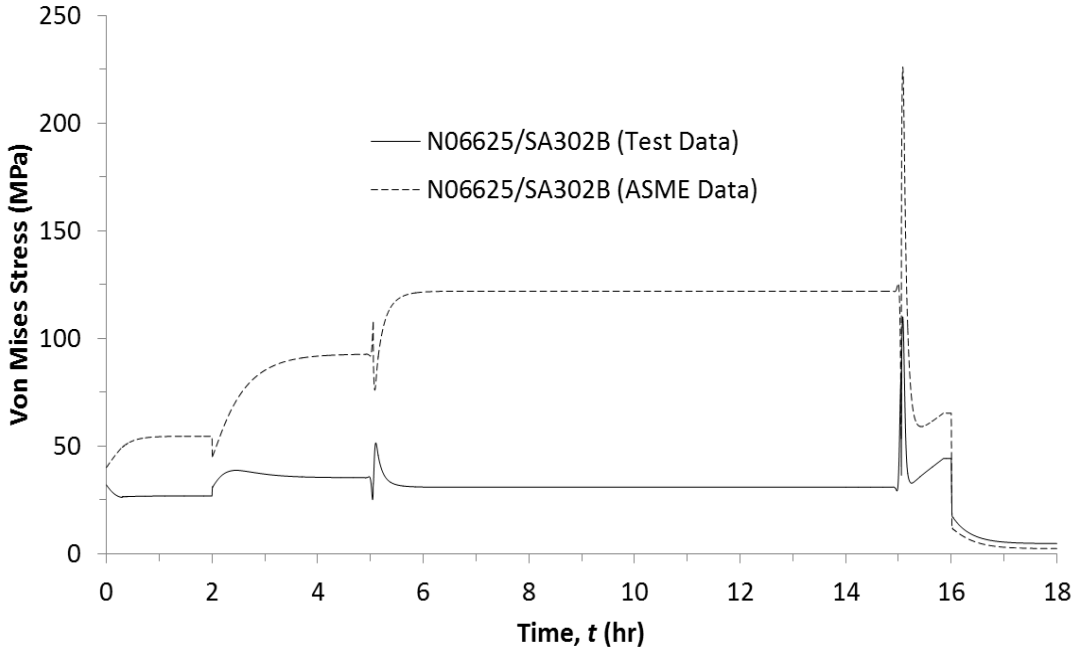

Figure 3.52: Von Mises stress at location 4 on the inner surface of coke drum in the process cycle.

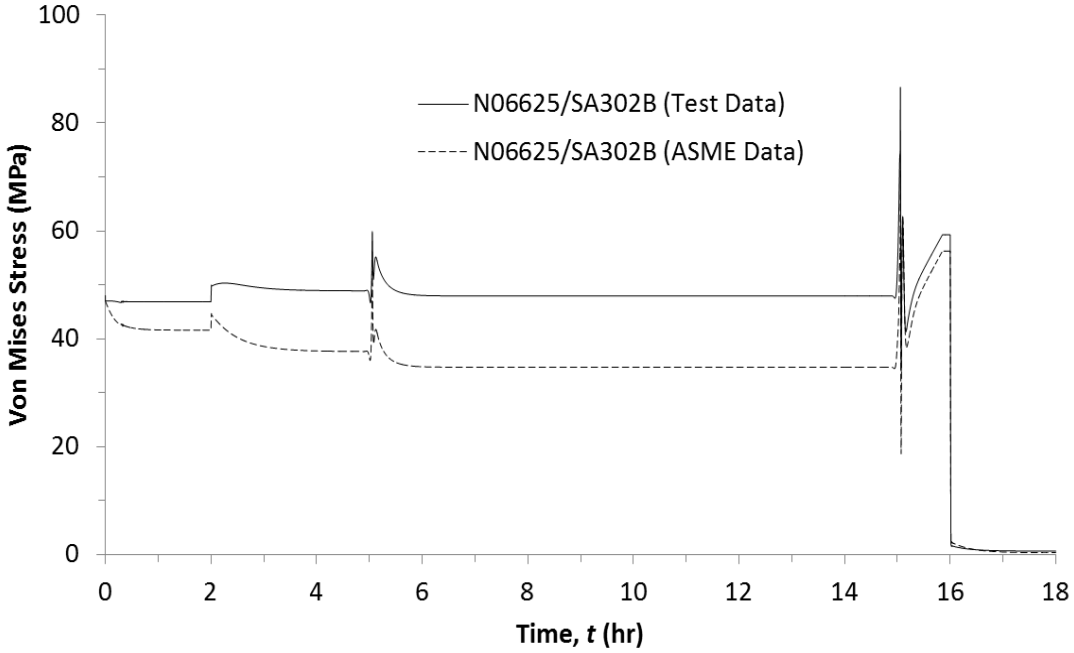

Figure 3.53: Von Mises stress at location 4 on the outer surface of coke drum in the process cycle.

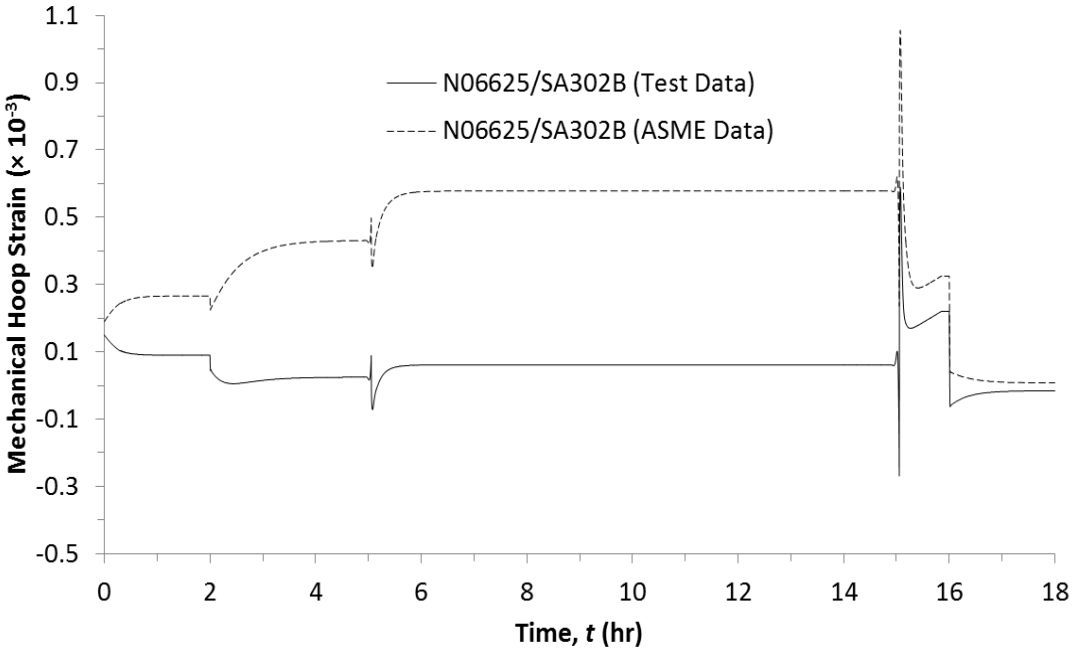

Figure 3.54: Mechanical hoop strain at location 4 on the inner surface of coke drum in the process cycle.

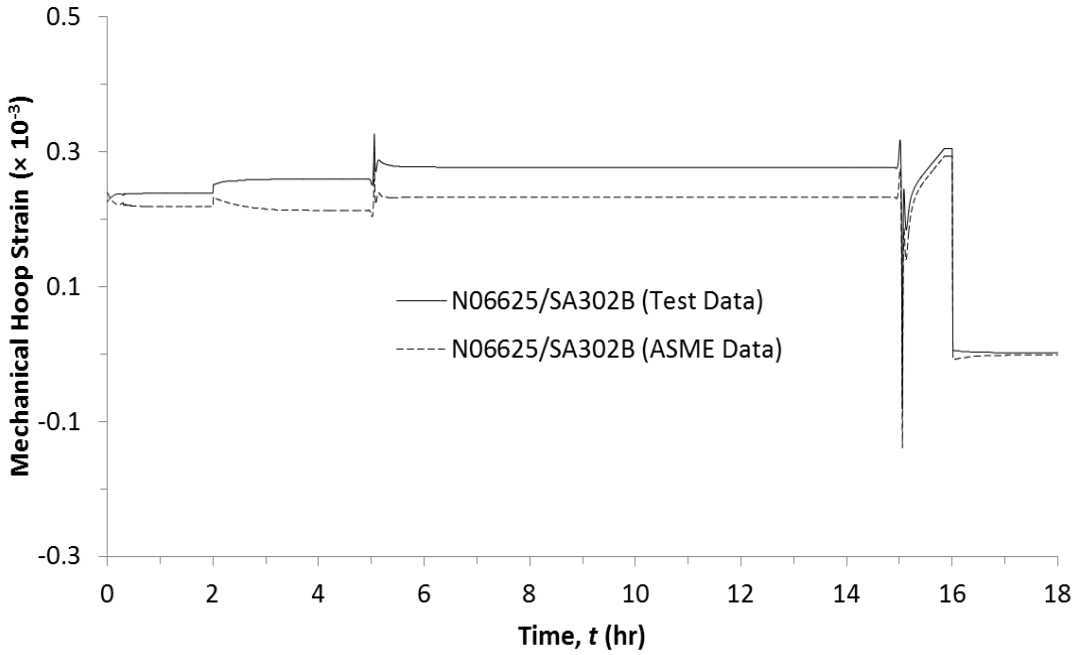

Figure 3.55: Mechanical hoop strain at location 4 on the outer surface of coke drum in the process cycle.

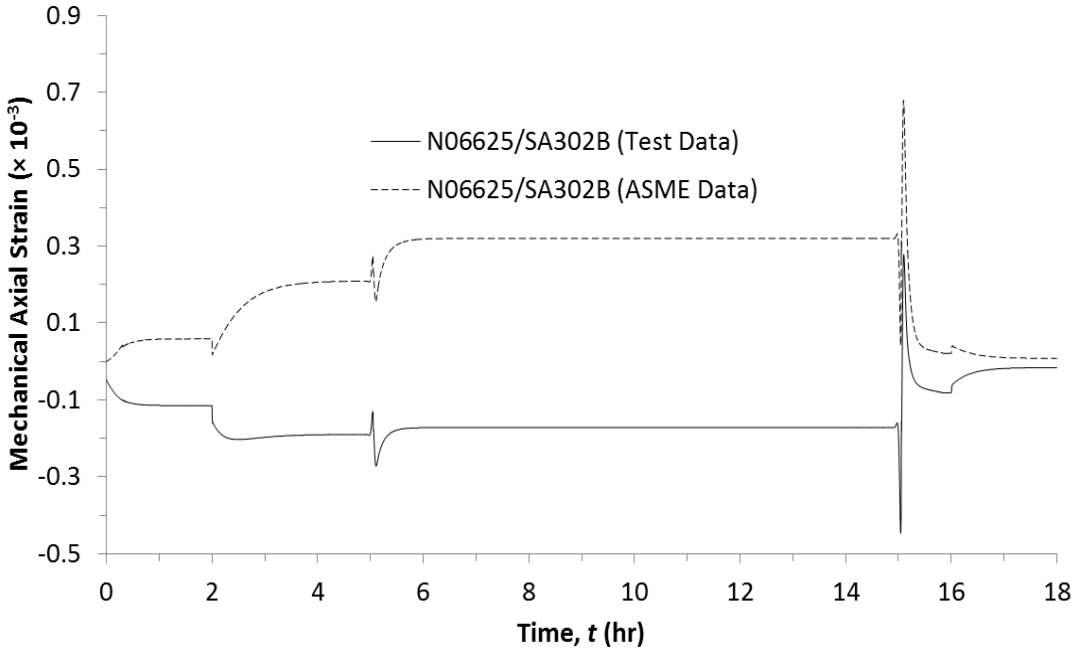

Figure 3.56: Mechanical axial strain at location 4 on the inner surface of coke drum in the process cycle.

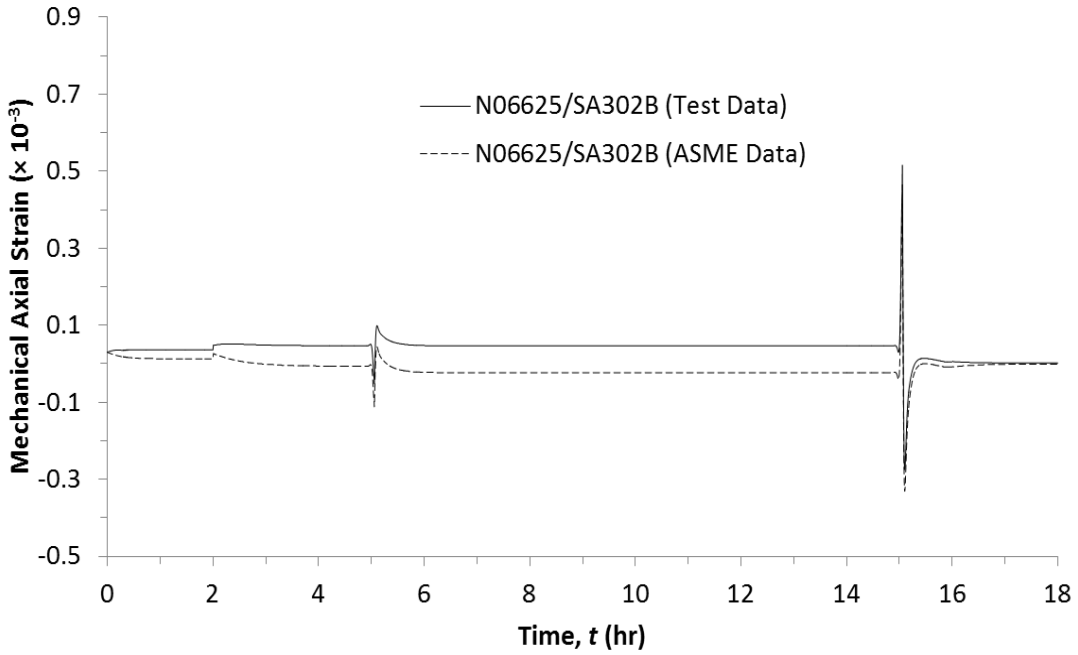

Figure 3.57: Mechanical axial strain at location 4 on the outer surface of coke drum in the process cycle.

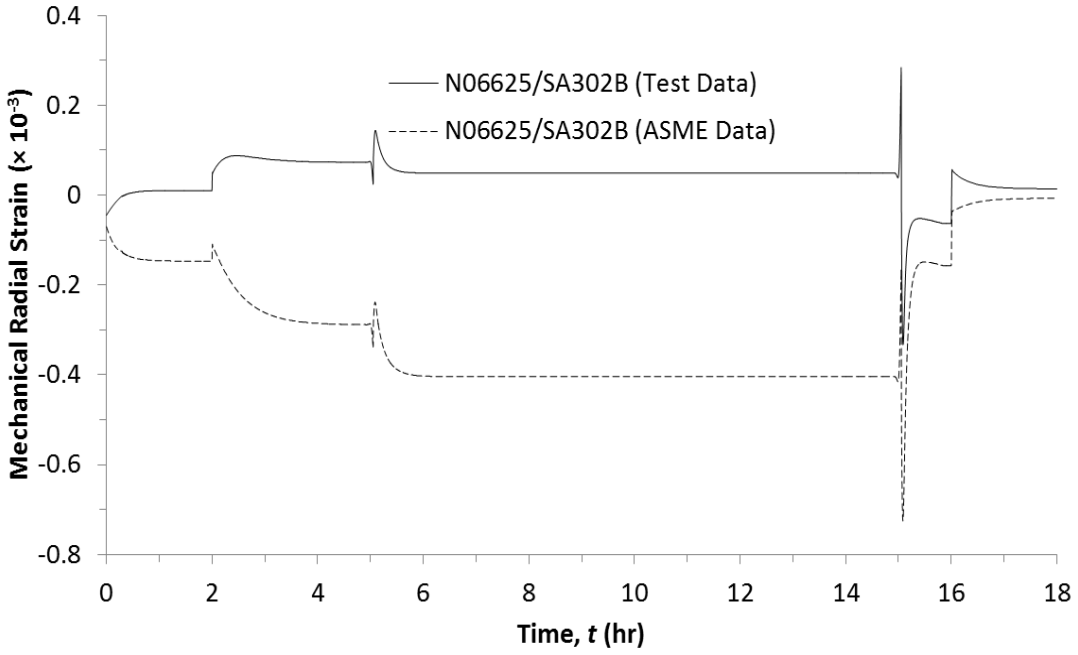

Figure 3.58: Mechanical radial strain at location 4 on the inner surface of coke drum in the process cycle.

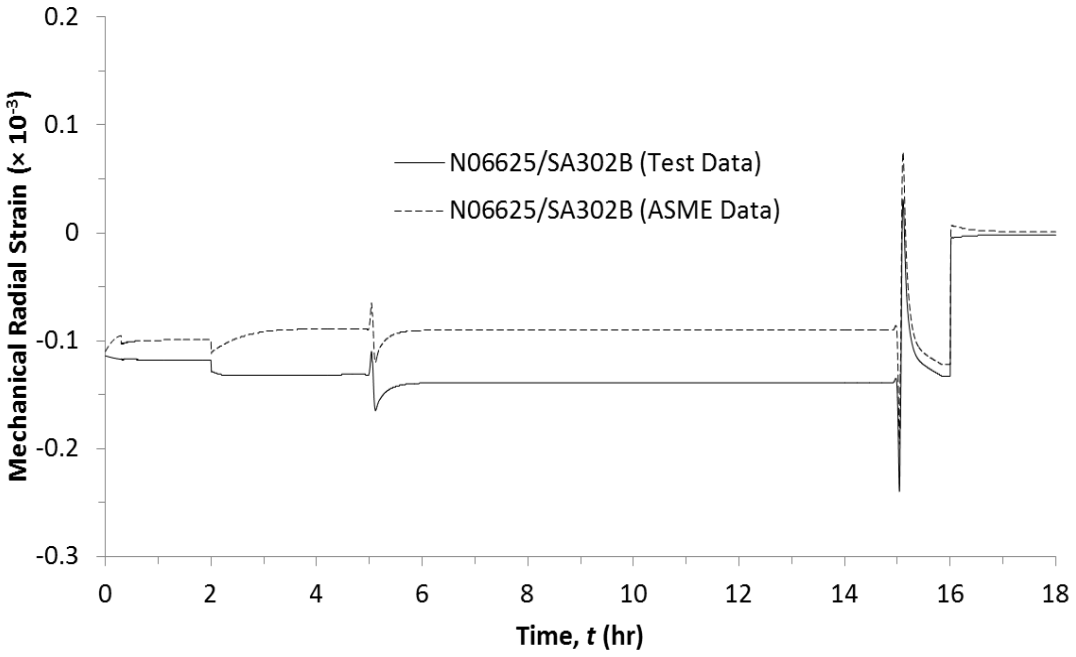

Figure 3.59: Mechanical radial strain at location 4 on the outer surface of coke drum in the process cycle.

Chapter 4 Thermal Elastic-Plastic Analysis of the Coke Drum

4.1 Introduction

In the previous chapter, coupled thermo-elastic analysis of the coke drum was carried out and temperature history and stress and strain over a complete operation cycle were obtained and analyzed. It was found that clad layer of the studied coke drum experienced yielding in a process cycle. To get more practical results as well as to account material nonlinearity, thermal elastic-plastic analysis is required [24].

The objective of this chapter is also to compare stress/strain field in the shell of the coke drum based on the elastic-plastic analysis for the same two pairs of base and clad materials as analyzed in the previous chapter. Since ANSYS does not provide the capacity of coupled thermal elastic-plastic analysis, temperature distribution data from the previous coupled thermo-elastic analysis was used in the analysis. The geometries of the coke drum and mechanical boundary conditions over a process cycle in this model are same as the coupled thermo-elastic analysis. PLANE182, a 2-D 4-Node structural solid element, was employed in the analysis for its plasticity analysis capability. But, to establish the elastic-plastic analysis, more material properties, as we will see below, are required as compared with the elastic analysis. The inelastic behavior of the materials of the coke drum was simulated by the kinematic hardening model to get accurate results.

4.2 Material Properties

Nonlinear cyclic stress-strain curve were experimentally obtained at four different temperatures as shown in chapter 2. Due to the adaptation of the bilinear kinematic hardening model, nonlinear cyclic stress-strain curve has to be represented by bilinear stress-strain curve to obtain three temperature-dependent properties such as yield strength (σ_y), Modulus of Elasticity (E) and tangent modulus (E_t). The minimum specified values of those properties from ASME Boiler and Pressure Vessel Code [12] were not utilized in this model to include practical material properties rather than being too conservative.

Yan and Xia et al [25] explained the procedure to find out those three material parameters from cyclic stress-strain curve as shown in Fig. 4.1. This curve is for base material SA-387-22-2 with the test temperature at 100^o C. Modulus of Elasticity (E) is obtained by the slope of the stress-strain curve in the proportional elastic region which is represented by line x as shown in Fig. 4.1. Since the absolute value of the obtained strain is always less than 0.5%, a vertical line y is drawn from the abscissa at 0.5% strain amplitude. A tangent line z is then drawn at the point of intersection of the line y and stress-strain curve. The slope of that line z represents the tangent modulus (E_t). Finally, the yield strength (σ_y) is obtained from the intersection of the two lines x and z. Following the same procedure, those three material properties of all base and clad materials at different temperatures were acquired and listed in Table 4.1 and Table 4.2.

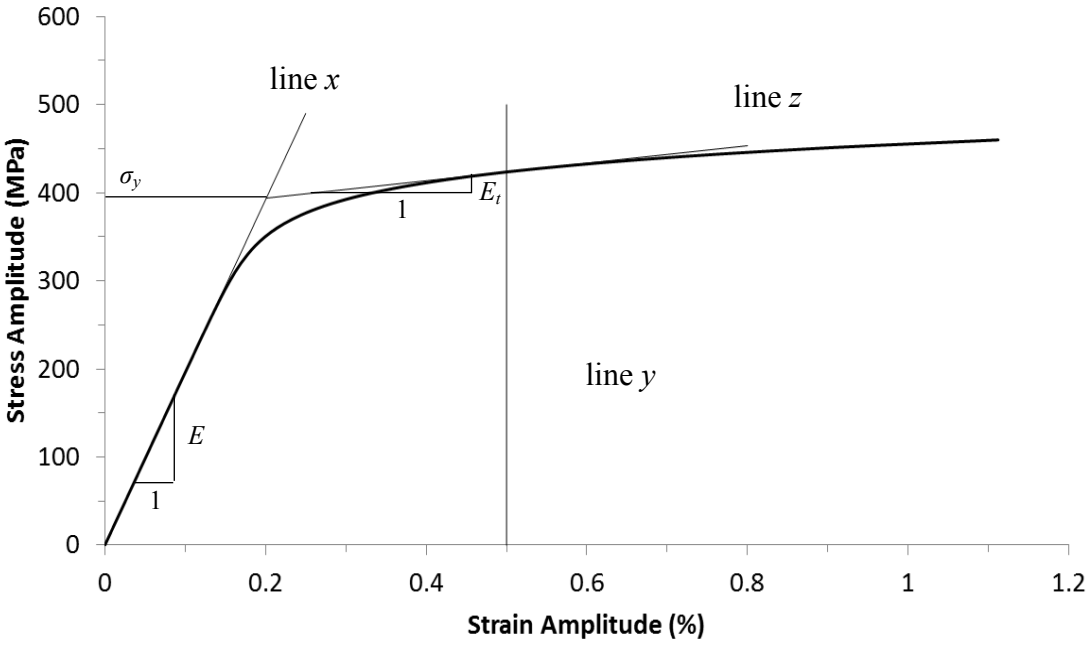

Figure 4.1: Typical cyclic stress-strain curve for base material at 100°C.

Table 4.1: Material properties of the clad materials based on cyclic stress-strain curve.

	SA240 TP410S			N06625		
Temp. (°C)	*E* (GPa)	σ_y (MPa)	E_t (MPa)	*E* (GPa)	σ_y (MPa)	E_t (MPa)
R.T.	179.3	280.0	11163	215.9	638.9	21117
100	178.0	274.0	8145	216.6	552.3	23112
250	165.5	222.0	10168	214.0	537.1	17576
480	167.3	192.4	5565	189.2	474.3	32473

Table 4.2: Material properties of the base materials based on cyclic stress-strain curve.

	SA387-22-2			SA302B		
Temp. (°C)	*E* (GPa)	σ_y (MPa)	E_t (MPa)	*E* (GPa)	σ_y (MPa)	E_t (MPa)
R.T.	204.0	438.8	8985	205.8	385.0	11372
100	196.0	394.0	9928	208.6	348.0	12556
250	187.9	364.5	9276	190.5	341.0	13576
480	176.0	330.9	8187	168.0	366.0	12845

4.3 Kinematic Hardening Formulations

Kinematic hardening models used to model the behavior of materials of coke drum, which is subjected to cyclic thermal and mechanical loadings, are suited to analyze the low cycle fatigue and ratcheting behaviors [24]. For bilinear kinematic hardening, the yield criteria is [26],

$$F(\{\sigma\}, k, \{\alpha\}) = 0 \qquad (4.1)$$

where, {σ} and $\{\alpha\}$ are the stresses and translation of yield surface or backstress respectively. *k* is the sum of the plastic work done over the history of loading.

But when equivalent stress (σ_e) is equal to the yield strength (σ_y), the material is starting to yield. Therefore the yield criteria from equation (4.1) becomes [26],

$$F = \sigma_e - \sigma_y = \left[\frac{3}{2}(\{s\} - \{\alpha\})^T [M](\{s\} - \{\alpha\})\right]^{\frac{1}{2}} - \sigma_y = 0$$

where, $\{s\}$ = deviatoric stress vector and $[M] = \begin{bmatrix} 1 & 0 & 0 & 0 & 0 & 0 \\ 0 & 1 & 0 & 0 & 0 & 0 \\ 0 & 0 & 1 & 0 & 0 & 0 \\ 0 & 0 & 0 & 2 & 0 & 0 \\ 0 & 0 & 0 & 0 & 2 & 0 \\ 0 & 0 & 0 & 0 & 0 & 2 \end{bmatrix}$

The associated flow rule for kinematic hardening model is [26]:

$$\{d\varepsilon^{pl}\} = \lambda\left\{\frac{\partial Q}{\partial \sigma}\right\}$$

where, λ is the plastic multiplier and $\left\{\frac{\partial Q}{\partial \sigma}\right\} = \left\{\frac{\partial F}{\partial \sigma}\right\} = \frac{3}{2\sigma_e}(\{s\} - \{\alpha\})$, and the back stress can be defined as $\{\alpha\} = 2G\{\varepsilon^{sh}\}$, where G is the shear modulus.

The shift strain at p-step can be calculated as follows:

$$\left\{\varepsilon_p^{sh}\right\} = \left\{\varepsilon_{p-1}^{sh}\right\} + \{\Delta\varepsilon^{sh}\}$$

where, $\{\Delta\varepsilon^{sh}\} = \frac{C}{2G}\{\Delta\varepsilon^{pl}\}$

$$C = \frac{2}{3}\frac{EE_t}{E - E_t}.$$

Here, all the material properties such yield strength (σ_y), modulus of elasticity (E) and tangent modulus of elasticity (E_t) are function of temperatures. More details of this elastic –plastic theory can be found in Ref. [26].

4.4 Results and Discussion

The time history of stresses and strains over a process cycle at location 4 of the base and clad layers are presented in Fig. 4.2 to Fig. 4.13. This current analysis gives a lower stress level as a result of higher strain level in the clad material of TP410S compared to the coupled thermo-elastic analysis. This is because of that TP410S yields during a process cycle. Additionally, elasto-plastic analysis gives more accurate and practical results compared to the elastic analysis. It is also found that the base layer SA387-22-2 is still in the elastic range. As explained in the previous chapter, due to the large difference of the coefficient of thermal expansion of these two materials and smaller thickness of the clad layer compared to the base layer, significant stress level beyond the yield strength develops in the clad layer of TP410S compared to SA387-22-2. The more severe fully reversed axial and hoop stresses develop in the clad layer during water quenching stage. The von Mises stresses in both clad and base materials of the optional material combinations are in the elastic stress range.

As seen in Figs. 4.2, 4.4, and 4.6 all the stresses in TP410S exceed the limit of yield strength, while stresses in N06625 are far below its yield strength. As a consequence, very high strains induced in TP410S as shown in Figs. 4.8, 4.10 and 4.12. Fig. 4.14 presents equivalent plastic strain over a process cycle in the clad layer at location 4. It is found that yielding starts at the oil filling stage in TP410S, while there is no sign of plastic strain in N06625 as shown in Fig. 4.14. That indicates that permanent plastic strain happens in the first process cycle in TP410S and accumulates in the subsequent cycle that will contribute the shakedown and ratcheting behavior in the coke drum. Summary of the stresses and strains developed in the clad layer at location 4 is listed in Table 4.3.

There is no significant amount of stresses developed in both base layers to exceed the yield strength as can be seen from Figs. 4.3, 4.5and 4.7. It is also visible from Table 4.4 where the summary of stresses and strains in the base layers is recorded. Though both base layers are still in the elastic range, maximum absolute strains induced in SA 387-22-2 are higher than SA302B as found in Figs. 4.9, 4.11 and 4.13. No permanent plastic strain occurs in both base layers as shown in Fig. 4.15.

Table 4.3: Summery of stresses (MPa) and strains ($\times 10^{-3}$) of the clad layers

	SA240 TP410S				N06625			
	Minimum	Maximum	Amplitude	Mean	Minimum	Maximum	Amplitude	Mean
σ_{zz}	-89.0	190.7	139.9	50.9	-97.6	93.6	95.6	-2.0
$\sigma_{\theta\theta}$	-106.3	222.6	164.5	58.1	-74.3	138.4	106.4	32.1
σ_{Mises}	-	204.3	-	-	-	119.0	-	-
ε_{rr}	-1.604	-0.108	0.748	-0.86	-0.334	0.280	0.307	-0.027
ε_{zz}	0.021	1.150	0.565	0.586	-0.439	0.276	0.358	-0.082
$\varepsilon_{\theta\theta}$	0.073	1.571	0.749	0.822	-0.269	0.590	0.430	0.161
$\widehat{\varepsilon_{pl}}$	-	0.900	-	-	-	0.000	-	-

Table 4.4: Summery of stresses (MPa) and strains ($\times 10^{-3}$) of the base layers

	SA387-22-2				SA302B			
	Minimum	Maximum	Amplitude	Mean	Minimum	Maximum	Amplitude	Mean
σ_{zz}	-56.0	74.9	65.5	9.5	-42.1	93.0	67.6	25.5
$\sigma_{\theta\theta}$	-8.80	75.6	42.2	33.4	0.63	68.4	33.9	34.5
σ_{Mises}	-	78.9	-	-	-	86.2	-	-
ε_{rr}	-1.054	-0.029	0.513	-0.54	-0.244	0.030	0.137	-0.107
ε_{zz}	-0.153	0.816	0.485	0.332	-0.276	0.526	0.401	0.125
$\varepsilon_{\theta\theta}$	0.162	0.861	0.350	0.512	-0.082	0.332	0.207	0.125

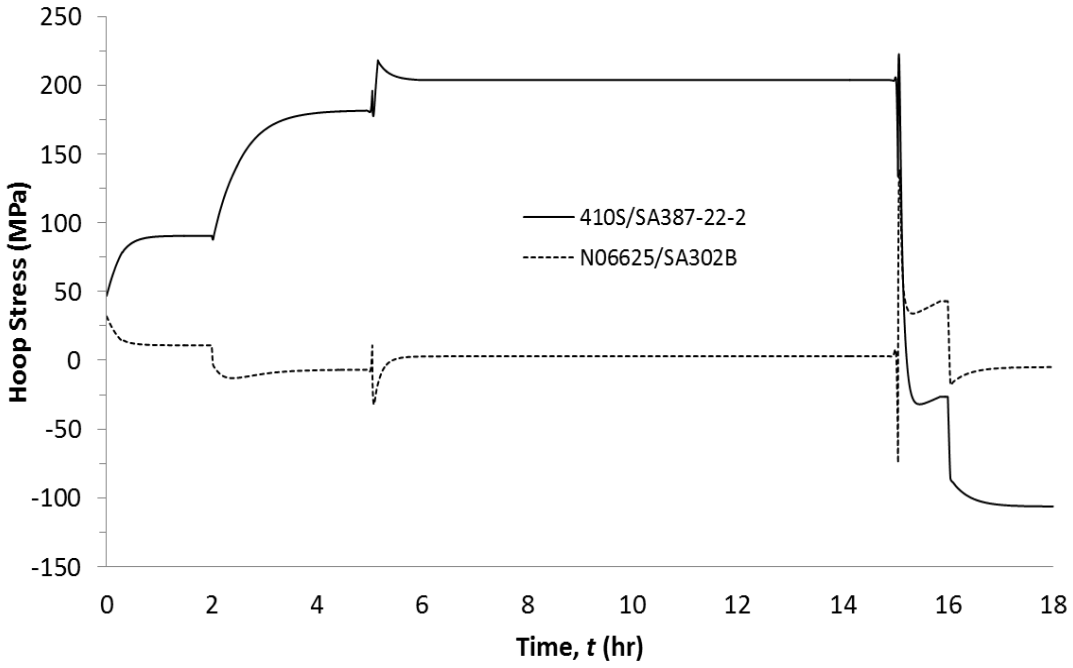

Figure 4.2: Hoop stress at the internal surface (Clad layer) for two different material combinations.

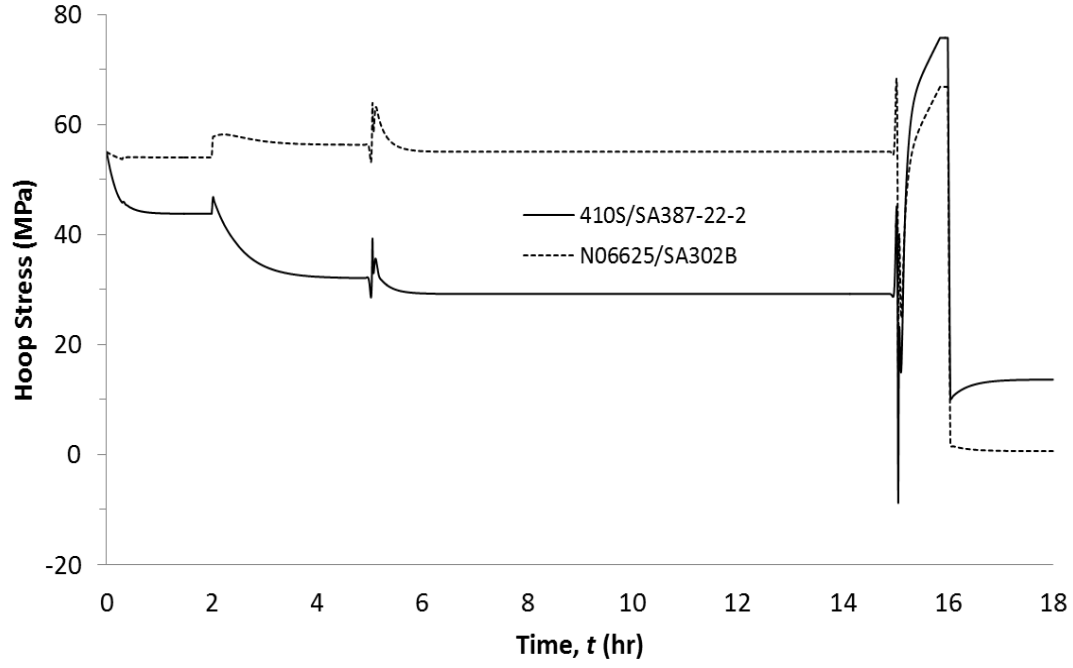

Figure 4.3: Hoop stress at the outer surface (Base layer) for two different material combinations.

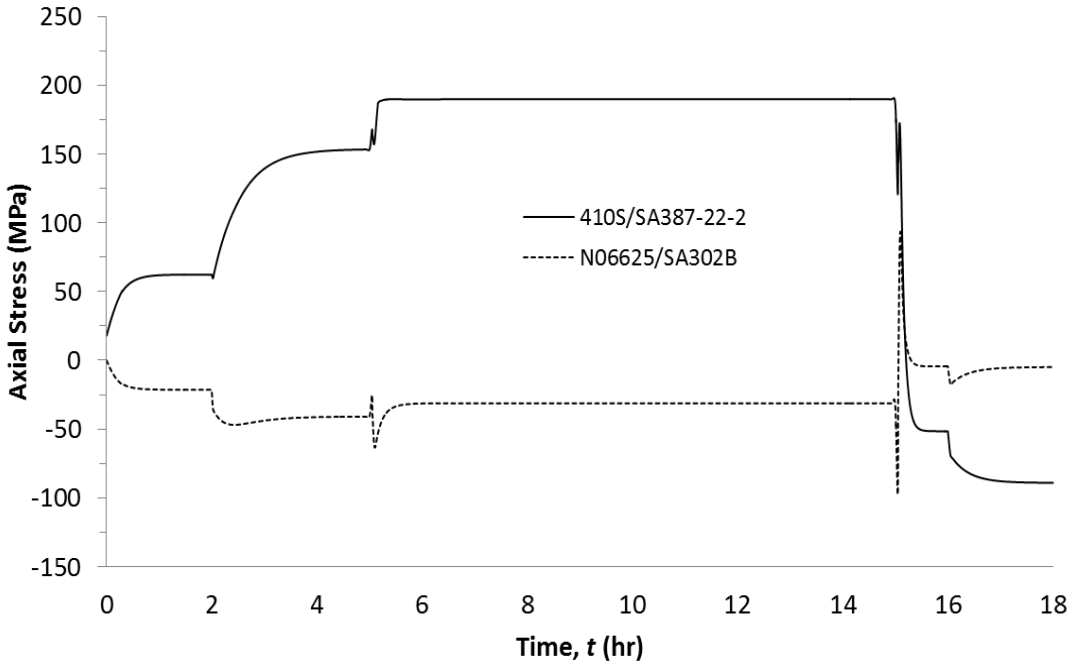

Figure 4.4: Axial stress at the internal surface (Clad layer) for two different material combinations.

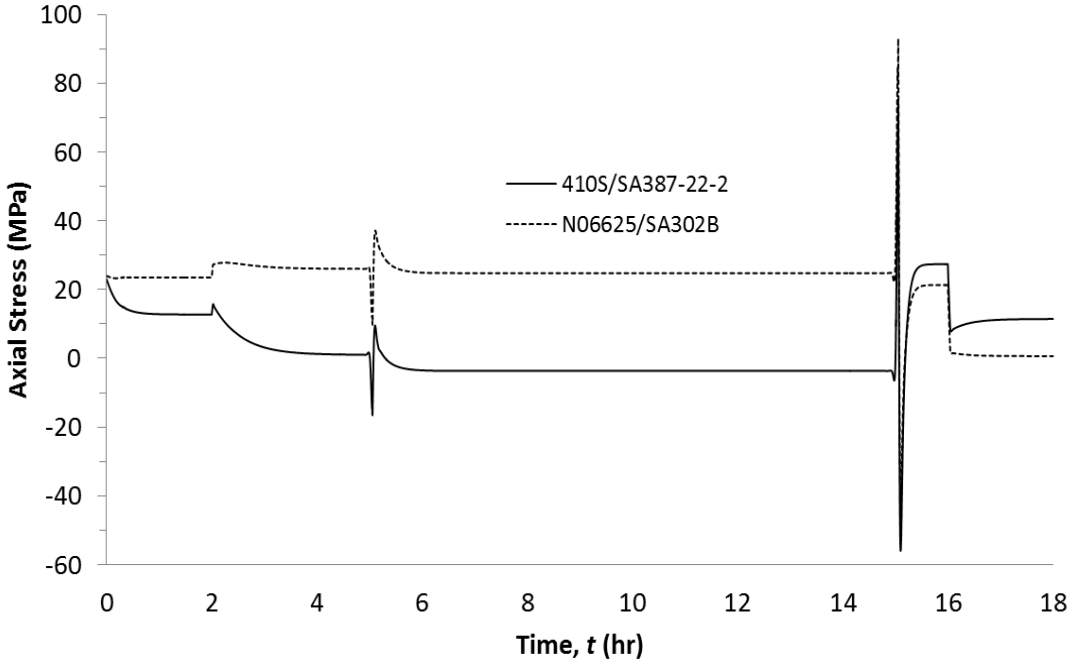

Figure 4.5: Axial stress at the outer surface (Base layer) for two different material combinations.

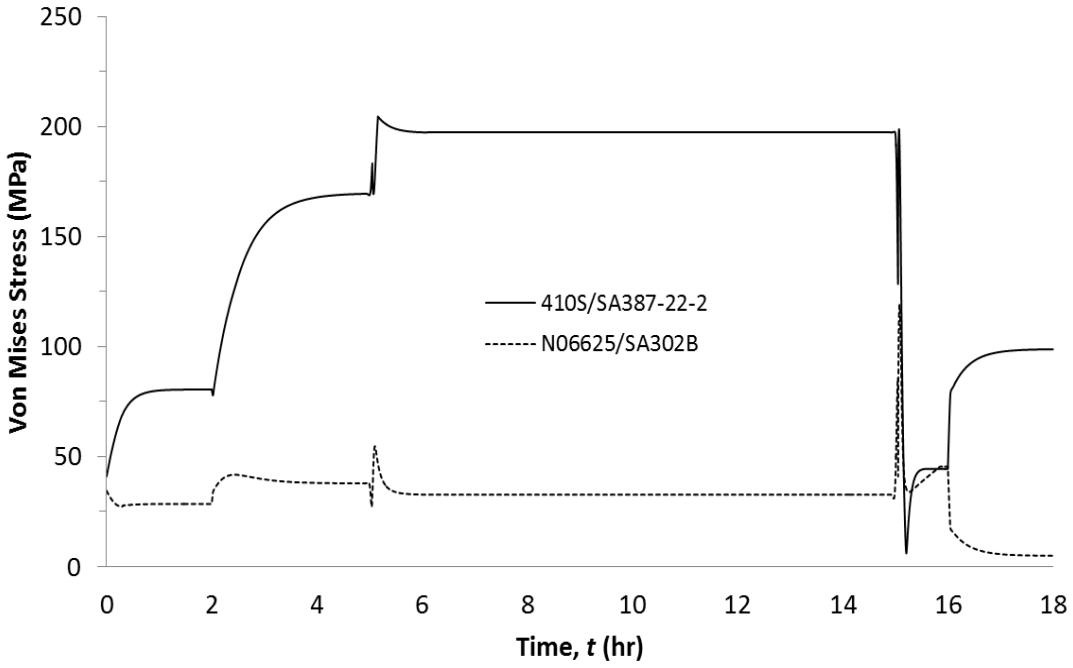

Figure 4.6: Von Mises stress at the internal surface (Clad layer) for two different material combinations.

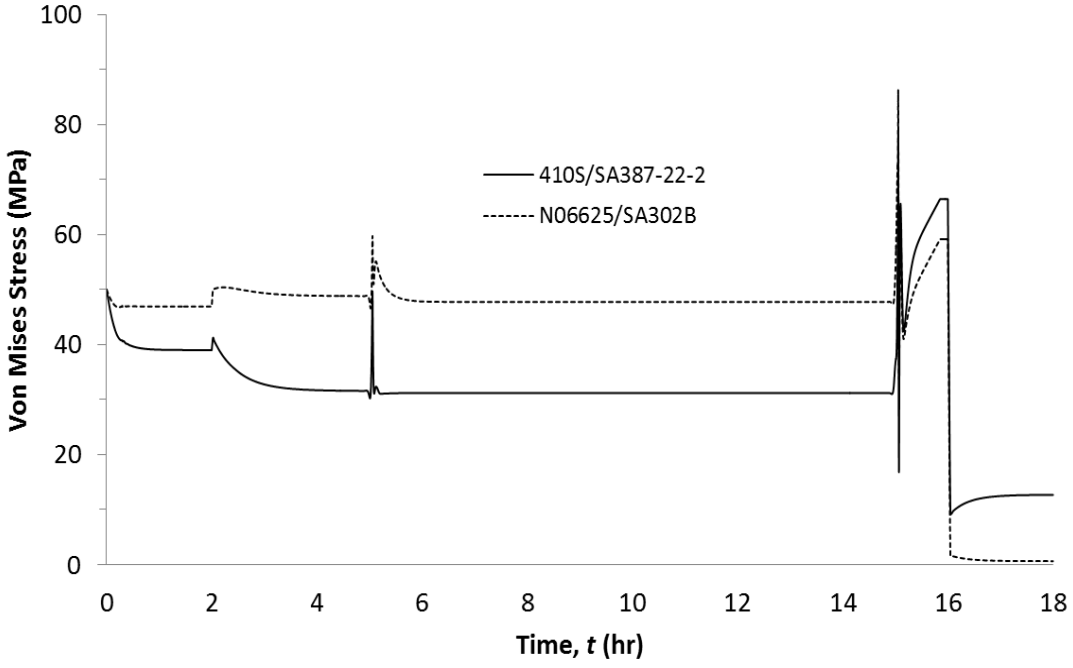

Figure 4.7: Von Mises stress at the outer surface (Base layer) for two different material combinations.

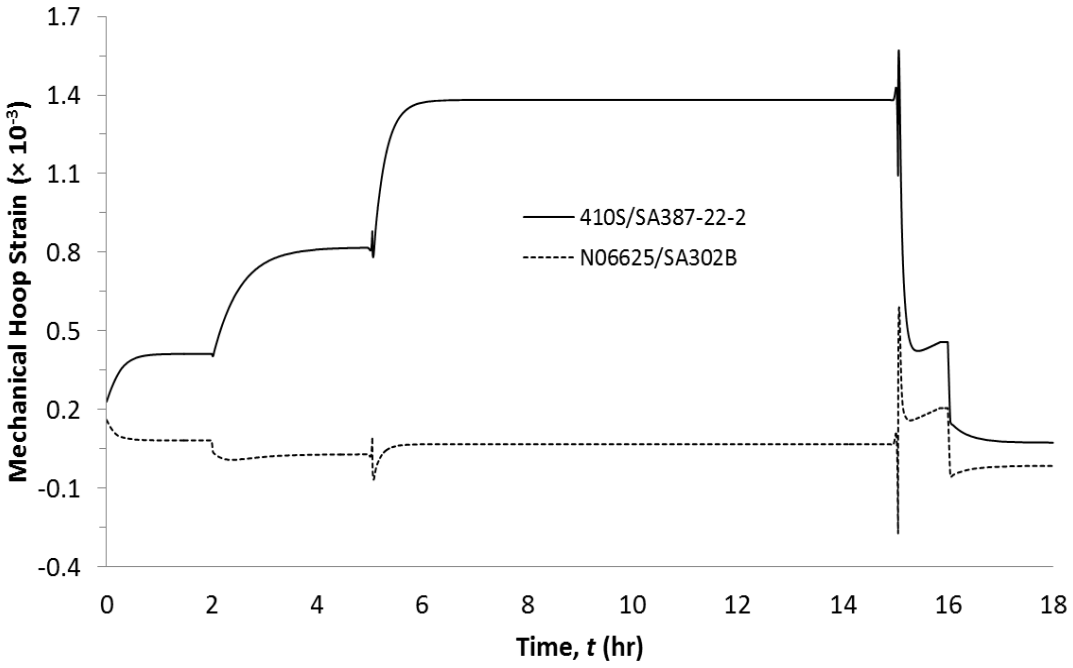

Figure 4.8: Mechanical hoop strain at the internal surface (Clad layer) for two different material combinations.

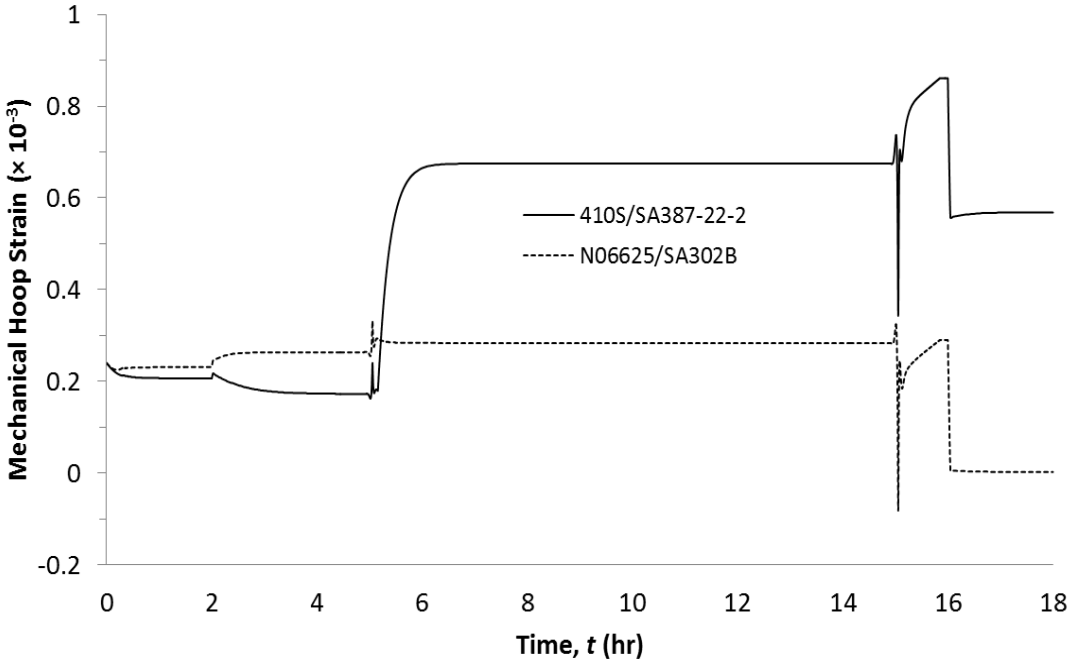

Figure 4.9: Mechanical hoop strain at the outer surface (Base layer) for two different material combinations.

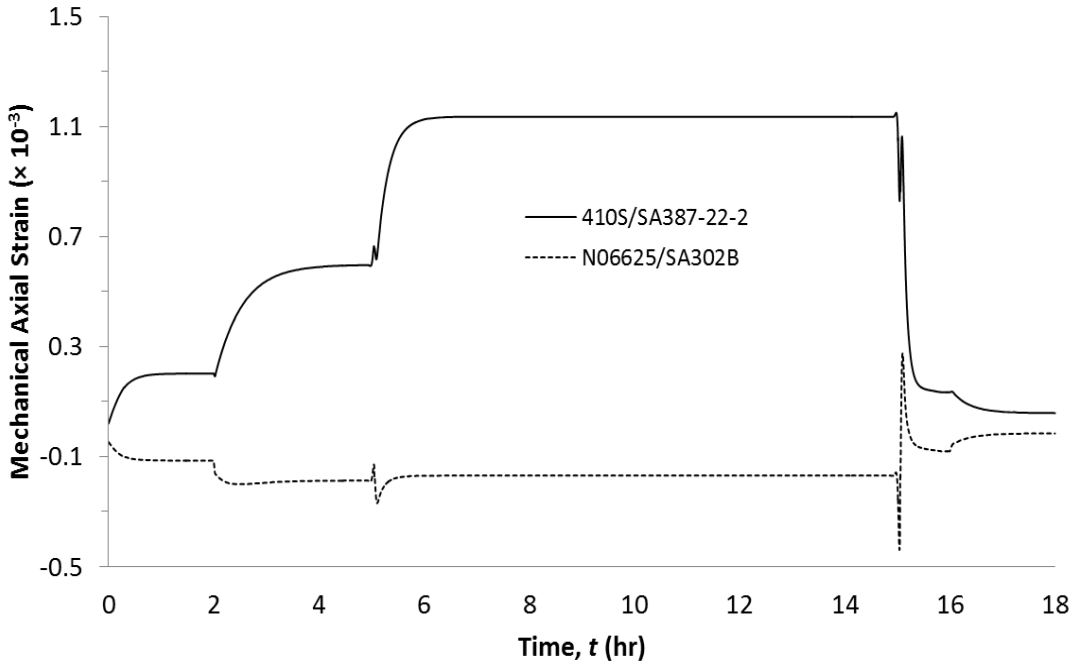

Figure 4.10: Mechanical axial strain at the internal surface (Clad layer) for two different material combinations.

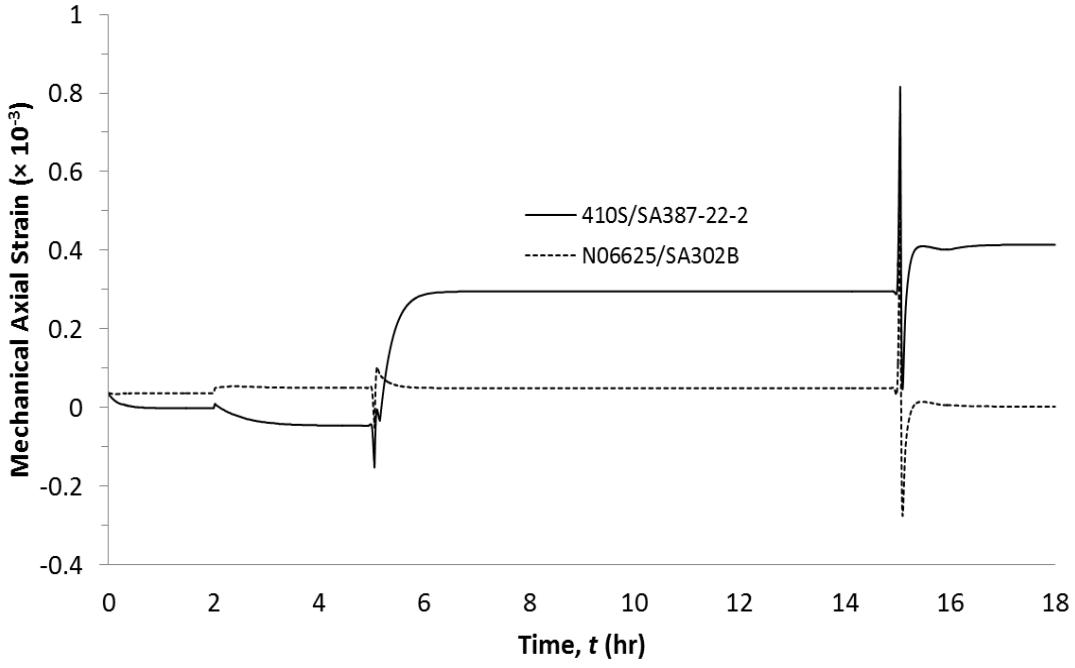

Figure 4.11: Mechanical axial strain at the outer surface (Base layer) for two different material combinations.

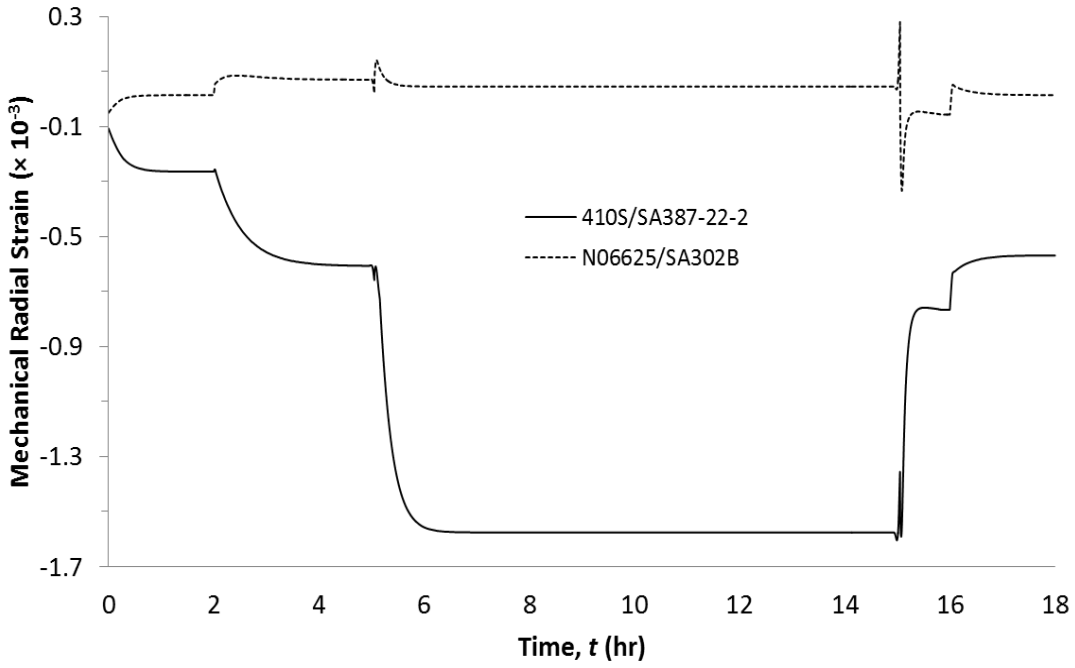

Figure 4.12: Mechanical radial strain at the internal surface (Clad layer) for two different material combinations.

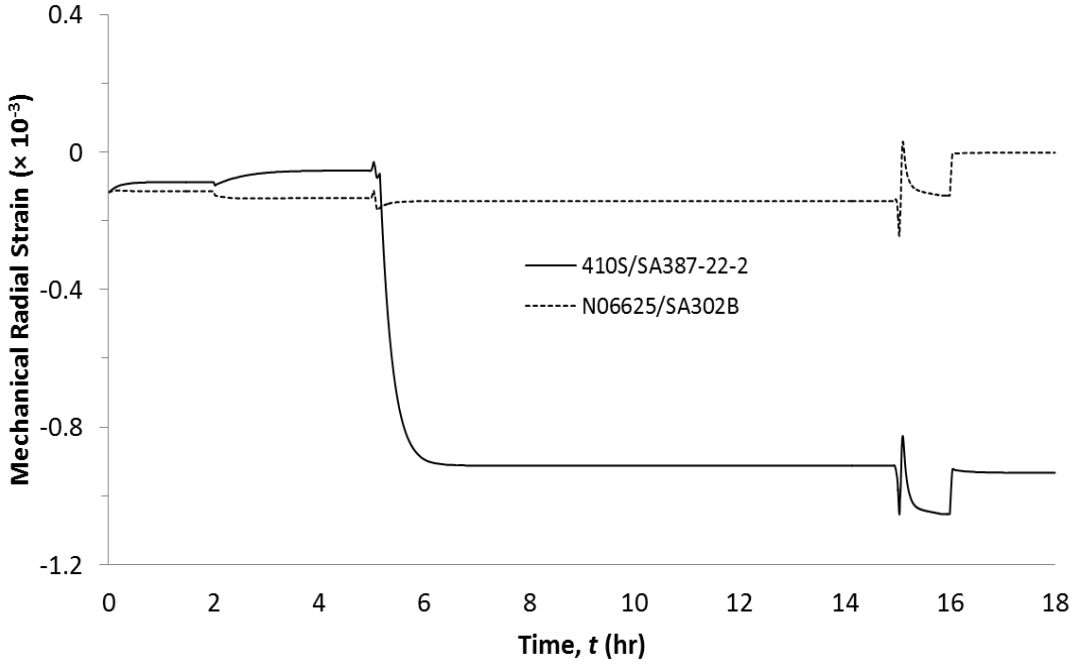

Figure 4.13: Mechanical radial strain at the outer surface (Base layer) for two different material combinations.

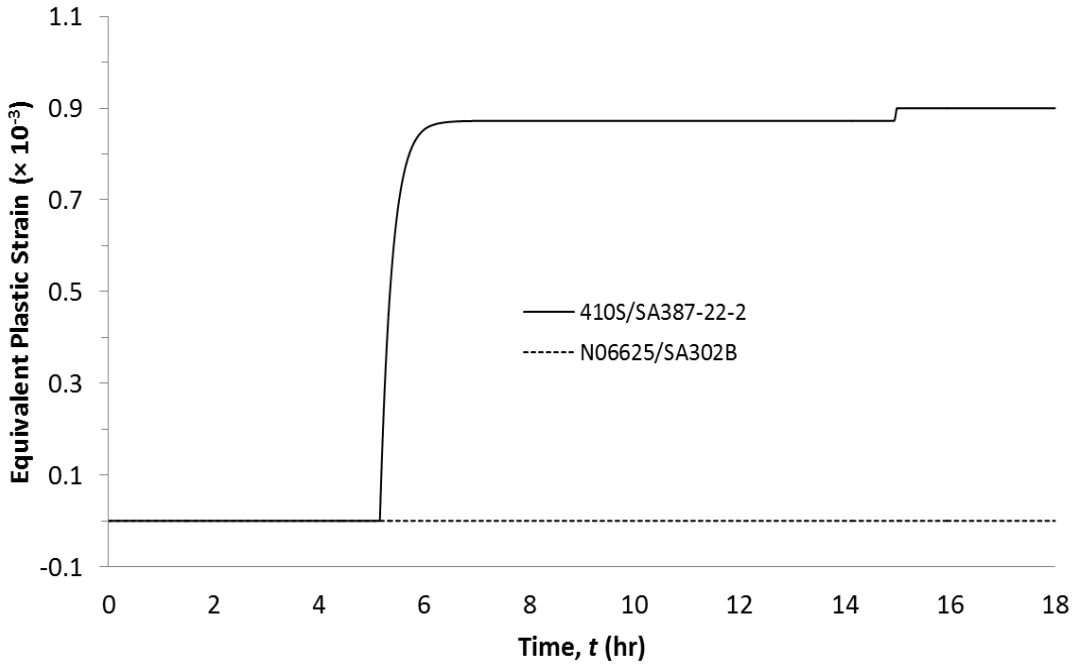

Figure 4.14: Equivalent plastic strain at the internal surface (Clad layer) for two different material combinations.

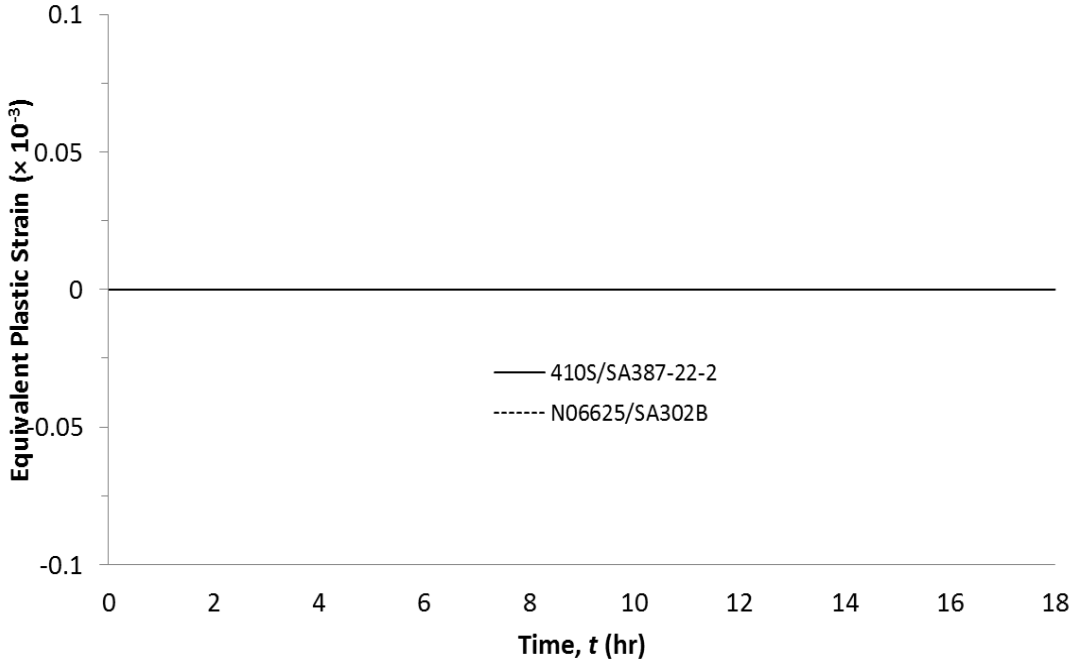

Figure 4.15: Equivalent plastic strain at the outer surface (Base layer) for two different material combinations.

Since the permanent plastic deformation happens in the material combinations of TP410S/SA387-22-2 in the first operational cycle, the performance and life of the coke drum will be reduced significantly due to elastic/plastic shakedown and ratcheting behavior of the coke drum. The mechanical behavior of the coke drum shell subjected to two cycles of thermal and pressure loadings is thus analyzed as shown in Fig. 4.16. The difference between the final equivalent plastic strains of the two cycles is 1.4×10^{-07}, which is very small. Since still there is accumulation of plastic strain after the first cycle, plastic shakedown happens in the clad layer of the currently used coke drum.

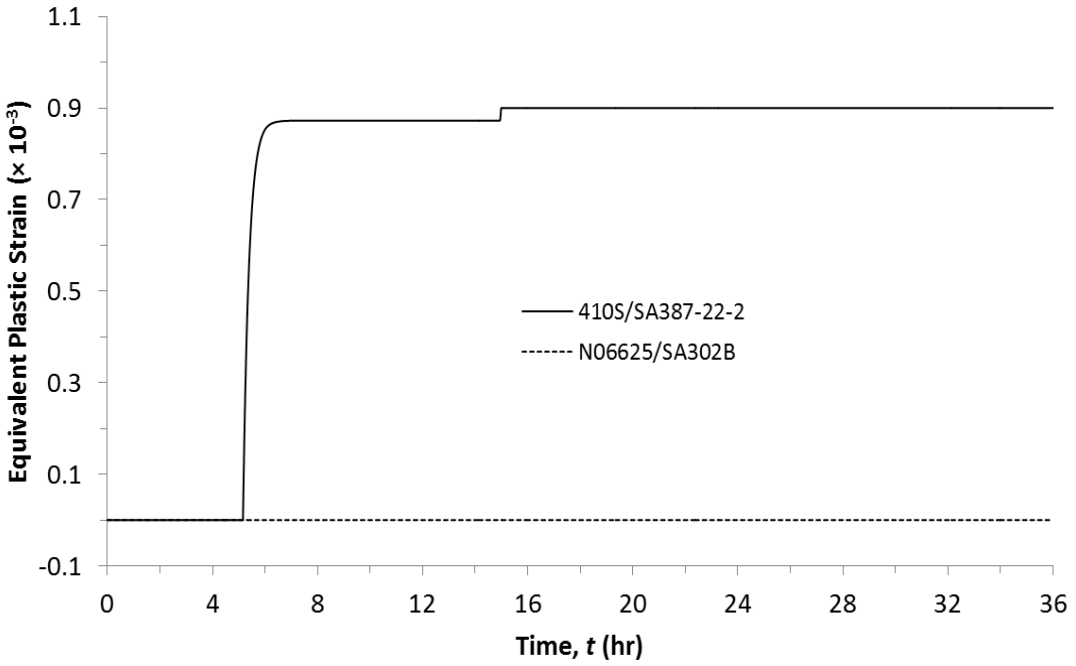

Figure 4.16: Equivalent plastic strain at the clad layer for two cycles of operation.

On the other hand, the maximum stress developed over an operational cycle in the clad/base layer for the material combinations N06625/SA302B is far below the elastic stress limit. So, it can be concluded that the performance of the coke drum can be improved by the selection of the optional material combinations N06625/SA302B.

Chapter 5 Conclusions

5.1 Summary

In order to choose an optimal material combination of the coke drums, the mechanical and thermal properties of the optional material combination of N06625 /SA302B are characterized and compared with the properties of currently used material combination of TP410S/SA-387-22-2. A thermal-mechanical material testing system, which is capable to perform tests under monotonic or cyclic loadings at room or elevated temperatures, is used to obtain monotonic and cyclic mechanical properties of those materials. This testing system is also employed to perform CTE measurements and isothermal low cycle fatigue (ILCF) tests. Monotonic mechanical properties of N06625 and SA302B satisfy the minimum requirement of section II of the ASME Boiler and Pressure Vessel Code. The monotonic mechanical properties of N06625 and SA302B are greater than ASME data with the exception of ultimate tensile strength of SA302B that has a lower value with a maximum difference of 2.4% at 100°C and 250°C compared to ASME data. N06625 has outstanding high strength compared to TP410S stainless steel.

The monotonic and cyclic stress-strain curves are obtained. Both clad materials cyclically harden at the temperatures of 100°C and 480°C. SA302B cyclically hardens at 480°C, while it shows the mixed behavior of hardening-softening at 100°C. On the other hand, SA387-22-2 cyclically softens at both temperatures, which indicates that properties of SA387-22-2 are deteriorated under the cyclic loading condition. From the CTE

measurement tests, it is found that the CTE of N06625 and SA302B are very close to each other without significant difference, which is the main reason to make these two materials as a better combination for coke drums. Based on the strain amplitude of low cycle fatigue (LCF) analysis, it can be concluded that N06625 has better fatigue life than TP410S. With the increase of temperature and strain amplitude, fatigue lives of both materials decrease.

Coupled thermo-elastic FE analysis of the coke drum was carried out to analyze the stress/strain distribution in the drum shell during entire operating cycle for the currently used material combination and the optional material combination. Temperature curves obtained from this FE analysis are in agreement with the measured temperature history of the coke drum. During quenching stage, severe bending stresses and strains are induced in the drum shell due to the temperature difference between the surfaces above and below the water level. The effect of different water rising rates on the stress and strains in the coke drum shell are compared to identify the suitable rising rate of water for the operation of coke drum. Stresses at base layers can be reduced by adopting higher water rising rate of $V_c = 3\ mm/s$ compared to the case of the slower water rising speed of $V_c = 1\ mm/s$. Due to the steeper temperature gradient along the axial direction of the coke drum shell, the von Misses stress to yield strength ratio at slower rising speed of $V_c = 1\ mm/s$ increases from 22.1 % (for the case of $V_c = 3\ mm/s$) to 61.2%.

The stresses and strains obtained from the FE analysis of the two material combinations, where the material properties are introduced from the ASME database, are also compared

with each other. It is found that stresses and strains in the clad layer of TP410S/SA387-22-2 combinations are much higher than the combination of N06625/SA302B. It is also revealed that the clad of the studied coke drum yields, while the clad layer of the coke drum with optional material combination is still in the elastic range due to their matching CTEs. The results obtained from the FE analysis using the test data of the optional material combination of the coke drum are then compared with the results obtained using ASME data in the analysis. It is noticed that the ratio between maximum von Mises stress to yield strength in the clad materials can be reduced significantly from 70% to 19% by using the test data in the analysis, because the test results of the CTE of N06625 is higher than the CTE of SA302B.

In addition, thermal elastic-plastic analysis was carried out for the same two pairs of the base and clad materials to get more practical and accurate results. The temperature distribution data from the previous coupled thermo-elastic analysis was used in this analysis. The bilinear kinematic hardening model is adopted in the FE analysis, where bilinear material properties of the coke drum materials are obtained from the cyclic stress-strain curves. The time history of stress and strain of the base and clad material are compared. It is noticed that this current analysis gives a lower stress level as a result of higher induced plastic strain in the clad material of TP410S compared to the values in the coupled thermo-elastic analysis. It is also found that the stresses of the base layer SA387-22-2 and, the stresses of both clad and base materials of the optional material combinations are still in the elastic range.

From the results, it is also shown that permanent plastic strain occurs only in TP410S in the first process cycle and accumulates in the subsequent cycle, which indicates that plastic shakedown happens in the clad layer of the currently used coke drum.

On the other hand, the maximum stress developed over an operational cycle in the clad/base layer for the material combinations N06625/SA302B is far below the elastic stress limit. Finally, based on the above analyses, it can be concluded that the performance of the coke drum can be improved by the selection of the optimal material combination N06625/SA302B.

5.2 Future work

This thesis mainly focuses on lowering the stress and strain developed in the drum shell during operation cycle by optimal selection of coke drum materials. Thus the skirt and head of the coke drum are removed from the FEA models to reduce the complexity. Additionally, the effect of the weld zone is not considered in the analysis. Welded section, skirt and head of the coke drum can be added to the finite element model in future work to investigate the effect of the discontinuity at the welding zones, the skirt to shell and cone junction on the performance of the coke drum. During oil filling stage radiation effect due to the hot oil inside the coke drum can be considered to obtain an accurate temperature history during the oil filling stage. Finally, multi-linear kinematic hardening rule can be adopted instead of using the relative simple bilinear kinematic hardening model in the elastic-plastic analysis to obtain more realistic simulation results.

Bibliography

1. J. A. Penso, , Y. M. Lattarulo, A. J. Seijas, J. Torres, D. Howden and C. L. Tsai, "Understanding Failure Mechanisms to Improve Reliability of Coke Drum," Operations, Applications, and Components, PVP ASME, 395, pp. 243–253, 1999.

2. Z. Xia, F. Ju and P. D. Plessis, "Heat Transfer and Stress Analysis of Coke Drum for a Complete Operating Cycle", Journal of Pressure Vessel Technology, 132, 2010.

3. J. Chen, "Experimental Study of Elastoplastic Mechanical Properties of Coke Drum Materials", Masters Dissertation, University of Alberta, Edmonton, 2010.

4. American Petroleum Institute, "1996 API Coke Drum Survey Final Report", November 2003.

5. A. Bagdasarian, J. Horwege, S. Kirk and T. Munsterman, "Integrity of Coke Drums (Summary of 1998 API Coke Drum Survey)," PVP ASME, 411, pp. 265–270, 2000.

6. R. S. Boswell and B. Wright, "State-of-the-Art Improvements in Coke Drum Design and Life Extension Practices," Proceedings of the PVP2007/ CREEP8, ASME, New York, pp. 379–388, 2007.

7. C. Alexander, and R. S. Boswell, "Techniques for Modeling Thermal and Mechanical Stresses Generated in Catalytic Cracker and Coke Drum Hot Boxes," Proceedings of the PVP2005, ASME, New York, pp. 527–537, 2005.

8. A. Ramos, C. Rios, J. Vargas, T. Tahara and T. Hasegawa, "Mechanical Integrity Evaluation of Delayed Coke Drums," Fitness for Adverse Environments in

Petroleum and Power Equipment, ASME, New York, Vol. 359, pp. 291–298, 1997.

9. A. Ramos, C. Rios, E. Johnsen, M. Gonzalez and J. Vargas, “Delayed Coke Drum Assessment Using Field Measurements and FEA,” Analysis and Design of Composite, Process and Power Piping and Vessels, ASME, New York, 368, pp. 231–237 , 1998.

10. M. Nikic and Z. Xia., "Alternative Selections of Delayed Coke Drum Materials Based on ASME Material Property Data." Proceedings of the ASME Pressure Vessels and Piping Conference, PVP2012-78548, Toronto, 2012.

11. T. Farraro and T. Walker, “Corrosion, Material and Inspection Considerations for Delayed Coking Units”, NACE, 1995.

12. ASME Boiler & Pressure vessel Code, Section II- Materials, Part D Properties, ASME, New York, 2007.

13. ASME, “Section II Part A Ferrous Material Specifications: SA-302/SA-302M”, ASME Boiler and Pressure Vessel Code, New York, 2007.

14. ASME, “Section II Part B Nonferrous Material Specifications: SB-446”, ASME Boiler and Pressure Vessel Code, New York, 2007.

15. ASTM, “Standard Test Methods for Tension Testing of Metallic Materials”, E 8/E 8M-08, 2008.

16. ASTM. “Standard Test Methods for Elevated Temperature Tension Tests of Metallic Materials”, E 21-09, 2009.

17. J. Chen, “Fatigue Behavior of Coke Drum Materials and Its Application to Extend the Service Lives of Coke Drums” PhD Dissertation, University of Alberta, Edmonton, 2014.

18. ASTM E2368-10, “Standard Practice for Strain Controlled Thermomechanical Fatigue Testing”, ASTM international, West Conshohocken, PA, 2010, DOI: 10.1520/E2368-10.

19. J. D. James, J.A. Spittle, S.G.R. Brown and R. W. Evans, “A Review of Measurement Techniques for the Thermal Expansion Coefficient of Metals and Alloys at Elevated Temperatures”, IOP, Measurement Science and Technology, 12, R1-R15, 2001.

20. ASTM E606-04, 2004, “Standard Practice for Strain-controlled Fatigue Testing”, ASTM international, West Conshohocken, PA, 2004, DOI: 10.1520/E606-04.

21. L. F. Jr. Coffin, “A Study of the Effects of Cyclic Thermal Stresses on a Ductile Metal”, Trans. ASME, 76, pp. 931-950, 1954.

22. S.S. Manson, “Behavior of Materials under Conditions of Thermal Stress”, Heat Transfer Symposium, University of Michigan, pp. 9-75, 1953.

23. Z. Ning and R. Liu, “Analysis of Transient Temperature Field in Coke Drums”, Applied Mathematics and Mechanics, 31(3), pp. 291-304, 2010.

24. F. Ju, J. Aummuler, Z. Xia and P. D. Plessis, “Global and Local Elastic-Plastic Stress Analysis of Coke Drum under Thermal-Mechanical Loadings”, Journal of Pressure Vessel Technology, 133, 2011.

25. Z. Yan, Y. Zhang, J. Chen and Z. Zia, “Statistical Method for the Fatigue Life Estimation of Coke Drums” Journal of Engineering Failure Analysis, 48, pp. 259-271, 2015.

26. ANSYS Manual 12.1, “Theory Reference for the Mechanical APDL and Mechanical Applications”, 2009.